LBL-36256
UC 404

CARBON DOPING OF III-V COMPOUND SEMICONDUCTORS

AMY JO MOLL

Center for Advanced Materials
Materials Sciences Division
Lawrence Berkeley Laboratory, 1 Cyclotron Rd.
Berkeley, CA 94720

and

Materials Science and Mineral Engineering Department
University of California
Berkeley, CA 94720

Ph.D. Dissertation

September 1994

This work was supported by the Director, Office of Energy Research, Office of Basic Energy Sciences, Materials Sciences Division, of the U.S. Department of Energy under Contract No. DE-AC03-76SF00098. A.J. Moll is supported by the Robert N. Noyce Memorial Fellowship from the Intel Foundation.

DISCLAIMER

Abstract

Carbon Doping of III-V Compound Semiconductors

by

Amy Jo Moll

Doctor of Philosophy in Engineering -

Materials Science and Mineral Engineering

University of California at Berkeley

Professor Eugene E. Haller, Chair

This thesis describes the behavior of carbon in III-V compound semiconductors. The focus of this study is C acceptor doping of GaAs which is of particular interest since the diffusion coefficient of C is at least one order of magnitude lower than the diffusion coefficients of the other common p-type dopants in GaAs. Doping with C by ion implantation results in a concentration of free holes in the valence band that is less than 10% of the concentration of C atoms implanted into the substrate when the implantation dose is greater than 10^{14} cm^{-2}. Ga co-implantation resulted in a dramatic increase in the activation of C. To study both the chemical and structural effects of co-implantation, a series of different elements was co-implanted. A second series of samples was studied in which the Ga dose was varied. The structural properties of the implanted layers were measured with channeling Rutherford backscattering spectrometry. The electrical characteristics were determined by Hall effect and electrochemical capacitance-voltage measurements. The amount of substitutional C_{As} was ascertained using local vibrational mode spectroscopy. The increase in activation of C due to co-implantation of Ga was shown to be a two-step process: first, the additional radiation damage creates vacant As sites that the implanted C can occupy, and second, it maintains the stoichiometry of the implanted layer thereby reducing the number of compensating native defects.

In InP, the behavior of C was found to be extremely different from its behavior in GaAs. C acts as an n-type dopant occupying the In site, however its incorporation by implantation was difficult to control. Results from experiments using P co-implants were inconsistent.

This thesis further addresses the lattice position of the inactive C in GaAs both in implanted and in epitaxial layers. A number of research groups have grown epitaxial layers with ultra-high concentrations ($>10^{21}$ cm^{-3}) of free holes using C doping. However, at high concentrations, the doping in these layers is not thermally stable. Annealing results in a rapid decrease in the free carrier concentration. Various models have been proposed to explain the loss of free carriers. Most assume a change in the lattice location of the carbon rendering it electrically inactive. Based on Raman spectroscopy and isotope substitution, the first direct evidence for the formation of C precipitates in GaAs was obtained. C precipitation was also shown to readily occur in C implanted InP. In GaAs, the presence of compensating native point defects was also found to affect the carrier concentration.

By correlating the results presented here with those in the literature for C doping in III-V semiconductors, a phenomenological description of the behavior of C in III-V compound semiconductors, in general, and in GaAs in particular, is presented. The behavior of C in III-V semiconductors is controlled by the chemical nature of C and by the intrinsic Fermi level stabilization energy of the particular semiconductor.

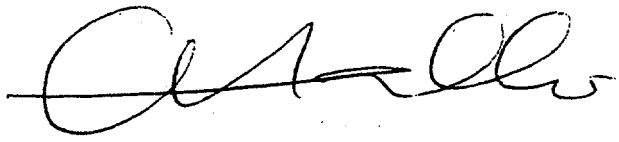

Sept. 23, 1994

Table of Contents

1. Introduction 1

1.1 Technological challenges in the applications of compound semiconductors 3

1.2 Motivation for the study of C in GaAs and InP 5

1.3 Questions addressed in this thesis 6

2. Review of Carbon Doping of III-V Compound Semiconductors 7

2.1 Basic properties of C in GaAs 7

2.2 Carbon doping during epitaxial growth of GaAs 9

2.3 GaAs:C epitaxial layers in devices 12

2.4 Stability of carbon doped GaAs epitaxial layers 14

2.5 Ion implantation of carbon in GaAs 25

2.6 Carbon doping in InP 29

2.7 Carbon doping of other III-V compounds and alloys 33

3. Experimental Procedures 42

3.1 Substrate preparation 42

3.2 Ion implantation 43

3.3 Annealing 50

3.4 Characterization techniques 53

3.4.1 Rutherford backscattering 53

3.4.2 Electrical measurements 56

3.4.3 Raman spectroscopy 63

3.4.4 Fourier transform infrared spectroscopy 65

3.4.5 Other techniques 67

4. Results and Discussion 68

4.1 GaAs:C implantation 68

4.1.1 Various elements as co-implants 69

4.1.2 Ga co-implant series 83

4.2 Inactive C in implanted and epitaxial layers 95

4.2.1 Carbon precipitation 97

4.2.2 Compensation by native defects 109

4.3 InP:C 113

4.4 A model to describe the behavior of carbon in III-V semiconductors 122

5. Conclusions 125

6. References 127

Acknowledgments

The completion of a Ph.D. degree is not a solitary venture and I would like to thank all who have contributed to this thesis. First I would like to thank my adviser, Professor Eugene Haller, for providing me with the resources required for my research and for his guidance throughout my graduate career. Dr. Joel Ager and Dr. Kin Man Yu assisted with the Raman and RBS measurements reported here. I would like to thank them not only for their technical expertise but for their help and guidance in all areas of my research. I am indebted to Wladek Walukiewicz as a source of inspiration, knowledge and journal articles. I would like to thank Professor Timothy Sands and Professor T. Kenneth Gustafson for reading my thesis.

In addition to those specifically mentioned above, I would like to acknowledge the assistance of each and every member of the Electronic Materials Group. Because of the unique environment of collaboration, unselfishness, and camaraderie, I have truly enjoyed my years as a graduate student. I have derived great pleasure in working with this group who I also consider as friends.

I would especially like to thank Kohei and Oscar. We began our journey together and now we will separate, but I have enjoyed their companionship along the way and I look forward to future collaborations.

Although they may not have always understood exactly what I was doing, my family has been a constant source of support throughout all of my many years of schooling.

Last of all I would like to thank my pack, Billy, Bica, and Duke. Their unconditional love and support bring great joy to my life, and their enthusiastic greetings when I return home after some very long days never fail to brighten my spirit.

1. Introduction

Semiconductors are a group of materials which have electrical conductivities between metals and insulators. The conductivity of semiconductors can be varied in a controlled way over orders of magnitude by changes in temperature, optical excitation, and impurity content. This variability in electronic properties is the reason semiconductors are the natural choice for electronic and optical devices. Silicon has become the workhorse of electronics due to several factors including its abundance, ease of growth in the form of single crystals, ease of purification, presence of a native oxide with excellent dielectric properties, interface state density, and virtually ideal bandgap. Other group IV elements are also used for specialized semiconductor devices, especially Ge. Recently, considerable effort is being placed on the use of diamond as a semiconductor.

The intrinsic limitations of Si as a semiconductor are the motivation for pursuing other materials for electronic devices. Silicon's indirect bandgap and relatively large effective mass of the free carriers are its principal limitations. The technological importance of III-V compound semiconductors, principally GaAs and InP, is their use in photonic and high-speed electronic devices. Both InP and GaAs are direct bandgap materials creating much more efficient photonic devices. For high speed electronics, GaAs and InP are superior materials because the electron saturation velocity is at least 1.5 times greater than that of Si. In addition, the low field electron mobility in GaAs or InP peaks at a few kV/cm where it is higher than that in Si by factors of 3 to 6. Therefore GaAs devices have the combined advantage of high speed and low power dissipation, which is particularly attractive for high frequency devices used in the communications industry. Figure 1.1 shows that the majority of the III-V compounds are miscible and therefore the bandgap and lattice constant can be tailored to the needs of the particular application.

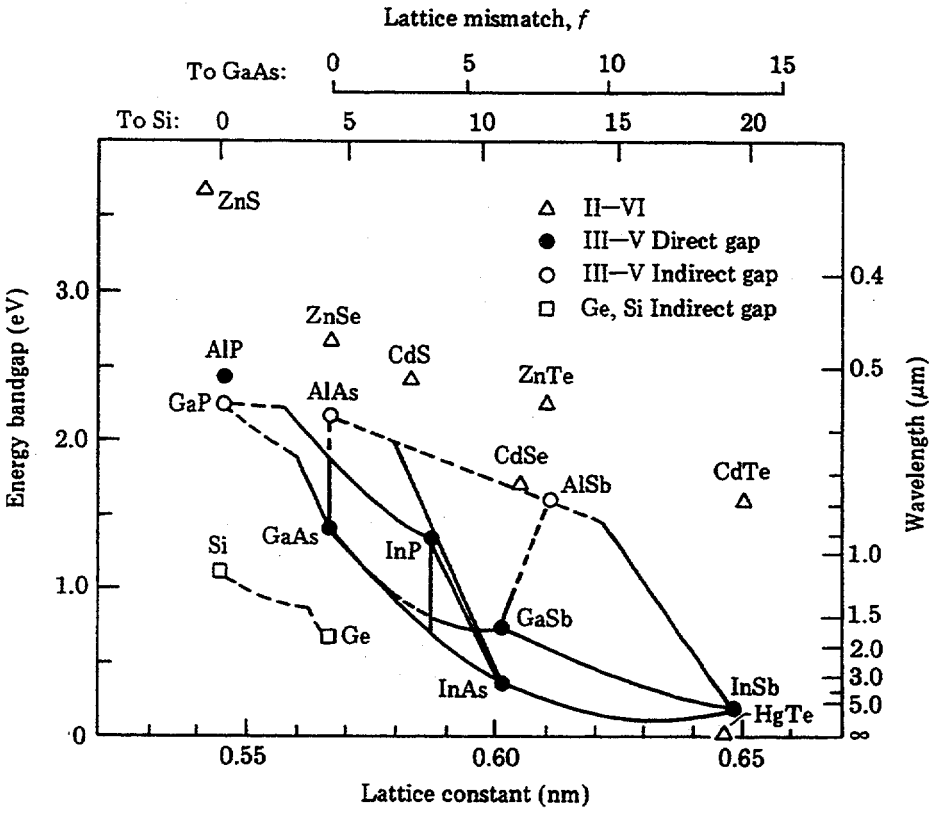

Fig. 1.1. Energy gap versus lattice constant for III-V, II-VI, and IV semiconductors. Open symbols are indirect-gap, closed are direct-gap materials. The lines joining the III-V compounds give the ternary energy gap and lattice constant. The lattic mismatch to Si and GaAs is shown at the top of the figure.(Tu, et al., 1992)

The technologically most important compound semiconductor is GaAs. It has a direct band gap of 1.421 eV at room temperature. The effective mass of the electrons is $0.063m_0$, and the effective mass of the holes is $0.5m_0$ in the heavy hole band and $0.076\ m_0$ in the light hole band. It is widely used for high frequency devices and as a substrate for the epitaxial growth of AlGaAs light emitting diodes, lasers, and a wide variety of superlattice and quantum well based structures. Room temperature X-ray detectors and far infrared photoconductors are being developed with GaAs.

Like GaAs, InP has high electron mobility and a large saturation drift velocity which make it attractive for high frequency electron devices and high speed logic applications. Currently, InP is principally used as a substrate for the alloy InGaAsP. This alloy system has a composition which can be adjusted so that its bandgap emission wavelength varies from 0.92 to 1.65 μm while its lattice constant remains matched to that of InP.

1.1 Technological challenges in the applications of compound semiconductors

Compound semiconductors are inherently more complex than elemental semiconductors. Growth, doping, and processing are less straightforward than in Si. Often one of the elements which make up the compound has a higher vapor pressure than the other. In the case of GaAs, this is As. Any thermal processing above 550°C results in loss of As except when measures are taken to prevent this loss.

Other difficulties arise during doping of compound semiconductors. Dopant atoms can in principle occupy either sublattice within the crystal. Any intentionally introduced dopant is expected to occupy only one kind of site within the crystal. If it occupies the wrong sublattice, it will act as a compensating dopant and diminish the doping efficiency. This fact is particularly important for the group IV dopants in III-V semiconductors. An

impurity or intentional dopant introduced into a single crystal semiconductor will occupy the lattice site which most close resembles its own electrical character. In theory the group IV elements, C, Si, Ge, and Sn, should be amphoteric in any III-V compound semiconductor. If the group IV element occupies a group III site it will act as a donor and if it occupies a group V site it will act as an acceptor. In general, each group IV element prefers one site or the other in each material.

Several factors may influence which substitutional site is chosen by the group IV element. These include the electronegativity, tetrahedral radius, and size. The doping method can influence the substitutional site as well. Dopant atoms introduced during bulk growth may behave differently than those which are introduced during epitaxial growth, implantation, or diffusion. The solubility of the dopant on the group III site is different than the solubility on the group V site, and the solubilities may have different temperature dependencies. For example, Ge may be more likely to occupy Ga sites at low temperatures in GaAs while at high temperatures it prefers the As site. The properties of the host lattice such as the tetrahedral radii of its constituents, the Fermi level, and dislocation density can also influence the substitutional site. In addition, the intentional dopants may occupy an interstitial site, form complexes or precipitate.

Another difficulty is associated with the role native defects play in a material. In group IV semiconductors, only two native point defects exist, the vacancy and the interstitial. In compound semiconductors, two types of vacancies, two types of interstitials and two antisite defects exist. In addition, the native point defects readily form complexes with each other and with intentional dopants which will affect the electrical characteristics of the material.

1.2 Motivation for the study of C in III-V compound semiconductors

In GaAs, C acts as a p-type dopant, substituting for an As site. The other common p-type dopants in GaAs are the group II elements such as Be, Mg, and Zn which have high diffusion coefficients. C has a much lower diffusion coefficient and is therefore a thermally more stable p-type dopant than the group II elements. In addition to its low diffusion coefficient numerous reports of ultra-high doping of C during epitaxial growth of GaAs have appeared in the literature in the last decade. Ultra-high C doped epitaxial layers have been used for the base layer of heterojunction bipolar transistors (HBTs). The high doping level allows improved performance of the HBT compared to similar devices doped with group II elements. Heavily doped C epitaxial layers have also been used to form nonalloyed ohmic contacts.

Implantation of carbon has not been as successful as doping during epitaxial growth. At doses higher than 1×10^{14} cm^{-2} less than 10% of the C implanted acts as an acceptor. The low activation of implanted C has limited the use of implantation as a method of C doping in GaAs.

Due to the success in attaining ultra-high doping levels in GaAs and its low diffusion coefficient, C doping has been studied in many other III-V semiconductors. In InP, the behavior of C is not well understood. No reports on C doping during bulk or epitaxial growth have been reported in the literature. C implantation results in an n-type InP surface layer however it is unclear whether these free carriers are due to C occupying an In site or due to radiation damage which remains in the layer following annealing. In other III-V compounds and in the ternary and quaternary III-V alloys, C doping has received limited attention. Research in this field is driven by the desire to achieve high p-type doping levels with a dopant atom which has a low diffusion coefficient.

1.3 Questions addressed in this thesis

One method of increasing the activation of C implanted into GaAs is to co-implant Ga. Co-implantation of Ga with implantation conditions chosen so that the atomic concentration profile of the two implanted species are similar, will maintain the stoichiometry of the implanted layer and increase the probability that C will occupy the As site. The Ga co-implant has a second effect. Since it must be implanted at much higher energies, and its mass is significantly larger than that of the C, it creates significantly more radiation damage to the crystal. In this thesis, the role of these two effects on the activation of implanted C in GaAs and InP will be examined.

The second question which will be addressed is the lattice position of inactive C in GaAs and InP. Several possibilities exist including self-compensation, compensation due to other native defects, isolated interstitials, and precipitation. The experimental evidence supporting each mechanism will be reviewed.

From the experiments described in this thesis an overall picture of the behavior of C in GaAs will be presented. The general behavior of C in III-V semiconductors will be discussed including the factors which determine the host sublattice on which C will reside within a particular material.

2. Review of Carbon Doping of III-V Compound Semiconductors

2.1 Basic properties of C in GaAs

Carbon acts as an acceptor in GaAs by substituting for As in the lattice. The ground state energy level is 28 meV above the valence band. The other common p-type dopants in GaAs are Be, Mg, and Zn. Their ground state energy levels are located 28, 28 and 31 meV above the top of the valence band respectively. The predominant photoluminescence (PL) lines associated with C acceptors appear at 1.494 eV which is assigned to the recombination of a free a conduction band electron with an acceptor bound hole and 1.490 eV which is assigned to the recombination of a donor bound electron with an acceptor bound hole.(Ashen, et al., 1975)(Stringfellow, et al., 1981) Although in principle C is an amphoteric dopant in GaAs (can occupy either the Ga site or the As site), no experimental evidence for C_{Ga} has been reported. Low et al.(Low, et al., 1983) examined high purity GaAs grown by several epitaxial techniques and found no evidence for C donors in either photothermal ionization spectroscopy (PTIS) or variable temperature PL measurements.

In bulk grown GaAs, C is one of the principal impurity species. Since C is an acceptor, it compensates residual donor contaminants, principally Si, in bulk crystals. The electron concentration in GaAs crystals is controlled by the balance between residual donors, EL2 deep donors, and carbon acceptors. The high resistivity of undoped, semi-insulating GaAs depends not only on the presence of the deep donor EL2 but also on an excess of acceptors over shallow donors. In commercially available semi-insulating GaAs wafers C is present in concentrations of 1×10^{15} to 1×10^{16} cm^{-3}.

The solubility of C in GaAs is not well known. C is not usually introduced during bulk growth as an intentional dopant. During epitaxial growth by metalorganic chemical

vapor deposition (MOCVD) or metalorganic molecular beam epitaxy (MOMBE), ultra-high doping levels can be achieved, as will be discussed later, however growth by these techniques is not an equilibrium process.

C is of special interest as a p-type dopant in GaAs because of its low diffusion coefficient. Reported values of the diffusivity of C in GaAs are given in Table 2.1. The diffusion coefficients of the group II acceptors are also listed for comparison. The diffusion coefficient of C is, in general, at least one order of magnitude smaller than that of any group II acceptor in GaAs.

Table 2.1: Diffusion Coefficients for p-type Dopants in GaAs

Dopant	Doping Level [cm^{-3}]	Growth Technique	Annealing Conditions	Diffusion Coefficient [$cm^2\ s^{-1}$]	Reference
C	1×10^{19} [p]	MOMBE	900°C 4 hr	6×10^{-15}	Konagai, et al., 1989
C	3×10^{20} [C]	MOMBE	900°C 30 sec	1×10^{-16}	Abernathy, et al., 1989
C	5×10^{19} [p]	MOMBE	900°C 1 hr	6×10^{-15}	Saito, et al., 1988
C	1×10^{19} [C]	MOCVD	800°C 1hr	2×10^{-16}	Kobayashi, et al., 1987
C	5×10^{18} [C]	MOCVD	825°C 24 hr	2.3×10^{-16} 1×10^{-16}	Cunningham et al., 1989
C	2×10^{19} [C]	MOCVD	920 C 1 hr	$<1\times10^{-16}$	Kuech, et al., 1987
Zn	8×10^{18}	MOCVD	800 °C 4 hr	6×10^{-14} undoped 3.6×10^{-16} n-type	Enquist, et al., 1988
Zn	2×10^{19}	MOCVD	800 °C 4 hr	9×10^{-14} undoped 3.6×10^{-16} n-type	Enquist, et al., 1988
Be	3.3×10^{19}	MBE	900 °C 30 min	5×10^{-14}	McLevige, et al., 1978
Be	1.5×10^{17}	MBE	800 °C 4hr	1×10^{-15}	Ilegems, 1977
Be	9×10^{19}	MOMBE	900°C 1hr	1×10^{-12}	Saito, et al., 1988

The local vibrational mode (LVM) of C_{As} was first reported by Newman.(Newman, et al., 1972) At 4K the C_{As} LVM appears at 583 cm^{-1}. High resolution infrared spectra can resolve the C LVM into 5 peaks which arise due to the two isotopes of Ga (69 and 71 amu). The area under the LVM peak is directly proportional to the concentration of C_{As} ($[C_{As}]$). If the optical cross-section is known then an absolute measure of the $[C_{As}]$ can be obtained. The reported cross-section for the C_{As} LVM varies from 8×10^{15} cm^{-1}(Brozel, et al., 1986) to 4×10^{16} cm^{-1}(Theis, et al., 1982) with several other values in between also reported.(Hunter, et al., 1984) The large spread in values is a result of the errors involved in verifying the $[C_{As}]$ by a second technique. If electrical measurements such as Hall effect are used then the concentration of compensating dopants must also be known since $p = N_C - N_D = [C_{As}] - N_D$. The other techique which is commonly used for calibration is secondary ion mass spectroscopy (SIMS). However, calibration of SIMS measurements requires the use of standards. In general, measurements are only accurate to within 25%. In addition, if C is present in other forms besides C_{As} (C clusters or interstitals), SIMS will measure this carbon but LVM spectroscopy will not. Therefore, LVM spectroscopy is best used as a relative measure of the $[C_{As}]$ in GaAs

2.2 Carbon doping during epitaxial growth of GaAs

Metalorganic chemical vapor deposition (MOCVD) and metalorganic molecular beam epitaxy (MOMBE) are common epitaxial growth techniques used for the growth of GaAs epitaxial layers. A successful growth method requires precise control of all dopant concentrations. This implies that the method should be capable of producing films with very low background doping. Carbon is one of the primary residual impurities found in epitaxial GaAs layers grown both by MOCVD and MOMBE. Trimethylgallium (TMGa)

is typically used as the source gas for Ga. C contamination is a particular problem in MOMBE growth of GaAs where use of TMGa as a source gas results in p-type layers with hole concentrations greater than 10^{18} cm^{-3}.(Putz, et al., 1985) Low et al.(Low, et al., 1983) found that C was the dominant acceptor impurity in MOCVD grown GaAs using TMGa as a source gas. The use of triethylgallium (TEGa) and careful control of growth parameters, including growth temperature and the V/III ratio results in minimal incorporation of C during both MOCVD(Chen, et al., 1993) and MOMBE(Chiu, et al., 1987) growth.

Tokumitsu et al.(Tokumitsu, et al., 1984) were the first to report the use of TMGa as a source of Ga for MOMBE growth of GaAs. A consequence of the use of TMGa was unintentional p-type doping in the range of 10^{18} to 10^{19} cm^{-3}. The dominant acceptor impurity was determined to be C. Subsequently, other groups have also used TMGa as a source gas to intentionally dope GaAs. As mentioned previously, C is particularly attractive as a p-type dopant because its diffusion coefficient is at least one order of magnitude lower than that of the group II p-type dopants. Careful control of the growth parameters has resulted in ultra-high doping levels with concentrations of C_{As} higher than 10^{21} cm^{-3}.

High concentrations of free holes by C doping of GaAs during MOMBE growth are routinely achieved by using TMGa as the source for Ga and C.(Abernathy, et al., 1989)(Abernathy, et al., 1990a) Typical growth temperatures range between 450°C and 600°C. The hole concentration (C concentration) is found to increase with decreasing growth temperatures and decreasing group V/group III growth ratio.(Saito, et al., 1988) Carrier concentrations greater than 1×10^{20} cm^{-3} have been reported(Konagai, et al., 1989) for epitaxial layers grown by MOMBE where the growth temperature was 450 °C and the V/III ratio was less than 1. The sample with the highest hole concentration of 1.5×10^{21} cm^{-3} had a hole mobility of 22 $cm^2V^{-1}s^{-1}$. SIMS measurements on these samples found the C concentration to be equal to the free hole concentration within the experimental

error. MOMBE growth also allows for excellent control of the C doping profile. Doping spikes with a free hole concentration of 7×10^{19} cm^{-3} and a full width at half maximum of 5 nm have been reported for C doping during MOMBE.(Abernathy, et al., 1990a) C doped layers with hole concentrations greater than 10^{18} cm^{-3} exhibited higher hole mobilities than layers doped with similar concentrations of either Be or Zn.(Stockman, et al., 1992b)

High free hole concentrations have also been achieved in the growth of C doped GaAs by MOCVD. Carrier concentrations greater than 1×10^{20} cm^{-3} have been reported.(Stockman, et al., 1992b)(Chen, et al., 1993) Typically, the source gases are TMGa or TEGa and AsH_3. TMGa can also be used as the source of C(Kushibe, et al., 1990) although CCl_4 is more commonly used.(Chen, et al., 1993)(Enquist, 1990) Growth temperatures range from 500° to 700°C. As in MOMBE, the carbon concentration was found to increase with decreasing growth temperature.(Hanna, et al., 1991)(Chen, et al., 1993) The amount of carbon incorporated also depended on the CCl_4 flow rate and the V/III ratio. The V/III ratio was varied from 1 to 100. Higher hole concentrations were achieved with smaller V/III ratios.(Hanna, et al., 1991)(Kushibe, et al., 1990) Mobilities for MOCVD epitaxial layers doped with C were similar or slightly better than MOMBE epitaxial layers with similar concentrations of Zn.(Hanna, et al., 1991)(Chen, et al., 1993) Abrupt doping profiles were also achieved with MOCVD growth.(Cunningham, et al., 1989)(Kobayashi, et al., 1987)

Traditional molecular beam epitaxy (not using metalorganic sources) eliminates most of the C contamination problem. As a consequence it is also more difficult to attain high C doping levels. Giannini used a solid carbon source and achieved C doping levels up to 5×10^{19} cm^{-3}.(Giannini, et al., 1992) Resistively heated graphite filaments have been used as a source of C in conventional MBE systems.(Malik, et al., 1988)(Hoke, et al., 1991) In this case, the evaporation rate and hence the incorporation rate of C is determined by the filament temperature. Doping levels as high as 1×10^{20} cm^{-3} with

abrupt doping profiles have been achieved.(Malik, et al., 1988) Several other methods have successfully been used for C doping during MBE growth. Zhang et al.(Zhang, et al., 1993) used injection of CBr_4 through a low pressure gas manifold to obtain C doped layers with carrier concentrations of up to 1.5×10^{20} cm^{-3}. Low energy C^+ ion implantation (100 eV) during epitaxial growth has been reported to dope layers up to 3×10^{18} cm^{-3} with no radiation damage and no unwanted impurities.(Iida, et al., 1993)

2.3 GaAs:C epitaxial layers in devices

C doped GaAs epitaxial layers are technologically important since such high doping levels can be achieved and because C has such a low diffusion coefficient. The principal applications for heavily doped C layers are nonalloyed ohmic contacts and the base layer of heterojunction bipolar transistors (HBT). In addition, C doping has been used in various other devices.

Ohmic contacts with resistances of less than 10^{-5} ohms cm^{-2} are required for adequate device performance. Typically, ohmic contacts to p-type material must be alloyed. During annealing, flow of the metal eutectic used for contacts limits the size of the devices. The ability to achieve low contact resistance without alloying is highly desirable. Several groups have successfully used C doping of GaAs to make nonalloyed ohmic contacts to p-type GaAs. Konagai et al. used Mo/Au contacts on a p-type C doped layer ($p=1.05\times10^{21}$ cm^{-3}) and attained ohmic contacts with a resistance of 7.6×10^{-8} Ω cm^{-2}. Non-alloyed ohmic contacts with resistances of 7.2×10^{-6} Ω cm^{-2} and 7.6×10^{-7} Ω cm^{-2} for doping levels of 1×10^{20} cm^{-3} and 5×10^{20} cm^{-3} were achieved using Pt/Ti contacts.(Abernathy, et al., 1989) Enquist(Enquist, 1990) reported a contact resistance of 4×10^{-7} Ω cm^{-2} for a Ti/Pt/Au contact on a C doped layer with $p=7\times10^{19}$ cm^{-3}.

HBT technology requires a base layer with well-controlled p^+ doping . The base region must be thin (< 100 nm) to keep the base transit time small. By increasing the base doping ($p>10^{19}$ cm^{-3}), it is possible to reduce the base transit time by growing a thinner layer and also to lower the parasitic capacitance due to the base contact resistance. Thus, the ability to grow thin p-type layers of very low resistivity is important to the HBT process, and is critical in determining the high-frequency performance of such devices. Other considerations for the base region include the minority carrier transport across the base and control over the location and abruptness of the emitter-base junction. Both Be and Zn are limited to doping levels in the range of mid 10^{19} cm^{-3}. Higher concentrations can lead to severe outdiffusion and poor surface morphology due to strain. Because C is a much slower diffuser it is possible to use high doping levels without degrading the junction quality. HBT's fabricated with base layers which were doped with carbon (10^{19} and 3×10^{20} cm^{-3}) had good ideality factors for both the base-collector junction (1.01) and the base-emitter junction (1.4).(Abernathy, et al., 1990a)

In GaAs metal semiconductor field effect transistors (MESFETS), the Schottky barrier height limits the performance of the device. The use of planarly doped p^+ layers significantly enhances the Schottky barrier height on n-type GaAs. Abernathy reported improved performance in GaAs MESFETS by use of two C planar doped layers near the surface.(Abernathy, et al., 1989) The turn-on voltage and the breakdown voltages in the MESFET were both increased with C doped layers. In addition, the thin p^+ layers did not add to the gate capacitance.

Another possible application for C doped GaAs, is in vertical cavity AlGaAs/GaAs surface emitting lasers.(Jewell, et al., 1991) The basic structure includes a bottom quarter wavelength distributed Bragg reflector and a lower cladding layer, both doped n-type, a thin intrinsic active region, an upper cladding layer, and a top distributed Bragg reflector both doped p-type. The top layers must have low resistance, therefore high p-type concentrations are desirable. Kopf et al.(Kopf, et al., 1992) studied p-type dopant profiles

in AlAs/GaAs structures. Use of Be as a p-type dopant resulted in diffusion of Be and accumulation of Be at the GaAs side of the heterointerface during growth of subsequent layers. When structures were doped with C, the targeted profiles were achieved.

2.4 Stability of carbon doped GaAs epitaxial layers

Although ultra-high doping levels have been achieved with C doping, these epitaxial layers are not thermally stable. The thermal behavior of C doped epitaxial layers is independent of the growth method but does depend on the free hole concentration. Layers doped with C concentrations less than approximately 5×10^{19} cm^{-3} have significantly different behavior when annealed than layers doped with C above 5×10^{19} cm^{-3}. In layers with free hole concentrations of less than 5×10^{19} cm^{-3}, annealing has either no effect on the free carrier concentration or the free hole concentration increases slightly following annealing.(Höfler, et al., 1992) The increase in the hole concentration is found in epitaxial layers grown by MOMBE or MOCVD and correlates with a reduction in the concentration of H in the layer(Höfler, et al., 1992) suggesting that in the as-grown layers some of the C is passivated by H. Metalorganic source gases provide an ample supply of hydrogen. Hydrogen is also used as a carrier gas in some cases.

In epitaxial layers doped above 5×10^{19} cm^{-3}, annealing has a dramatic effect on the properties of the layers. Again, these effects are independent of the growth technique. Anneal temperatures up to 600°C can cause a slight increase in the hole concentration as described above. Annealing above 600°C results in a measurable decrease in the free hole concentration. Independent of the initial C concentration, the free hole concentration tends towards an ultimate value of approximately 5×10^{19} cm^{-3}. At the same time, the mobility of the holes decreases as does the lattice contraction of the epitaxial layer with respect to the substrate (the strain in the epitaxial layer).

In heavily C doped epitaxial layers the lattice constant is reduced due to the high concentration of C. C has a covalent radius of 0.77 Å while the covalent radii of Ga and As are 1.21 and 1.26 Å respectively. The heavily C doped epitaxial layers are therefore under compressive strain since the average lattice constant is smaller in this layer than in the semi-insulating GaAs substrate. The strain can be measured by X-ray diffraction and several groups have found that the lattice constant is reduced in accordance to Vegard's law.(Höfler, et al., 1992)(Hanna & Majerfeld, 1991)(Hoke, et al., 1991)

The results from annealing experiments reported in the literature are tabulated in Table 2.2. Two detailed studies will be highlighted. Nozaki et al.(Nozaki, et al., 1993) grew two structures by MOMBE to study the effects of annealing on C doped layers. The growth temperature was varied to grow multilayered structures with varied C doping levels. A series of annealing experiments were then carried out. The results of the annealing experiments are shown in Fig. 2.1, 2.2, and 2.3. In all cases, the hole concentration decreases following annealing (Fig. 2.1) while the C concentration remains the same.(Fig. 2.2) Furthermore, Nozaki et al. found that the hole concentration tends toward an ultimate value independent of the initial concentration. (Fig. 2.3) That is, the change in hole concentration was more rapid in layers which were more highly doped and the steps (in concentration) became less pronounced with annealing. Significant decreases in the hole concentration were seen at early stages in the annealing process. Although significant reduction in the hole concentration occurs during annealing, the C concentration measured by SIMS remains the same. No change is found in the C concentration profile even after a 240 min. anneal at 800°C.

Watanabe and Yamazaki(Watanabe & Yamazaki, 1991) conducted a series of annealing experiments at varying temperatures on MOCVD layers grown with a hole concentration of either 1.3×10^{20} cm^{-3} or 3.5×10^{19} cm^{-3}. In the heavily doped sample, the carrier concentration increased slightly for annealing temperatures up to 600°C. At higher temperatures the hole concentration and the mobility both decreased as shown in

Table 2.2: Effects of annealing on heavily C doped GaAs epitaxial layers

Growth method	Anneal condtions	p (as grown) [cm^{-3}]	p (annealed) [cm^{-3}]	μ (as-grown) [cm^2/Vs]	μ (annealed) [cm^2/Vs]	Strain (as-grown)	Strain (annealed)	Reference
MOMBE	700°C, 60 min.	1.5×10^{20}	1.1×10^{20}	68	39	.7%	0	(Abernathy, et al., 1989)
MOMBE	900°C, 4 hr.	1×10^{19}	1×10^{19}	nr	nr	nr	nr	(Konagai, et al., 1989)
MOMBE	900°C, 1 hr.	5×10^{19}	5×10^{19}	nr	nr	nr	nr	(Saito, et al., 1988)
MOMBE	900°C, 30 min.	6×10^{20}	4×10^{18}	nr	nr	.55%	.05%	(Sohn, et al., 1992)
MOCVD	600°C, 30 sec.	4.7×10^{19}	6.6×10^{19}	77	74	.15%	.2%	(Han, et al., 1992)
MOCVD	900°C, 30 sec.	4.7×10^{19}	6.4×10^{19}	77	68	.15%	.16%	(Han, et al., 1992)
MOCVD	600°C, 30 sec.	9.8×10^{19}	1.7×10^{20}	69	64	.05%	.006%	(Han, et al., 1992)
MOCVD	900°C, 30 sec.	9.8×10^{19}	1.2×10^{20}	69	56	.05%	.07%	(Han, et al., 1992)
MOCVD	600°C, 14 min.	1.5×10^{20}	4×10^{19}	70	55	.2%	.1%	(Enquist, 1992)
MOCVD	800°C, 5 min.	1×10^{20}	5×10^{19}	70	60	.17%	.09%	(Hanna & Majerfeld, 1991)
MOCVD	800°C, 5 min.	2×10^{19}	2×10^{19}	90	90	.02%	.02%	(Hanna & Majerfeld, 1991)
MOCVD	900°C, 10 min.	1.3×10^{20}	7×10^{19}	70	40	nr	nr	(Watanabe & Yamazaki, 1991)
MOCVD	900°C, 10 min.	3.5×10^{19}	4×10^{19}	80	60	nr	nr	(Watanabe & Yamazaki, 1991)
MBE	950°C, 10 sec.	5.2×10^{19}	4.8×10^{19}	60	66	nr	nr	(Hoke, et al., 1991)

nr = not reported

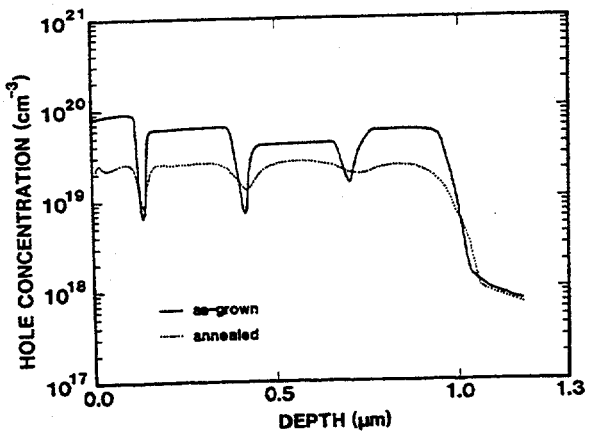

Fig. 2.1. Hole concentration depth profile in C doped MOMBE GaAs layers before and after a 750°C, 60 min. anneal.(Nozaki, et al., 1993)

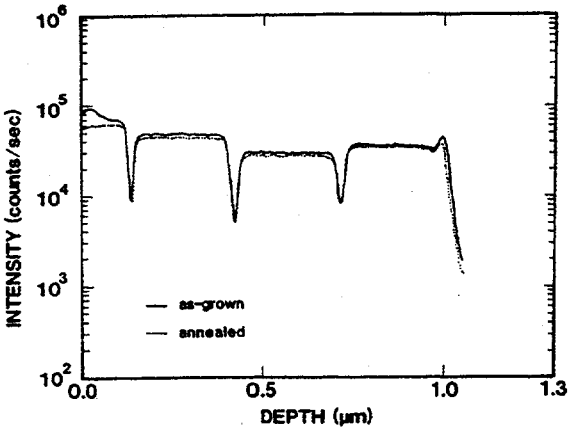

Fig. 2.2. SIMS depth profile of carbon distribution in C doped MOMBE GaAs layer before and after a 750°C, 60 min. anneal.(Nozaki, et al., 1993)

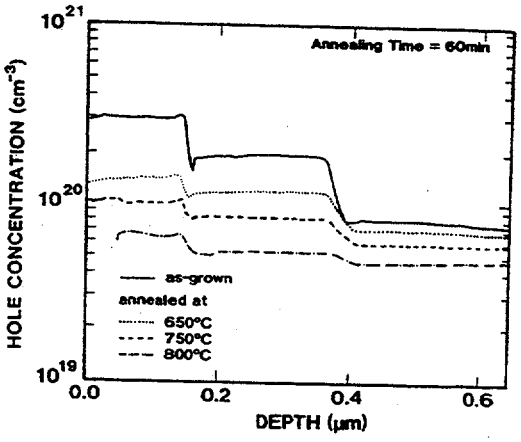

Fig. 2.3 Hole concentration depth profile for a C doped MOMBE GaAs layer before and after annealing at 650, 750, and 800 °C for 60 min.(Nozaki, et al., 1993)

Fig. 2.4. However in the lower doped sample the carrier concentration increased slightly and then remained steady following annealing (Fig. 2.5). To further characterize the sample, the PL spectra at 4.2K were measured. In the heavily doped, annealed sample, a broad peak at 1080 nm appeared in the PL spectra (Fig. 2.6). No such peaks were present in the more lightly doped sample.(Fig. 2.7)

Several mechanisms to describe the decrease in carrier concentration with annealing have been suggested. An effective model must take into account the decrease in hole concentration, decrease in hole mobility and the decrease in strain. The ultimate hole concentration of approximately 5×10^{19} cm^{-3} implies that this may be the solid solubility limit of C in GaAs. The decrease in mobility suggests compensating centers are forming,

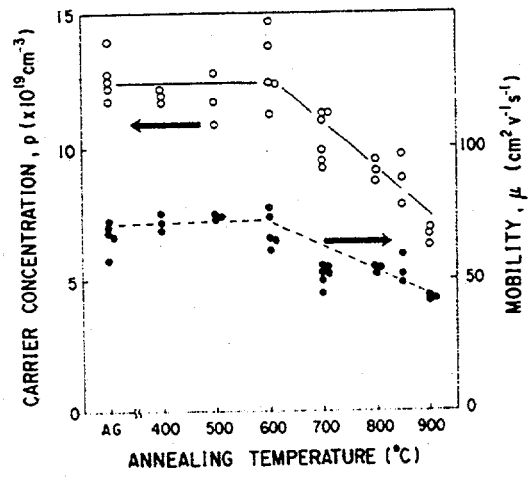

Fig 2.4 Annealing temperature dependencies of the carrier concentration and hole mobility in heavily C doped MOCVD GaAs layers. Open dots and the solid line represent carrier concentration; closed dots and the broken line represent mobility.(Watanabe & Yamazaki, 1991)

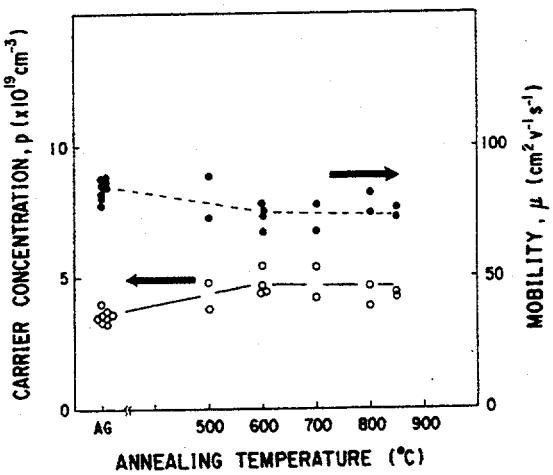

Fig. 2.5. Annealing temperature dependencies of the carrier concentration and hole mobility in lightly C doped MOCVD epitaxial layer. Open dots and the solid line represent carrier concentration; closed dots and the broken line represent mobility.(Watanabe & Yamazaki, 1991)

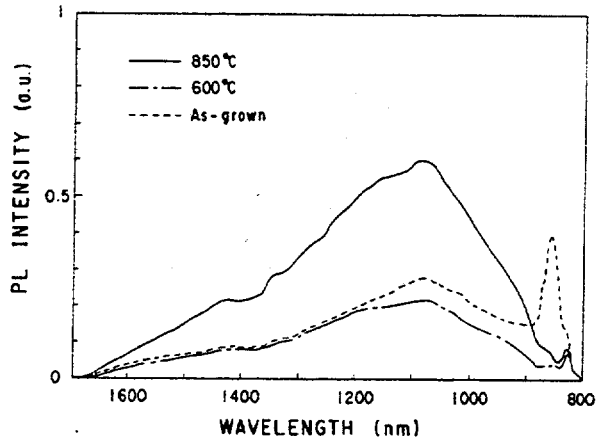

Fig. 2.6. Annealing effect on PL deep level spectra in heavily C doped MOCVD GaAs layer. Solid line is for the 850°C annealed sample; solid and dotted line is for the 600°C annealed sample; broken line is for the as-grown sample.(Watanabe & Yamazaki, 1991)

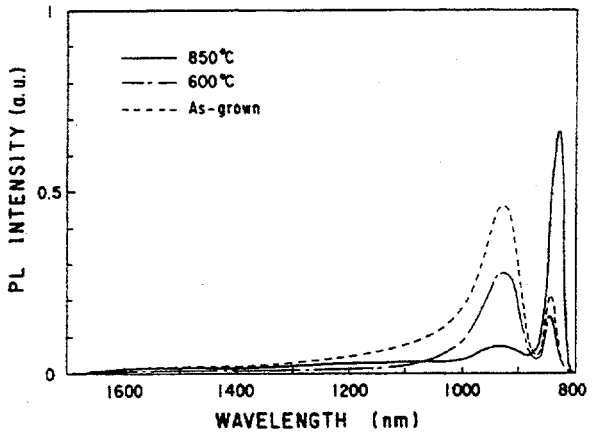

Fig. 2.7. Annealing effect on the PL specta in lightly C doped MOCVD GaAs layer. Solid line is for the 850°C annealed sample; solid and dotted line is for the 600°C annealed sample; broken line is for the as-grown sample.(Watanabe & Yamazaki, 1991)

assuming that the mobility at such high concentrations is inversely proportional to the number of ionized impurities in the sample. Finally an effective model must also account for relaxation of the strained epitaxial layer.

The first and most commonly cited mechanism is self-compensation. Theoretically C is amphoteric in GaAs. Therefore, it is proposed that during annealing a fraction of the C switches from As sites to Ga sites. This mechanism has two effects. The concentration of C_{As} is reduced by the formation of C_{Ga} (C which has switched sites).

$$[C_{As}]_{annealed} = [C_{As}]_{as\ grown} - [C_{Ga}]_{annealed}$$

The free hole concentration is further reduced due to compensation by the C_{Ga}.

$$p = [C_{As}]_{annealed} - [C_{Ga}]_{annealed} = [C_{As}]_{as\ grown} - 2[C_{Ga}]_{annealed}$$

The decrease in the hole mobility following annealing supports this mechanism. However site switching of C does not explain the relaxation of strain in the epitaxial layers upon annealing. The covalent radius of As (1.21Å) is slightly smaller than that of Ga(1.26Å) Therefore C atoms switching from As sites (acceptor) to Ga sites (donor) would have either no effect on the strain in the epitaxial layer or slightly increase the strain. In addition, no C_{Ga} LVM peak has been found. From first principles calculations,(Jones, et al., 1992) the expected frequency of the C_{Ga} LVM would be about 6 cm^{-1} lower than that of C_{As}. The LVM of C_{As} is observed at 583 cm^{-1} at 4K,(Newman, et al., 1972) therefore the C_{Ga} LVM could be expected around 575 cm^{-1}. Davidson et al.(Davidson, et al., 1993) have completed detailed studies of all peaks present in both C doped GaAs and AlAs. All peaks within from 500 cm^{-1} to 650 cm^{-1} have been identified as arising from C-H modes or C_{As}. No peaks which could be assigned to C_{Ga} were found. These findings suggest that no significant fraction of C occupies Ga sites and that there must be another reason for the reduction in the free hole concentration after annealing.

A second suggestion for the reduction of free carriers following annealing is that C forms complexes with itself in the form of C-C pairs on adjacent lattice sites or as split interstitials. As well as reducing the $[C_{As}]$, these defects could further reduce the hole

concentration by compensating the remaining C_{As}. No experimental evidence for this to occur has been found.

Another model speculates that during annealing misfit dislocations form in the heavily C doped epitaxial layers to accommodate the strain.(Han, et al., 1992) It is further suggested that these dislocations have electrical character (donor) which compensate the C acceptors. It is unlikely that dislocations would exist in heavily C doped GaAs and that they would create a sufficient concentration of electrically active donors to compensate C acceptor cocentrations greater than 10^{20} cm^{-3}. Dislocations would only form in epitaxial layers which are greater than the critical thickness. If dislocation formation is the mechanism by which the carrier concentration is reduced, then samples thinner than the critical thickness should not show any change in their electrical character following annealing. However, in samples grown with thicknesses less than the critical thickness, the carrier concentration was reduced following annealing in the same way as the reduction during annealing of layers greater than the critical thickness.(Enquist, 1992) Transmission electron microscopy (TEM) of annealed epitaxial layers which were heavily doped with C and show a significant reduction of free carrier concentration showed no evidence of the formation of dislocations.(Han, et al., 1992)(Han, et al., 1992) Although dislocations were not seen with TEM the strain was relieved in the epitaxial layers following annealing.

Formation of C interstitials has also been suggested as a mechanism which accounts for the reduction in free carriers. Non-substitutional C has been observed by nuclear reaction analysis (NRA).(Höfler & Hsieh, 1992) The nuclear reaction used in this experiments is $^{12}C(d,p)^{13}C$. Experiments were conducted on annealed GaAs and AlGaAs epitaxial layers which had a range of doping levels before annealing.(Höfler, et al., 1992) Figure 2.8 shows the backscattered particles in the (100) channel in GaAs before and after annealing for an epitaxial layer with an as-grown hole concentration of 1×10^{20} cm^{-3}. The increase in backscattered yield indicates additional non-substitutional C in the epitaxial

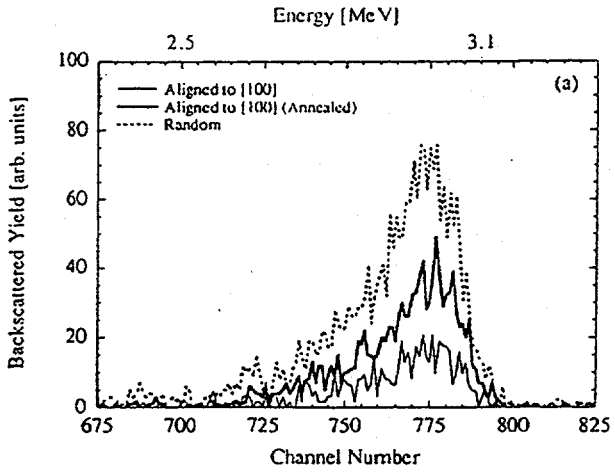

Fig 2.8. [100] aligned and randomly aligned nuclear reaction backscattered carbon signal versus energy obtained on an as-grown and annealed C doped MOCVD GaAs layer with [C]=1×10^{20} cm^{-3}.(Höfler, et al., 1992)

layer following annealing. Experiments were not performed along other channels to locate the specific position of the non-substitutional C. Unfortunately, nuclear reaction analysis does not provide information on the chemical character of the nonsubstitutional C. Therefore, the nonsubstitutional C seen in these experiments could be in the form of isolated interstitials, split interstitials, C complexes or even precipitates.

The neutral C atom is small enough to occupy an interstitial site in GaAs. C has a radius of 0.77 Å and will readily fit into the tetrahedral and octahedral interstitial sites in GaAs. By moving from a substitutional site to an interstitial site the strain in the epitaxial layers could be relieved. The loss of free carriers following annealing can also be accounted for by the formation of C interstitials. However, the reduction in the hole

mobility following annealing is not as easily explained. If a C interstitial is a neutral species it should have little effect on the mobility. Therefore with a decrease in free holes, the mobility would increase. Since the mobility decreases, the compensation in the epitaxial layer must increase following annealing. The C interstitial would have to act as a donor to compensate the C acceptors. No experimental evidence for the C interstitial acting as a donor is reported in the literature. Another possibility is that As vacancies are present which compensate the C acceptors. Each interstitial C atom can create an As vacancy As vacancies are known to be donors and also may form n-type complexes with other native defects.

Finally, it has been suggested that C precipitates form in the epitaxial layers during annealing. Precipitation would occur if the C concentration is above the solid solubility limit in GaAs. It is well known that both MOMBE and MOCVD are non-equilibrium processes. The nonsubstitutional C seen in NRA could be in the form of precipitates. You et al.(You, et al., 1993) have suggested that the reduction in the hole concentration in C doped epitaxial layers during annealing is due to a precipitation process for which C_i^- is the mobile entity:

$$C_i^- + h \rightarrow (C^0)_{ppt.}$$

Precipitates have been observed in annealed epitaxial layers using TEM.(Sohn, et al., 1992) C doped MOMBE layers with initial hole concentrations of 5.8×10^{20} cm^{-3} were annealed at 900°C for 30 minutes. Following annealing the hole concentration was reduced to 3.4×10^{18} cm^{-3}. The lattice mismatch in the epitaxial layers changed from -.55% before annealing to -.05%. The precipitates seen in TEM were 1-3 nm in diameter and were homogeneously distributed throughout the epitaxial layer. Based on the correlation of free carrier reduction with the appearance of precipitates, it was suggested that the precipitates contain carbon, but a direct identification of their crystallographic structure was not achieved.

To summarize this section, in heavily C doped epitaxial layers, the carrier concentration is reduced upon annealing above 600°C. Not only is the carrier concentration reduced, but the hole mobility is reduced, and the strain in the epitaxial layers is relieved. Although many mechanisms have been suggested to explain this effect, no clear experimental evidence has been presented which fully explains the phenomena.

2.5. Ion implantation of carbon in GaAs

Although C doping during epitaxial growth has been highly successful, implantation of C is more problematic. The concentration profile of an implanted dopant is determined by the implantation parameters, in particular the energy and implantation dose. Concentration profiles follow a modified Gaussian distribution. Implantation with low doses of C which correspond to peak bulk concentrations of less than 5×10^{18} cm^{-3} are fairly successful. The activation lies typically near 50%. Activation is defined as the sheet free hole concentration divided by the implant dose. However when the implantation parameters are such that the bulk concentration is 5×10^{18} cm^{-3} or higher over more than 10 nm, activation remains very low, in general less than 10%.

The results of any implantation study will depend on a variety of experimental variables. Obviously the implantation dose and energy determine the concentration profile. In addition, the initial substrate and the annealing conditions can be very important. A summary of the C implantation results reported in the literature is presented in Table 2.3. At low doses and moderate energies, activation is fairly high. When the C dose is between 1×10^{13} and 5×10^{13} cm^{-2} (the peak concentration remains below 5×10^{18} cm^{-3}), activation from 40 to 50% can be attained.(Shin, 1976)(van Berlo, 1993)(Jiang, et al., 1994) Increasing the dose beyond 5×10^{13} cm^{-2} causes a significant deterioration in the activation. Doses greater than 1×10^{14} cm^{-2} result in activation of less

Table 2.3 Summary of implantation schedules and results from the literature

Ion	Energy (keV)	Dose (cm^{-2})	Anneal-ing Temp. (°C)	Sheet Carrier Conc. (cm^{-2})	Activ. Effic. (%)	Reference
C	70	1×10^{13}	700	2×10^{11}	2	(Sansbury & Gibbons, 1970)
C	70	1×10^{14}	700	1×10^{11}	1	(Sansbury & Gibbons, 1970)
C	70	1×10^{15}	700	6×10^{11}	0.1	(Sansbury & Gibbons, 1970)
C	200	2×10^{14}	800	3×10^{12}	1.5	(Harris, 1971)
C	200	2×10^{14}	800	1.4×10^{13}	7	(Harris, 1971)
C	120	1×10^{13}	900	5×10^{12}	50	(Shin, 1976)
C	120	1×10^{14}	900	1.2×10^{13}	12	(Shin, 1976)
C	60	1×10^{14}	700	3.6×10^{12}	3.6	(Shin, et al., 1978)
C	60	1×10^{14}	900	9.5×10^{12}	9.5	(Shin, et al., 1978)
C	80	3×10^{13}	850	2.7×10^{12}	9	(Paulson & Tam, 1984)
C	80	5×10^{13}	850	2.7×10^{12}	5	(Paulson & Tam, 1984)
C	50 + 150	6×10^{11} + 2×10^{12}	850	6×10^{11}	27	(Paulson & Tam, 1984)
C	40	1×10^{13}	800	3.4×10^{12}	34	(Pearton & Abernathy, 1989)
C	40	5×10^{14}	800	1.3×10^{12}	2.5	(Pearton & Abernathy, 1989)
C	45	5×10^{13}	950	1.2×10^{13}	25	(Chan & Chen, 1993)
C	100	3×10^{13}	1000	1.2×10^{13}	40	(van Berlo, 1993)
C	100	1×10^{14}	1000	1.5×10^{13}	15	(van Berlo, 1993)
C	100	3×10^{14}	1000	2.4×10^{13}	8	(van Berlo, 1993)
C	100	1×10^{15}	1000	2×10^{13}	2	(van Berlo, 1993)
C	70	1×10^{14}	1000	2.2×10^{13}	22	(van Berlo, 1993)
C	90	5×10^{13}	800	2.6×10^{13}	52	(Jiang, et al., 1994)
			850	3.7×10^{13}	73	
C	90	1.6×10^{14}	800	6.9×10^{13}	43	(Jiang, et al., 1994)
			850	8.8×10^{13}	55	
C	90	5×10^{14}	800	1.5×10^{14}	30	(Jiang, et al., 1994)
			850	1.3×10^{14}	26	
C	90	1.6×10^{15}	800	1.8×10^{14}	11	(Jiang, et al., 1994)
			850	1.4×10^{14}	9	
C	90	5×10^{15}	800	1×10^{14}	2	(Jiang, et al., 1994)
			850	1×10^{14}	2	

Table 2.3 (cont.) Summary of implantation schedules and results from the literature

Ion	Energy (keV)	Dose (cm^{-2})	Anneal-ing Temp. (°C)	Sheet Carrier Conc. (cm^{-2})	Activ. Effic. (%)	Reference
C + Ga	60 120	1×10^{14} 1×10^{14}	700	1.2×10^{13}	12	(Shin, et al., 1978)
C + Ga	60 120	1×10^{14} 1×10^{14}	900	3.2×10^{13}	32	(Shin, et al., 1978)
C + Ga	40 180	1×10^{13} 1×10^{13}	800	6×10^{12}	60	(Pearton & Abernathy, 1989)
C + Ga	40 180	5×10^{14} 5×10^{14}	800	2.1×10^{14}	43	(Pearton & Abernathy, 1989)
C + Al	50 90	3×10^{14} 3×10^{14}	850	2×10^{13}	7	(Leier, et al., 1992)
C + Ar	50 120	3×10^{14} 3×10^{14}	850	5×10^{13}	17	(Leier, et al., 1992)
C + Ar	45 130	5×10^{13} 5×10^{13}	950	5×10^{13}	100	(Chan & Chen, 1993)
C + Ga	70 350	1×10^{14} 1×10^{14}	1000	1×10^{14}	100	(van Berlo, 1993)

than 15%(Sansbury & Gibbons, 1970)(Harris, 1971)(Paulson & Tam, 1984) with activation falling to below 5% for most experiments(Pearton & Abernathy, 1989)(van Berlo, 1993) where the C dose is greater than 5×10^{14} cm^{-2}.

An implanted dopant into a compound semiconductor like GaAs typically substitutes for atoms on only one host sublattice. This fact results in a change in the stoichiometry of the implanted layer. Heckingbottom and Ambridge(Heckingbottom & Ambridge, 1973) proposed the co-implantation of a complementary species to reduce stoichiometry effects. In the case of C implanted into GaAs, Ga or another group III element (B, Al, or In) would be implanted to maintain the stoichiometry of the implanted layer. Typically the energy and dose of the co-implant is chosen so that the concentration profile of the co-implant closely matches that of the dopant ion.

Ga co-implantation has been shown to increase the activation efficiency of implanted C particularly at high doses. Shin et al.(Shin, et al., 1978) found that co-implantation of Ga increases the activation efficiency of C from 9 to 32% for a C dose of 10^{14} cm^{-2} after annealing at 900°C. The bulk concentration in co-implanted samples was 2×10^{18} cm^{-3}. Ga co-implantation made a dramatic difference in the activation efficiencies obtained by Pearton et al.(Pearton & Abernathy, 1989) Activation efficiencies increased from 34 to 60 % for a 1×10^{13} cm^{-2} implants and from 2.5 to 43% for 5×10^{14} cm^{-2} implants after annealing at 800°C. In the fabrication of heterojunction bipolar transistors with C implantation, Leier et al.(Leier, et al., 1992) found that Al and Ar co-implantation dramatically enhanced the C activation by more than one order of magnitude leading to p-type doping levels of 7×10^{18} cm^{-3}. Chan and Chen(Chan & Chen, 1993) found that co-implantation of Ar increased the activation to nearly 100% for C implanted at a dose of 5×10^{13} cm^{-2} and an energy of 45 keV. C implanted alone at the same energy and dose resulted in an activation of only 25%. Results for carbon and co-implants are also shown in Table 2.3

2.6 Carbon doping in InP

The behavior of C in InP is not well understood. C does not appear to incorporate in significant amounts during bulk growth of InP. Undoped, melt-grown InP is usually n-type due to incorporation of S or Si. To obtain semi-insulating behavior, Fe which acts as a deep acceptor is added to the melt.

In bulk growth of liquid encapsulated Czochralski InP crystals, Cockayne et. al(Cockayne, et al., 1981) used spark source mass spectrometry and radiochemical gamma photon activation analysis to measure the concentration of C in a series of crystals. The mean concentration of C from 8 samples was found to be 1.3×10^{16} cm^{-3}. The concentration of C varied from 5×10^{15} cm^{-3} to 1×10^{17} cm^{-3} however no correlation was found between the concentration of C in the samples and N_D or N_A as measured by 77K Hall mobility and free-electron concentration.

Hess et al.(Hess, et al., 1974) were the first to associate a peak in the PL spectrum of InP with a C acceptor (C_P). The sample was an InP epitaxial layer grown by liquid phase epitaxy (LPE) on an InP substrate. The peak at 1.3832 eV was labeled as a conduction band to acceptor transition in InP. Hess speculated that the residual "A_1" acceptor seen in his PL experiments was due to a C acceptor (C_P). Previously, C had been identified as a major contaminant in LPE InP by Dean et al.. Other groups also found conduction band to acceptor transitions with approximately the same energy in PL experiments on polycrystalline InP,(Barthruff, et al., 1979) bulk single crystals(Temkin & Bonner, 1981) and InP grown by MOCVD.(Zhu, et al., 1985)

Skromme et al.(Skromme, et al., 1984) used intentional doping by low dose ion implantation of C, Be, and Mg acceptors to evaluate the identification of the A_1 acceptor. Implantation of C resulted in additional peaks in the PL spectrum, however the ionization energy of the C acceptor was found to be 44.6 meV. The ionization energy of the A_1

acceptor seen by Hess was 41.2 meV. The A_1 acceptor was assigned to either Mg or Zn. Skromme only found the A_1 acceptor peak in intentionally doped InP. A comparison with the ionization energies of residual acceptors in LPE, MOCVD, bulk LEC, and polycrystalline InP indicated that C is not present as a residual acceptor in undoped InP. Skromme did not report the electrical characteristics for the intentionally C doped InP. Strong PL peaks associated with a C acceptor were evident after implantation of C ions.

Doping of InP with C during MOCVD growth was attempted by Cunningham et al.(Cunningham, et al., 1990b) Use of CCl_4 and growth conditions similar to those used for high C doping levels in GaAs resulted in C incorporation into InP below the detection limit of SIMS (3×10^{16} cm^{-3}). To further increase the detection limit, doping with ^{13}C from $^{13}CCl_4$ was attempted. Again C concentrations in epitaxial layers grown at 630°C and 580°C were below the detection limit, 2×10^{14} cm^{-3}, of SIMS experiments. In addition, no change in the net free carrier concentration (N_D-N_A) was detected in any of the samples. Cunningham therefore concluded that C is not incorporated in InP grown by MOCVD. Kibbler et al.(Kibbler, et al., 1991) was also unsuccessful in doping InP with C using CCl_4 as a source in MOCVD. The carrier concentration of InP epitaxial layers did not vary from the undoped value regardless of the CCl_4 flow (T_g=600 to 700°C).

Benchimol et al. (Benchimol, et al., 1990) studied chemical beam epitaxial growth of InP. The carbon concentration in the epitaxial layer was measured by SIMS with a detection limit of 1×10^{16} cm^{-3}. Their data is shown in Fig. 2.9. The carbon concentration increased with increasing PH_3 flow rate and decreasing growth temperature. At low growth temperatures they correlate the carbon concentration with the net electron concentration implying that C is an n-type dopant, substituting for an In atom. This correlation is based on one data point as shown in Fig. 2.9. Clearly at high growth temperatures, no correlation between the net electron concentration and the C concentration exists. Clearly, the identification of C as a donor in their material is far from certain.

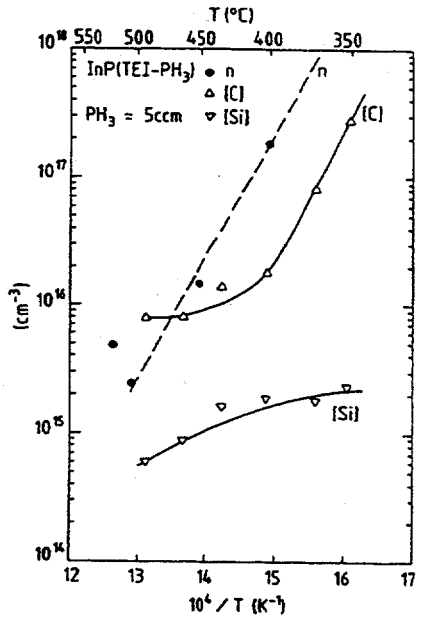

Fig. 2.9. C and Si concentration, measured by SIMS, and net electron concentration, measured by Hall effect, versus inverse growth temperature in InP grown by CBE.(Benchimol, et al., 1990)

Recent reports in the literature confirm that C acts as a donor in InP. Stockman et al.(Stockman, et al., 1994) were successful in incorporating C from TMIn during MOCVD growth of InP with growth temperatures below 500°C. The highest C concentration achieved (T_g = 440°C) was 2.3×10^{19} cm^{-3}, however, the free electron concentration was only 1.3×10^{18} cm^{-3}. In all C doped layers, the electrical activation was only 5 to 15%. The electron mobility and the PL intensity were reduced in C doped InP compared to Si doped InP with the same concentration of free electrons. Gas source MBE growth of InP using CCl_4 as the C source at a growth temperature of 515°C resulted in a C concentration of 1×10^{21} cm^{-3} as measured by SIMS.(de Lyon, et al., 1991a) The electron concentration in the layer was only 9×10^{17} cm^{-3} with a Hall mobility at 77K of 740 $cm^2\ V^{-1}\ s^{-1}$. In comparison, undoped InP grown under the same conditions

resulted in a free electron concentration of 3.2×10^{17} and a 77K mobility of 2650 $cm^2\ V^{-1}\ s^{-1}$.

Several attempts have also been made to dope InP with C by implantation. Donnelly and Ferrante(Donnelly & Ferrante, 1980) report n-type activity following implantation of C which they attribute to C substituting for In. The activation was less than 5% for a C dose of 1×10^{14} cm^{-2} at 400 keV. This activation is significantly lower than activation of Si, Ge, and Sn implanted into InP under similar conditions. Pearton et al.(Pearton, et al., 1989) also reported n-type behavior following implantation of C in InP. The C was implanted at an energy of 40 keV with doses ranging from 5×10^{12} cm^{-2} to 5×10^{14} cm^{-2}. In all cases the activation of C is very low. The free electron concentration was found to increase with increasing doses of C, although the increase was not linear with ion dose and appeared to saturate as shown in Figure 2.10. Various co-implants

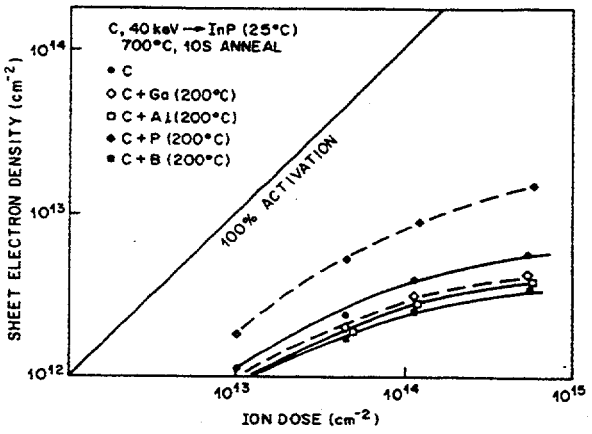

Fig. 2.10. Sheet electron density obtained for C, C=P, C+Ga, C+B, or C+Al implantation into InP, as a function of ion dose for an annealing temperature of 700°C for 10s. The dose of C and the group III or group V ions was the same in each case.

were used (Ga, Al, P, and B) to determine their effect on activation. The co-implantation was performed at both room temperature and 200°C. The highest activation achieved was a result of P co-implantation performed at 200°C. The activation percentages remained very low (<10% at doses greater than 10^{14} cm^{-2}).

To summarize, C may act as an acceptor in InP at very low concentrations. It is difficult to intentionally dope with C during epitaxial growth. The growth temperature must be relatively low (approximately 500°C) before C incorporation occurs. In other words, the growth process must be far from equilibrium before C will incorporate into InP. Implantation of C results in n-type implanted layers. In both epitaxial layers and implanted layers, C is a very inefficient n-type dopant. The C atomic concentration is at least an order of magnitude higher than the free electron concentration.

2.7 Carbon doping of other III-V compounds and alloys

The motivation for studying C doping in other III-V compound semiconductors and their alloys is two-fold. One concern is the effect of C contamination on the electrical properties of epitaxial layers. Therefore, intentional C doping experiments are performed to determine C incorporation rates due to various source gases and also to determine the electrical behavior of C. Second, the low diffusion coefficient and extreme p-type doping levels achieved during epitaxial growth of GaAs has led many groups to research the possibility of p-type doping of C in other III-V compound semiconductors. In principal, C should act as an amphoteric dopant in any III-V compound semiconductor or alloy semiconductor. However, experimental results suggest that C either acts efficiently as a p-type dopant or it is weakly n-type.

AlAs and the alloy AlGaAs are compound semiconductors of considerable interest because of their many applications including HBTs, quantum well lasers and vertical

surface emitting lasers. The epitaxial growth of AlAs and AlGaAs is very similar to the growth of GaAs. In MOCVD and MOMBE, C from the metalorganic sources is the principle acceptor contaminant.(Tamamura, et al., 1987) Kuech et al.(Kuech, et al., 1987) found that in MOCVD growth of AlGaAs the residual C incorporation is strongly dependent on the Al content in the alloy. With increasing Al content in the layers, the undoped epitaxial material changed carrier type from n- to p-type conduction. This crossover occurred around x = 0.1-0.2 in $Al_xGa_{1-x}As$ at growth temperatures greater than 700°C. Lee et al.(Lee, et al., 1990) showed that C contamination could be reduced in AlGaAs epitaxial layers grown by MOMBE by using triisobutylaluminum rather than TEAl as the aluminum source. The substrate temperature for the growth of AlGaAs with a minimum carbon concentration was found to be 560°C. Carbon incorporation increased when the growth temperature was either less than or greater than 560°C.

As in GaAs, it is easy to attain high p-type doping levels in $Al_xGa_{1-x}As$ for the whole composition range by intentionally doping with C during epitaxial growth. MOCVD, (Abernathy, et al., 1990b)(Watanabe & Yamazaki, 1993) MOMBE(Konagai, et al., 1989) and MBE with a graphite filament as the C source(Wagner, et al., 1993)(Micovic, et al., 1994)(Giannini, et al., 1993) have all been successful in growing p-type AlGaAs with free hole concentrations above 5×10^{19} cm^{-3}. Konagai et al. reported free hole concentrations as high as 2.5×10^{21} cm^{-3} in C doped $Al_{0.35}Ga_{0.65}As$ layers grown by MOMBE. Several groups report that C is more readily incorporated as the mole fraction of AlAs increases.(Cunningham, et al., 1990a)(Makimoto & Kobayashi, 1993)

C doping of AlGaAs has also been used in a variety of devices. Atomic layer doping in AlGaAs has been reported by Makimoto and Kobayashi.(Makimoto & Kobayashi, 1993) These workers grew a p-type modulation doped AlGaAs/GaAs structure which resulted in a high quality two-dimensional hole gas at the heterojunction interface. Guido et al.(Guido, et al., 1988) demonstrated that C doping during MOCVD

growth could be used as the active p-type dopant in AlGaAs-GaAs quantum well lasers. In another study, Guido(Guido, et al., 1990) reported that C doped AlGaAs-GaAs quantum well heterostructures had less Al-Ga interdiffusion compared to similar structures doped with Be. Micovic et al.(Micovic, et al., 1994) demonstrated that high quality epitaxial layers with abrupt doping profiles for the fabrication of graded index separate confinement heterostructure single quantum well lasers could be grown using solid source MBE with a graphite filament as the C source.

Although epitaxial growth of AlAs and AlGaAs allows for doping to very high levels, the free carrier concentration decreases following annealing,(Watanabe & Yamazaki, 1993) as is found in the GaAs epitaxial layers. Annealing above 600°C results in a decrease of the free hole concentration in AlGaAs doped with C above 10^{20} cm^{-3}. At the same time the lattice constant of the layers is found to increase.

Although GaAs, AlAs, and the alloy AlGaAs can be p^+-doped with C, C is reported to act as a donor in InAs. InAs is an attractive material for infrared light sources and detectors because of its direct bandgap of only 0.36 eV. Several groups have reported that residual C in epitaxial layers is responsible for the n-type behavior of their layers. Kamp et al.(Kamp, et al., 1990) grew InAs on GaAs by MOMBE with both TMIn and TEIn as source gases. SIMS measurements indicated that the C concentration increased by at least one order of magnitude while the free electron concentration increased by two orders of magnitude in the layers grown with TEIn. Therefore, they correlated the increase in free electron concentration with the increase in C. Chiu et al.(Chiu & Ditzenberger, 1990) identified a donor level seen in PL experiments at 20 meV in InAs grown by MOMBE using TMIn as due to C contamination.

Intentional doping of In As with C during epitaxial growth has not been successful. Using a CBr_4 as a C source in gas source MBE growth, free electron concentrations of 3×10^{17} cm^{-3} in InAs where similar growth conditions resulted in incorporation of C at a level of 1×10^{19} cm^{-3} in InGaAs. (Zhang, et al., 1993)

The ternary $In_xGa_{1-x}As$ is interesting with regard to the behavior of C since C has the opposite electrical behavior in the two pure compounds (GaAs and InAs). Ito et al.(Ito & Ishibashi, 1989) studied the behavior of C in InGaAs with the mole fraction of InAs varying from 0 to 1. The epitaxial layers were grown by MBE with C doping achieved using a graphite filament. Regulating the filament currents to attain a hole concentration in pure GaAs:C of 6×10^{19} cm^{-3}, they found that the carrier type switched from p-type to n-type when the InAs mole fraction was approximately 0.6 (Fig. 2.11). The maximum free electron concentration in InAs:C was 7×10^{17} cm^{-3}, which by low temperature Hall mobility measurements appears to be highly compensated.

Even a small amount of In content in InGaAs affects the free hole concentration. A small amount of In in GaAs:C layers grown by MOMBE expands the lattice constant so that the heavily C doped GaAs layers are lattice matched to the semi-insulating GaAs substrate. Akatsuka et al.(Akatsuka, et al., 1990) found that when the InAs mole fraction was greater than 0.1 the free hole concentration dropped as shown in Fig. 2.12. Similar results were obtained by Konagai et al.(Konagai, et al., 1990)

The alloy $In_{0.57}Ga_{0.43}As$ has attracted significant interest because it is lattice matched to InP. Kamp et al.(Kamp, et al., 1989) studied the effect of source gases on the free electron concentration of MOMBE grown $In_{0.53}Ga_{0.47}As$ layers on InP substrates. Use of TMGa was found to result in C concentrations of $3\text{-}4\times10^{18}$ cm^{-3} which was an order of magnitude higher than the C concentration in layers grown with TEGa. The free electron concentrations in these layers was 5×10^{17} cm^{-3} and 7×10^{16} cm^{-3} respectively. Switching the In source gas from TMIn to TEIn did not have a significant effect on either the C concentration or the free electron concentration. Abernathy et al.(Abernathy, et al., 1990a) were able to dope InGaAs p-type with carbon and achieved hole concentrations of 1×10^{19} cm^{-3} when elemental In, TMG and elemental As were used for MOMBE growth. Using a resistively heated graphite filament as a source of C during conventional MBE

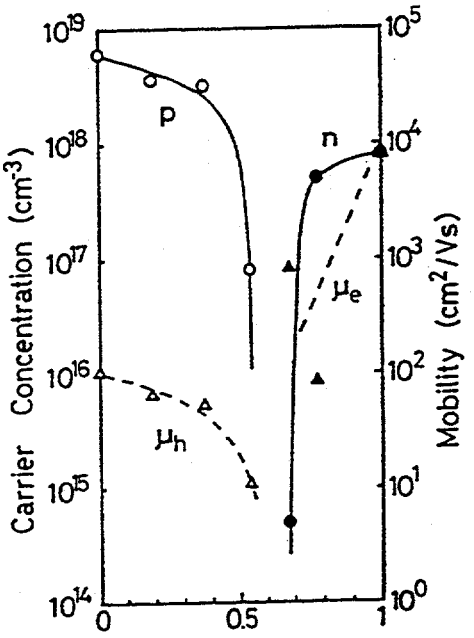

Fig. 2.11 Dependence of free carrier concentration and mobility on the InAs mole fraction in (In,Ga)As sytems grown by MBE.(Ito & Ishibashi, 1989)

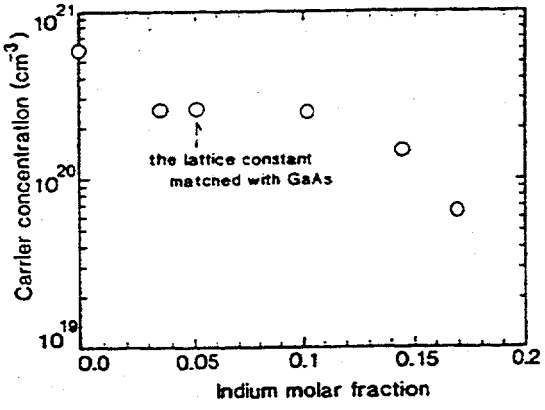

Fig. 2.12. The hole concentration in C doped InGaAs MOMBE layers as a function of the indium molar fraction.(Akatsuka, et al., 1990)

growth, free hole concentrations as high as 4.4×10^{19} cm^{-3} were obtained in $In_{0.53}Ga_{0.47}As$.(Zhang, et al., 1993)

A post growth annealing step has been shown to increase the free electron concentration in MOCVD and gas source MBE grown InGaAs layers doped with C. Stockman et al.(Stockman, et al., 1992a) grew C doped InGaAs MOCVD layers with a free hole concentration of 1.7×10^{18} cm^{-3} and a room temperature Hall mobility of 82 cm^2 V^{-1} s^{-1}. A 5 minute anneal at 400°C in a H_2 free environment increased the free hole concentration to 1×10^{19} cm^{-3} with a Hall mobility of 70 cm^2 V^{-1} s^{-1}. Chin et al.(Chin, et al., 1991) found similar results for C doped layers grown by gas source MBE using CCl_4 as the C source. As grown layers had a free hole concentration of 3×10^{18} cm^{-3}. Annealing at 420°C for 5 minutes increased the hole concentration to 3×10^{19} cm^{-3}. The increase in hole concentration in both cases is likely to be a result of eliminating H which passivates the C acceptors in the epitaxial layers.

Pearton et al.(Pearton, et al., 1990) studied C implantation in $In_{0.53}Ga_{0.47}As$ and $Al_{0.52}In_{0.48}As$ grown by MOCVD on InP. The C was implanted at an energy of 40 keV and with doses ranging from 5×10^{12} to 5×10^{14} cm^{-2}. C only implantation did not result in any change in the electrical characteristics of either alloy. Co-implants of Ga, As, Al, or Ar created p-type layers in both samples. C+Ga co-implantation into InGaAs and C+As in AlInAs created the highest activation. Even the As co-implant created a p-type layer in both compounds (see Fig. 2.13).

Because of their ability to emit radiation in the visible portion of the electromagnetic spectrum, GaP and GaInP are important semiconductor materials for optical devices such as light emitting diodes and laser diodes. Very little work on doping with C in the phosphide based compounds has been reported. In GaP, C acts as a p-type dopant. The use of methyl and ethyl metalorganic precursors as carbon doping sources for MOMBE growth of GaP on GaP substrates was studied by de Lyon et al.(de Lyon, et al., 1991b) Hole concentrations as high as 1.8×10^{20} cm^{-3} were obtained in epitaxial

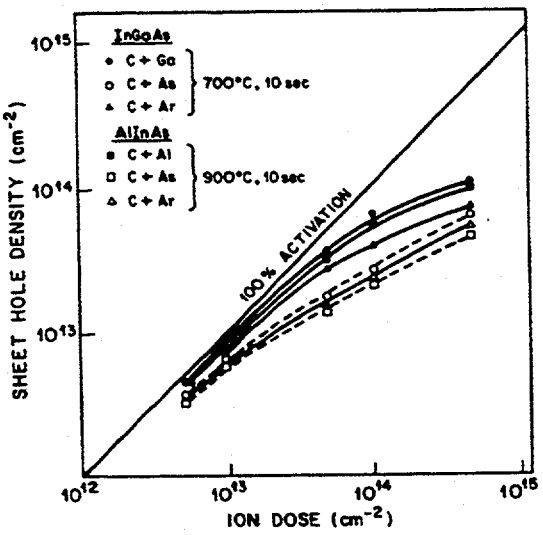

Fig. 2.13. Sheet hole densities obtained in C+Ga, C+Ar,or C+As implants in InGaAs or C+Al, C+Ar or C+As in AlInAs as a function of ion dose of each species.(Pearton, et al., 1990)

growth of GaP using TMGa as the precursor. SIMS measurements indicated that the atomic concentration of C was also 1.8×10^{20} cm^{-3} implying 100% electrical activity of C within the error of Hall effect and SIMS measurements. Similar success was achieved by using CCl_4 as a C source during growth by MBE.(de Lyon, et al., 1991a) A hole concentration of 1×10^{20} cm^{-3} with a Hall mobility of 25 cm^2 V^{-1} s^{-1} at room temperature was attained.

Similar to the ternary InGaAs, GaP can be readily doped p-type while C incorporation into InP is difficult and results in n-type layers. C incorporation into $Ga_xIn_{1-x}P$ epitaxial layers was found to depend on the In content. A series of GaInP films were grown by MOMBE (T_g = 560°C) with the mole fraction of InP increasing from 0 to 8%.(de Lyon, et al., 1991b) As seen in Fig. 2.14, as the InP mole fraction exceeds about

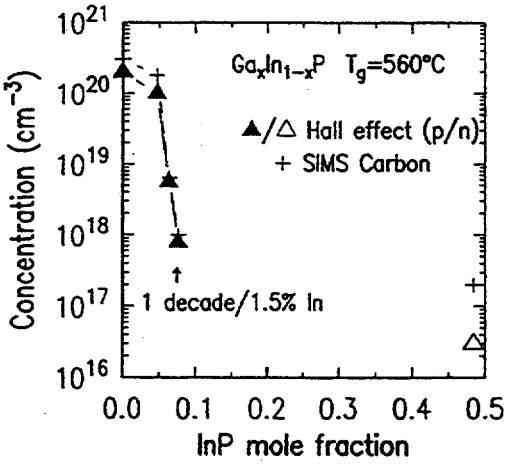

Fig. 2.14. Dependence of hole concentration determined from Hall effect and atomic concentration measured with SIMS on InP mole fraction in films of GaInP grown by MOMBE.(de Lyon, et al., 1991b)

5%, the hole concentration drops rapidly. SIMS measurements indicate that the carbon is not being incorporated into the samples.

Doping of $Ga_{0.51}In_{0.49}P$ (lattice matched to GaAs) with C during epitaxial growth is also difficult. Although carbon was incorporated during MOMBE growth at a temperature of 500°C as shown by SIMS measurements, the net electron concentration N_D-N_A remained the same.(de Lyon, et al., 1991b) The C concentration varied from $<2\times10^{17}$ cm^{-3} (detection limit of SIMS) for samples grown at 560°C to 5×10^{18} cm^{-3} when grown at 500°C. However in both of these samples, N_D-N_A = 3×10^{17} cm^{-3}. Kibbler et al.(Kibbler, et al., 1991) were also unsuccessful in doping $Ga_{0.5}In_{0.5}P$ with C during MOCVD growth using CCl_4 as a C source. Hole concentrations were less than 1×10^{17} cm^{-3} for layers grown at temperature between 600°C and 700°C. Chin et al.(Chin, et al., 1991) found that a post growth anneal significantly increases the free hole

concentration in GaInP. Epitaxial layers grown by MOMBE using CCl_4 as a C source were weakly p-type as grown ($p=2\times10^{17}$ cm^{-3}). Annealing at 550°C for 5 minutes increased the free hole concentration to 5×10^{18} cm^{-3}.

AlInP and AlGaInP are of interest as cladding layer materials for visible semiconductor lasers. Carbon could be incorporated up to a level of 1×10^{19} cm^{-3} as measured by SIMS in AlInP.(de Lyon, et al., 1991b) However the layers were highly resistive.

To summarize, the doping behavior of C varies widely in the III-V compound semiconductors and their alloys. In GaAs, AlAs, and GaP, C is an effective p-type dopant with a low diffusion coefficient. It can be incorporated during epitaxial growth or by ion implantation. Doping during epitaxial growth results in nearly 100% of the C atoms residing on As lattice positions and contributing a free hole. Ultra-high doping levels have been achieved in all three of these compounds. In the alloy, AlGaAs, C is also and efficient p-type dopant. On the other hand, in InP and InAs C acts as an n-type dopant. C is difficult to incorporate in these compounds and when it does incorporate only a very small percentage of the C present contributes a free electron. The behavior of C in the ternary alloys, GaInAs and GaInP, depends on the composition. As the In content increases in these alloys C switches from a p-type dopant to an n-type dopant.

3. Experimental Procedures

3.1 Sample preparation

GaAs substrates used for all of the implantation studies in this thesis are (100) oriented wafers cut from a boule grown by the liquid encapsulated Czochralski technique. The substrates are semi-insulating and are obtained commercially. The background C level in the substrates ranges from 1×10^{15} cm^{-3} to 1×10^{16} cm^{-3}. InP substrates were obtained commercially from CrystaComm Inc. They are semi-insulating due to doping with Fe. They are (100) oriented.

All substrates are solvent cleaned at several instances during the experiment including prior to implantation and prior to annealing. Solvent cleaning entails the following steps. Samples are boiled in trichloroethane, acetone, and methanol for five minutes each. They are then cooled and rinsed in methanol and dried with flowing N_2. Immediately prior to implantation, the GaAs substrates are etched with concentrated HCl, rinsed with deionized water and blown dry with N_2.

Partitioning of the samples is accomplished by cleaving along the (110) plane using a diamond scribe.

Etching of GaAs is performed using a mixture of H_2SO_4:H_2O_2:H_2O. Depending on the rate of etching desired, the composition varies from 3:1:1 to 3:1:50. Following etching, samples are rinsed in deionized water and dried in flowing N_2.

For lapping and polishing, samples are mounted on a hand held polishing block using wax. Al_2O_3 powder with a grit size of 3 μm is used with deionized water on a glass plate for lapping both GaAs and InP samples. GaAs is polished using a 1:1:1 mixture of Syton:H_2O_2:H_2O. Syton is a colloidal suspension of SiO_2. InP is polished using 0.1 μm Al_2O_3 in deionized water on a polishing cloth. The surface of the InP is not specular

following this procedure, however, the surface is sufficiently polished for infrared transmission experiments. After lapping and polishing samples are removed from the polishing block and solvent cleaned.

3.2 Ion implantation

Ion implantation is performed in a Varian Extrion machine with a modified endstation which allows for cooling of samples with liquid nitrogen. For singly ionized species, energies from 20 keV to 200 keV can be implanted. Energies up to 400 keV can be obtained for doubly ionized species. All samples are tilted 7° from the normal during implantation to prevent channeling. Samples are mounted onto Al plates which are then screwed onto the endstation paddle. Two methods are used: in the first, samples are mounted with wax and a dot of silver paint on the corner to establish electrical contact to the plate. In the second method, several springs hold the sample in place, and In foil is used between the Al plate and the substrate to maintain good thermal contact.

Samples are implanted at either room temperature or at approximately 100 K. Low temperatures are attained by filling the hollow paddle with liquid nitrogen. The temperature is measured with a type K thermocouple on the surface of the paddle next to the Al mounting plate. When samples are implanted at low temperatures, the samples are held onto the Al plate with springs since wax does not perform well at low temperatures due to the mismatch in thermal coefficients. The dose rate is carefully controlled in all implantations. In general, the beam current is kept below 50 μamps during implantation.

The important considerations when characterizing samples doped by ion implantion are the concentration profile of the implanted dopant and the radiation damage created during implantation. Fortunately, at least in the first case, the physical principles governing the implantation process are well studied and well understood. Both the

concentration profile and the damage profile can be derived when the mechanisms responsible for stopping the implanted ions are known. Implanted ions are slowed and stopped by either inelastic or elastic collisions. Inelastic collisions, also known as electronic stopping occur when the implanted ion loses energy to the electrons in the substrate either by ionization or excitation of the host atom. Elastic collisions (nuclear stopping) are a result of collisions between the incoming ion and the nuclei of the substrate. A fraction of the kinetic energy of the incoming ion is transferred to the nuclei.

Nuclear stopping is generally modeled as a collision between two point masses. Consider the collision of two hard spheres shown in Fig. 3.1, each of radius r_0. The incident sphere has a mass of M_1 and energy E_0, and the struck sphere has mass M_2 and is initially at rest. The distance between the two center of masses is p which is called the impact parameter. From conservation of momentum and energy, the energy transferred to M_2, E_2, and the angle of scattering, θ, can be determined by

$$E_2 = E_0\left\{1-\left[\frac{\left(M_2^2 - M_1^2\sin^2\theta\right)^{1/2} + M_1\cos\theta}{(M_1+M_2)}\right]^2\right\} \qquad [3.1]$$

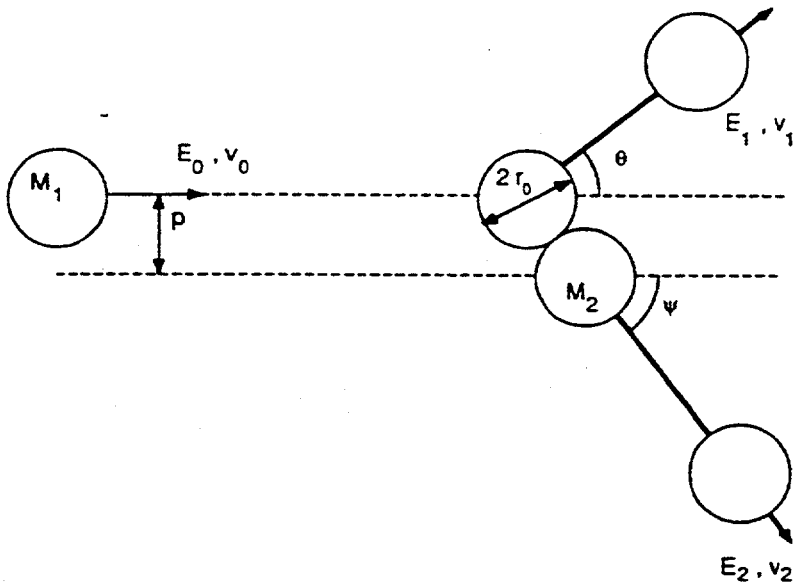

Figure 3.1. The geometry of a collision between two point masses.

In ion implantation, a flux of ions is incident upon the substrate. Only ions with $p<2r_0$ will collide with a particular atom. The area $(2r_0)^2$ defines a total collision cross-section. A flux of ions, each with impact parameter p will be deflected through an angle θ, into a cone of half angle θ about the center of the struck atom. Similarly, ions incident at impact parameter $p+\delta p$ will be uniformly deflected into a cone of half angle $\theta+\delta\theta$ as shown in Fig. 3.2. The plane area defined by the radii p and $p+\delta p$ determines which ions are scattered between angle θ and $\theta+\delta\theta$. This area is known as the differential scattering cross section, $d\sigma$, and is given by

$$d\sigma = 2\pi p \delta p \qquad [3.2]$$

for scattering between impact parameters of p and $p+\delta p$ and scattering angles of θ and $\theta+\delta\theta$.

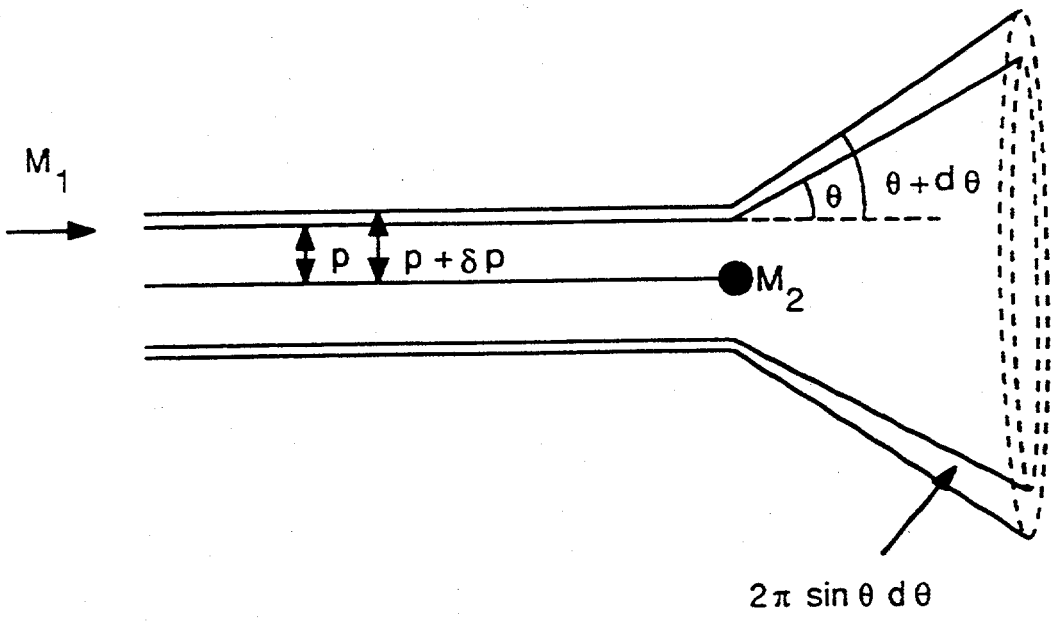

Figure 3.2. Illustration of the differential scattering cross-section.

The energy transferred to the substrate atom, T (=E_2) is determined by the incident energy and the scattering angle. The energy transfer can be calculated in terms of the impact parameter, p, by use of the following equation:

$$p^2 = 4r_0^2\left(1-\frac{T}{T_m}\right) \qquad [3.3]$$

where T_m is the maximum energy which can be transferred (θ=180°) given by

$$T_m = \frac{4M_1M_2}{(M_1+M_2)^2}E_0. \qquad [3.4]$$

This analysis assumes that the collision between the implanted ion and the substrate atom can be modeled as a collision between two point masses which can be described as hard spheres. In this model the interatomic forces and potentials are replaced by a step function which rises from zero at the hard sphere radius. However, the Coulomb force between the atoms extends to infinity so the atomic collision will occur over all values of the interatomic separation r and not only at $r=2r_0$. Because of the infinite extent of the Coulomb potential, the substrate atom moves as soon as the incident particle moves toward it. Therefore both the incident and struck atoms move along constantly changing trajectories and not with the rectilinear motion described above. In this case, the quantitative evaluation of scattering angles for given initial conditions (energy and impact parameter) is only possible if the form of the force and potential laws are known analytically. Even then in only a few special cases of an assumed potential can an exact analytic solution be obtained.

In both the hard sphere model and more realistic models, the energy lost (transferred) is determined for individual collisions between isolated atoms. In ion implantation, the moving ion experiences a succession of collisions along its path. Each collision results in a loss of energy and a change in direction of the incident ion. The collisions can be averaged statistically and a mean rate of energy loss per unit path length calculated. If the energy lost by an ion in a single collision is T, the average loss of energy in a collision is

$$\overline{T} = \frac{\int_0^{T_m} T d\sigma}{\int_0^{T_m} d\sigma}. \qquad [3.5]$$

Assuming N target atoms per unit volume randomly spatially distributed relative to the primary ion, the total number of atomic encounters by the ion is $N\int_0^{T_m} d\sigma$ in unit distance travelled. Thus the mean rate of energy loss per unit path length is

$$\frac{dE}{dx} = N\int_0^{T_m} T d\sigma. \qquad [3.6]$$

As well as losing energy in nuclear collisions, the incident ion loses energy in inelastic collisions. Energy is lost due to electron excitations and ionizations which occur in the substrate atoms as the ion passes. This energy loss can only be calculated using a quantum mechanical approach. It can be qualitatively understood as the energy transferred from the incident ion to the substrate atom which must exceed the minimum energy for electronic excitation.

The stopping cross section S of a solid is given by

$$S = \frac{1}{N}\left(\frac{dE}{dx}\right)_{e,n} \left[eVcm^2\right]. \qquad [3.7]$$

where the subscripts, e and n, refer to electronic and nuclear stopping powers respectively. The relative importance of the two stopping mechanisms is determined by the energy and mass of the implanted ions and the mass and atomic density of the solid. Typical implantation energies fall in the range where nuclear stopping is dominant.

Once the stopping cross-section is known, the total path length and range of the implanted ions can be determined. The total range, R, depends on the initial incident ion energy and is given by:

$$R = \frac{1}{N}\int_0^E \frac{dE}{S_n(E) + S_e(E)}. \qquad [3.8]$$

The projected range R_p is the projection of R in the incident direction of the ion beam. Lindhard, Scharff, and Schiott(Lindhard, et al., 1963) were the first to show theoretically

that the ion range can be described by a Gaussian distribution. The ion concentration profile as a function of distance from the surface of the substrate, x, is given by

$$N(x) = \frac{\phi}{\sqrt{(2\pi)}\Delta R_p} \exp - \frac{(x - R_p)^2}{2\Delta R_p^2}. \qquad [3.9]$$

This equation represents a Gaussian distribution where ϕ is the implant dose and ΔR_p is the standard deviation. The maximum dopant concentration occurs at $x=R_p$ and is given by

$$N_{max} = \frac{\phi}{\sqrt{(2\pi)}\Delta R_p}. \qquad [3.10]$$

More sophisticated models of the distribution have been evaluated by using joined Gaussians or by taking into account higher order moments of the standard deviation. The Pearson IV distribution uses four moments to calculate the profile. They are the projected range, straggling, skewness and kurtosis. The skewness and kurtosis affect the symmetry and tail shape of the distribution respectively. These two moments are, in general, determined empirically. The theorectical ion profiles presented in this thesis are calculated using a Pearson IV distribution generated by the Profile Code.(I. S. Corporation)

The theoretical predictions for ion range are only valid in amorphous material. In general, most implantations are performed in crystalline materials. Single crystal materials have relatively open structures. Channeling occurs when the implanted ion travels along a row of lattice sites. Very few nuclear collisions occur, and the only energy losses are due to electronic stopping. The implanted ions therefore penetrate much deeper into the substrate than if they were not channeled.

Once the ion enters a channel it is "guided" or "steered" by the repelling potential of the row of atoms. If the angle of entry is below a critical angle, the implanted ion will be confined to a channel (Fig. 3.3). The range of the ion is then directly proportional to the velocity of the ion. The critical angle can be determined by dividing the incoming energy of the ion into components which are perpendicular to ($E_\perp$) and parallel to ($E_\parallel$) the

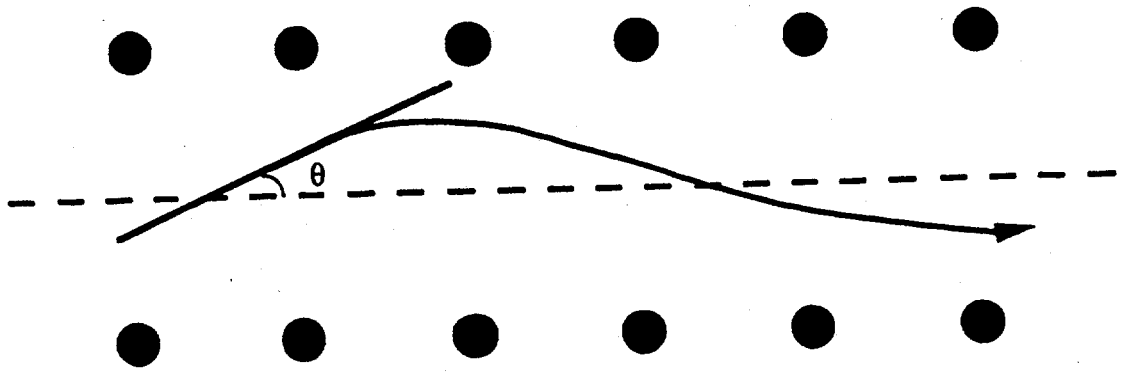

Figure 3.3. Channeling of an implanted ion.

channel axis. If $E_{\perp} < V(r)$, the repelling potential of the atomic chain, the ion will remain in the channel. The critical angle in GaAs lies between 1° and 10° for the major crystal axes and typical implant energies. The principal channelling direction in zinc blende cubic cyrstals are <100>, <111>, and <110>.

Complete channelling is never achieved due to randomization of the beam caused by surface scattering. Ions can be channeled immediately upon entering the crystal or scattered into a channel after undergoing a few nuclear collisions. Channeling can be minimized by orienting crystals in a nonchanneling direction or by implanting through thin deposited amorphous layers which randomize the beam. At higher doses damage created by the implanted ions will randomize the beam.

3.3 Annealing

Thermal annealing is required following implantation for two reasons, to repair the radiation damage created during implantation and to activate the implanted ions by short range diffusion of the ion to a lattice position. Radiation damage occurs as the implanted ion undergoes nuclear collisions with substrate atoms which can displace the host atoms from their lattice position creating Frenkel defects. The recoiling host atoms may have enough energy to displace other lattice atoms. Along the track of the implanted ion, a damage cascade is created. When the damage clusters overlap throughout the volume of the substrate, an amorphous layer is created.

Ions which are substantially lighter than the atomic mass of the constitutents of the substrate only cause a small amount of damage. The light ions are initially slowed by electronic stopping which causes little damage to the lattice. At the end of their range they are stopped by nuclear collisions. The possiblity of scattering through large angle after a nuclear collision creates a particularly tortuous track for a light ion. Nearly all the damage caused by the implanted ion of small atomic weight occurs at the end of its range. On the other hand, heavy ions create considerable damage along their entire path. They displace target atoms from the surface inwards due to a relatively higher number of nuclear collisions. Recoiling substrate nuclei can also displace other nucli resulting in considerable lattice damage in a small volume, i.e., damage clusters.

For both light and heavy ions the volume of crystal in which the energy of the implanted ion is deposited is larger than the volume in which damage occurs. Near the end of its path in the crystal, the ion no longer has enough energy to displace substrate atoms. Therefore, the range of the damage does not coincide precisely with the ion profile in the solid with the peak of the damage occurring at 0.7 to 0.8 R_p.

The simplest defects created during implantation are Frenkel pairs consisting of a vacancy and an interstitial. More complex defects can also be formed; di-vacancies,

trivacancies, clusters of vacancies and clusters of interstitials. Vacancies and interstitials can have various charge states and may form complexes with impurities thus affecting diffusion and electrical characteristics of the implanted layer. Line defects will occur due to the accumulation of point defects. Dislocations can grow during annealing into the undamaged part of the crystal.

Damage accumulation during implantation, damage recovery and dopant activation are sensitive to implantation parameters. Self annealing during implantation readily occurs in GaAs. The amount of damage and therefore the crystalline to amorphous transition in implanted GaAs has been shown to strongly depend on the substrate temperature during implantation.(Haynes & Holland, 1991a) A study of GaAs substrates implanted with 100 keV Si^+ ions demonstrated the existence of a distinct transition temperature above which the substrate did not become amorphous during implantation. The transition temperature was found to be very near room temperature. The amount of damage created in the implanted GaAs has been shown to also depend on the dose rate during implantation.(Haynes & Holland, 1991b)

The damage caused by implantation consists of either amorphous layers or extended crystalline defects (dislocation loops and stacking faults). In GaAs several stages of damage removal exist. At fairly low temperatures, 150 to 200°C, the amorphous layers recrystallize however the layers are highly defective and contain twins, stacking faults and other extended defects. From 400 to 500°C, the extended defects begin to disappear but leave behind a high density of dislocation loops. Above 700°C, the dislocation loops expand and eventually annihilate by combining with other dislocations and the remaining point defects anneal out.

The temperatures required to repair the radiation damage are high enough (>600°C) to cause dissociation of the group V element. Therefore, measures must be taken to prevent surface degradation of the implanted layers. Several methods can be used. Encapsulating dielectric layers such as SiO_2 and Si_3N_4 are often used to protect the

surface. Si_3N_4 often suffers from cracking and pealing. SiO_2 has a significantly different coefficient of thermal expansion and therefore near surface strains result which can lead to significant enhancement of diffusion in the implanted layers. Both layers cause outdiffusion of both Ga and As atoms during annealing. In these experiments either the proximity method or an overpressure of As is used during annealing.

Samples are annealed by either rapid thermal annealing (RTA) or furnace annealing (FA). Activation of implanted dopants takes place within the first 10 seconds at high temperatures. Therefore any additional time spent above this temperature can result in diffusion of the implanted dopants and further detrimental surface degradation. For this reason, the RTA was developed. In this experiment, samples were annealed for 10 seconds in a Heatpulse 210 RTA system. GaAs samples are annealed at 950° C. InP samples are annealed at 850° C. Flowing N_2 or Ar is used as the annealing ambient. To protect the surface, the proximity method is used. Samples are placed on a 4 inch Si wafer within the chamber, implanted side up. Another piece of clean GaAs or InP is then placed on top of the sample. This method creates an As or P overpressure inhibiting loss of the group V element during annealing. The temperature within the RTA is measured by a type K thermocouple embedded in the 4 inch Si wafer.

Furnace annealing is performed in a horizontal tube furnace. GaAs samples annealed in the furnace are sealed in an ampoule with solid As. The amount of solid As required is calculated assuming that As_4 is the dominant species in the gaseous phase and that 1 atm of As_4 overpressure will be present in the ampoule at the annealing temperature. The quartz ampoule is cleaned and etched using a 10% HF solution, rinsed with DI water and then dried with flowing N_2. The samples and As are solvent cleaned and etched in HCl before loading into the ampoule. The ampoule is then purged with Ar and sealed under vacuum. Typically, 3 purge cycles are used to ensure cleanliness of the ampoule. The ampoules are typically at a vacuum of 10^{-5} Torr when sealed. Sealing is accomplished with a hydrogen torch. Samples are then loaded into the furnace at the

annealing temperature. N_2 is flowing through the quartz furnace tube during annealing. Following annealing the ampoule is slowly pulled from the furnace to allow the As to condense on the end of the ampoule opposite the samples. When the samples are removed from the ampoule they are etched in 10% HF to remove any As oxide which may have deposited on the surface.

3.4 Characterization techniques

3.4.1 Rutherford backscattering

In Rutherford backscattering (RBS), a collimated beam of He ions with energies in the MeV range are incident on the sample. The backscattered ions are collected and their energy is measured by a solid state detector to give the RBS spectra. RBS can be used to determine the type and quantity of elements present in the crystal and measure the depth of individual layers in multilayered structures. No standards are required for any of these analyses. Three important physical concepts are involved in RBS: the kinematic scattering factor, the scattering cross section, and the energy loss.

The kinematic scattering factor, K, is given by the energy of the scattered particle, E_s, divided by the energy of the incident particle, E_i,

$$K = \frac{E_s}{E_i}. \qquad [3.11]$$

The energy of the scattered particle is a function of the scattering angle, the particle mass and the target mass. K can be derived from conservation of energy and momentum for a projectile of mass M_1 and scattering from target M_2 at a laboratory angle θ (Fig. 3.4) and express as:

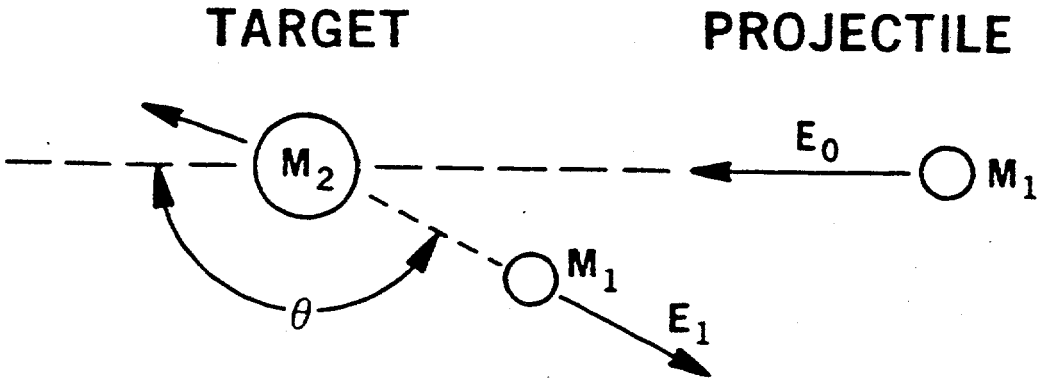

Figure 3.4. Scattering of an incident particle in Rutherford backscattering spectrometry.

$$K = \left[\frac{\left(M_2^2 - M_1^2 \sin^2 \theta\right)^{1/2} + M_1 \cos\theta}{\left(M_1 + M_2\right)} \right]^2 . \qquad [3.12]$$

In RBS experiments, the scattering angle and the particle mass are known, hence the different elements in the target can be identified by measuring the energies of the scattered particles.

Quantitative information about the target material can be obtained through the scattering cross section. The scattering cross section is the probablility that a particle will be elastically scattered by a target atom in a unit solid angle. The scattering cross section can be calculated by assuming a Coulombic reaction between the incident ion and the substrate atom. Once the scattering cross section is known, the atomic fraction of an element in a target can be calculated from the relation,

$$A = \frac{d\sigma}{d\Omega} Q N t \Delta\Omega \qquad [3.13]$$

where A is the number of detected backscattered particles, Q is the total number of incident particles, Nt is the amount of target material in atoms per unit area, and $d\sigma/d\Omega$ is the scattering cross section.

The energy lost by the backscattered particle provides depth information. As the energetic ion travels through the crystal it loses energy in nuclear and electronic scattering as described above. In RBS experiments, electronic stopping is the principal mechanism. The energy difference between particles scattered from the target surface and those scattered at a depth t below the surface is given by

$$\Delta E = KE_0 - E_1 = N[S]t. \qquad [3.14]$$

[S] is the energy loss factor which can be calculated. If the energy loss factor is known, the depth, t, can then be determined.

RBS can also be used as a measure of the crystalline perfection of a material. Crystalline materials have open channels along specific directions. If the ion is incident on one of these channels then the probability of a backscattering event occurring is much smaller than in an amorphous material. As described in the section on implantation, there is a maximum incident angle, the critical angle, where the incident particle can be steered by the atomic rows. If the incident angle is less than the critical angle then the incident particle is channeled and has a very low probability of scattering as it travels along the channel. Figure 3.5 is a schematic of the energy spectra for a beam aligned with a symmetry direction of the crystal and in a random direction.

The presence of defects causes the ion to be dechanneled and greatly increases the probablility of backscattering. Point defects, dislocations, precipitates and amorphous clustsers present in the crystal will result in higher backscattered counts.

Channeling Rutherford backscattering is an excellent technique for characterizing the radiation damage caused by implantation. In these experiments, it is also used to measure the residual damage in the implanted layers following annealing. Channeling Rutherford backscattering spectra are taken along the <110>, and <111> directions in the

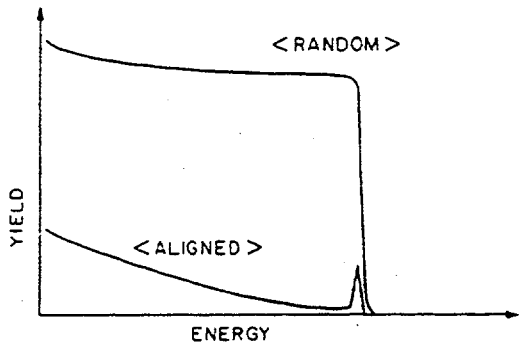

Figure 3.5 Schematic of the energy spectra for a beam aligned with a symmetry direction of the crystal and in a random direction.

crystal. Additional spectra are taken in a random direction from each sample. A random direction denotes a beam misaligned with any major crystallographic direction as is a good representation of the spectrum from an amorphous solid. A 1.8 MeV He^+ ion beam is used in all experiments.

3.4.2 Electrical measurements

For electrical measurements contacts have to be formed on the samples. For GaAs:C, InZn alloyed contacts are created by annealing at 250°C for 10 minutes in flowing N_2. For InP, In alloyed contacts are formed by annealing at 200°C for 10 minutes in flowing N_2. Copper wires with In coated tips are then pressed onto the contacts. Carrier concentration, mobility and resistivity are determined by van der Pauw geometry

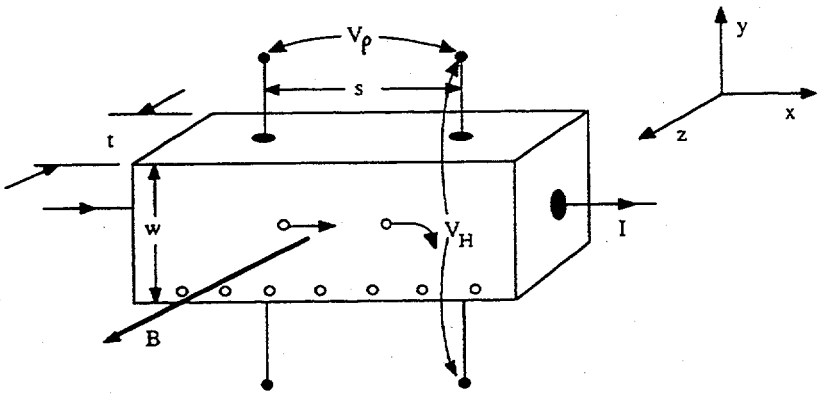

Figure 3.5. Geometry of a Hall effect measurement.

Hall effect measurements. All measurements are taken using a magnetic induction of 3kG. The current is chosen so that the voltage across the contacts is between 5 and 50 mV. Variable temperature Hall effect measurements are also made using the same configuration.

The Hall effect is a consequence of the Lorentz force which acts on electric charges moving in an electric field. Hall effect measurements provide information on the carrier concentration, type of carrier, and resistivity. From measurement of the resistivity and the carrier concentration, mobilities can be derived.

If electrons are moving with a velocity, v in the positive x direction then a magnetic field, **B** along the z axis displaces the electrons in the y-direction. (Fig. 3.5) This displacement sets up an electric field $\mathbf{E_H}$ in the material which in equilibrium balances the Lorentz force.

$$q\left(\bar{v}\times\bar{B}\right)=\overline{q\,E_H} \qquad [3.15]$$

The resulting electric field (for holes) is given by

$$E_H = v_x B_z = \frac{J_x B_z}{qp} = R_H J_x B_z \qquad [3.16]$$

where J_X is the current density, p is the concentration of free holes and q is the electric charge. The Hall coefficient is given by

$$R_H = \frac{1}{qp}. \qquad [3.17]$$

Hall measurements taken here are performed in the van der Pauw configuration. Van der Pauw applied conformal mapping to an arbitrarily shaped sample of constant thickness. Van der Pauw's method allows the resistivity to be determined with only four point contacts on the surface of the sample if the following conditions are met: 1) the contacts are at the circumference of the sample, 2) the contacts are sufficiently small, 3) the sample is uniformly thick, and 4) the surface of the sample is singly connected, i.e., the sample does not contain any isolated holes. The resistivity is given by

$$\rho = \frac{\pi t}{\ln 2} \frac{\left(R_{12,34} + R_{23,41}\right)}{2} F. \qquad [3.18]$$

The resistance is defined as $R_{12,34} = V_{34}/I_{12}$ where the current I_{12} enters the sample through contact 1 and leaves through contact 2 and $V_{34} = V_3 - V_4$. (Fig. 3.6) F is only a weak function of the ratio $R_{12,34}/R_{23,41}$. as shown in Fig. 3.7.

Hall effect measures the total concentration of free carriers throughout the entire sample. For implantation experiments, the carrier concentration as a function of depth is also of interest. For these measurements an electrochemical capacitance-voltage (C-V) profiler is used. In this technique an electrolyte is used to both etch the substrate and to form a Schottky contact. The electrochemical cell used for these measurements is shown in Fig. 3.8. In addition to the semiconductor (working) electrode, three other electrodes are used in the cell. The platinum electrode is used for the C-V measurement; the carbon (counter) electrode is used to complete the circuit for etching; and the saturated calomel electrode is used as a reference against which the equilibrium (rest) and overpotential can be measured. The working electrode (semiconductor) is etched by passing a current between it and the counter electrode. When no current is flowing between the counter

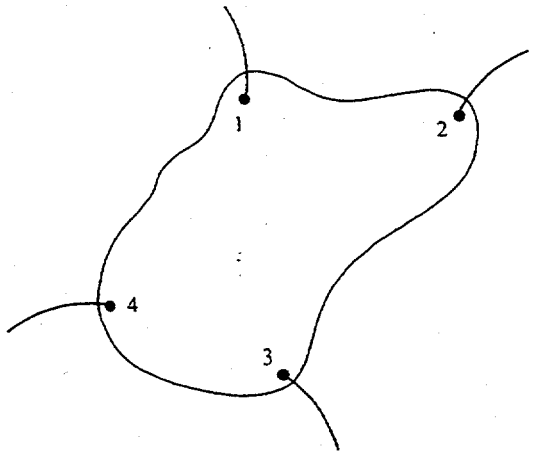

Figure 3.6. Sample geometry for the Van der Pauw method.

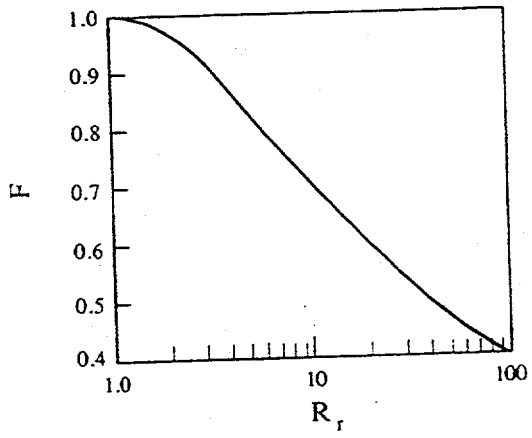

Figure 3.7. The dependence of F on the ratio $R_{12,34}/R_{23,41}$.

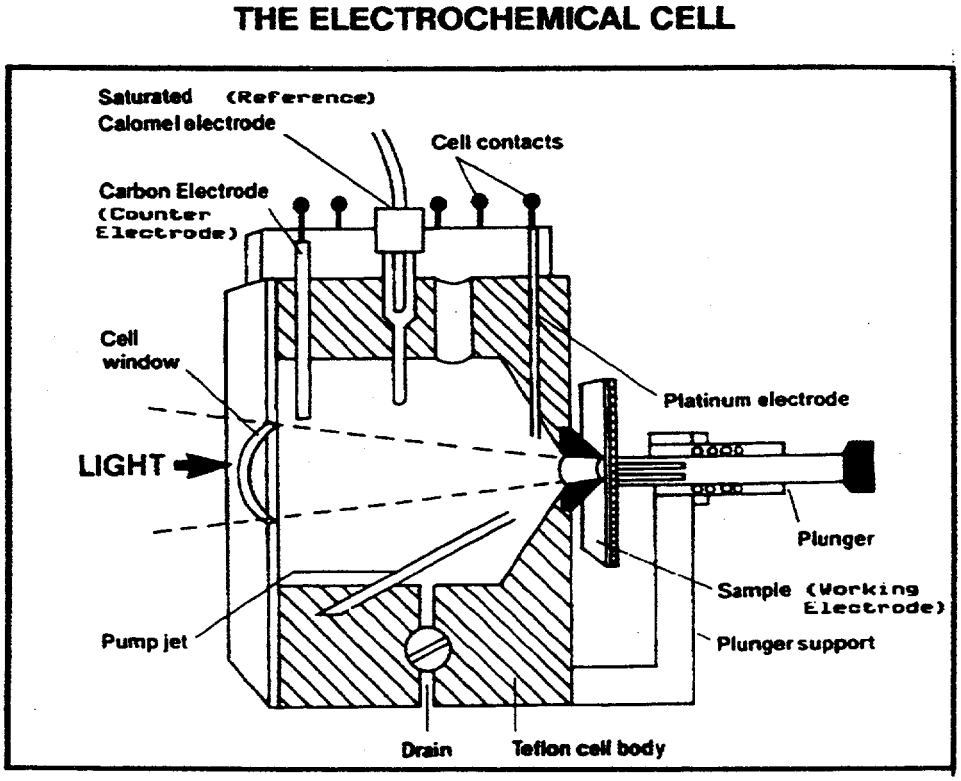

Figure 3.8. Schematic of the electrochemical cell for capacitance-voltage measurements.

and working electrodes, the measured potential is referred to as the rest potential which is the equilibrium or base point in the system. From measurement of the rest potential with and without illumination the semiconductor type can be determined. During illumination, eletron-hole pairs are created in the depleted region and swept out in opposite directions by the electric field. As p and n type materials produce photovoltages of opposite sign, they can be differentiated. For p-type material the electrode potential will become more positive and conversely for n-type material it will become more negative.

If the electrolyte used is fairly concentrated (0.1M), the semiconductor/electrolyte interface behaves as a Schottky junction and the equations for depletion width and capacitance can be used. To determine the carrier concentration, the semiconductor is reverse biased and the carrier density at the edge of the depletion layer is obtained from this equation:

$$N = \frac{1}{q\varepsilon_r\varepsilon_o A^2}\frac{C^3}{dC/dV} \qquad [3.19]$$

For n-type semiconductors the capacitance of the depletion layer will decrease as the semiconductor is made more positive than its rest potential. Consequently dC/dV and N will be negative. For p-type semiconductors the capacitance of the depletion layer will decrease as the semiconductor is made more negative than its rest potential. dC/dV and N will be positive.

To determine the carrier concentration experimentally, C and dC/dV are obtained by using a slowly modulated high frequency voltage. The electrochemical cell along with a reference resistor and various stray admittances form a potential divider (Fig. 3.9). The semiconductor/electrolyte interface is represented by its equivalent parallel circuit of a capacitor and resistor. The capacitor is the depletion layer capacitance and the resistor represents leakage current.

A composite drive voltage (carrier + modulator + DC bias) is applied across the potential divider (Y1 + Y2). The output signal is measured across Y1. For good signal to

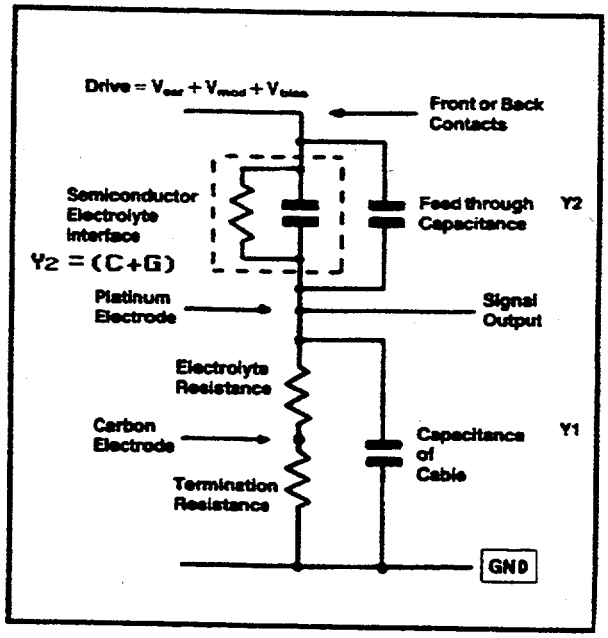

Figure 3.9. Potential divider circuit for the electrochemical capacitance-voltage measurement.

noise ratio, the resistor is chosen so that Y1 is approximately equal to Y2. The various stray admittances are determined experimentally. Because all of the admittances are independent of potential, dC/dV can be extracted from the amplitude and phase of the modulated component of the waveform, and N can be readily calculated.

Etching of the semiconductor is carried out by the appropriate choice of electrode potential. For p-type material, the forward bias region is used. That is, the working electrode must be more positive than the rest potential. For n-type material, reverse bias is used, and the sample is illuminated. The etching rate is proportional to the current flowing between the working and counter electrodes. The amount of material removed (the etch depth, W_r) is given by Faraday's law of electrolysis

$$W_r = \frac{M}{zF\rho A}\int_0^t I dt. \qquad [3.20]$$

The depth at which the carrier concentration is measured is given by the sum of the etch depth and the depletion depth.

$$W_{tot} = W_r + W_d \qquad \text{where} \qquad W_d = \frac{\varepsilon_r \varepsilon_o A}{C}. \qquad [3.21]$$

Electrochemical C-V profiles presented in this thesis are performed on a BioRad Polaron instrument. Ohmic contacts are the same as those described previously. The electrolytic solution is 0.2M NaOH with EDTA. To etch the sample, the voltage applied is chosen so that the etching current is approximately .3 mA cm^{-2}. Typically, C-V measurements are taken every 0.01 μm. The bias voltage for measurement is chosen from the region of the C-V curve which is well behaved. That is, $1/C^2$ vs. V is a straight line.

3.4.3 Raman spectroscopy

Raman scattering occurs when photons are scattered with the emission or absorption of phonons. Conservation of energy and crystal momentum in a one phonon process requires

$$\omega_s = \omega_i \pm \omega_j \qquad [3.22]$$

and

$$\mathbf{k}_s = \mathbf{k}_i \pm \mathbf{k}_j. \qquad [3.23]$$

where ω is the angular frequency and **k** is the wave vector. The subscripts s and i refer to the scattered and incident photon respectively. The subscript j refers to the phonon which is emitted or absorbed. The + sign refers to the anti-Stokes process where a phonon is absorbed. The - sign refers to the Stokes process (a phonon is emitted). Since the photon wave vectors are very small (**k** = 0) only optical phonons at the Brillouin zone center are involved in Raman scattering.

The Raman effect in all solid state materials is very weak. The total scattering efficiency in GaAs is about 8.5×10^{-6} sterad^{-1}cm^{-1}. The interaction length is given by $L=1/2\alpha$ where α is the absorption coefficent at the photon energy. In GaAs, α equals 9×10^{4} cm^{-1} for a wavelength of 500 nm. Since the scattering is so weak, an intense monochromatic source (laser) is required.

Raman spectra were collected with 2 cm^{-1} resolution at room temperature in the $z(x,y)\bar{z}$ pseudo-backscattering geometry. The 488 nm (2.54 eV) line of an Ar ion laser was used. The interaction length in GaAs for this wavelength is approximately 50 nm. Under these conditions, the Raman scattering is not resonance-enhanced. The laser was incident at 65° from the surface normal. Scattered light was collected normal to the sample by a f/1 camera lens and imaged through a holographic edge filter onto the entrance slit of a single pass monochromator equipped with a two-dimensional detector. Some measurements were performed with a home-built Raman microprobe with a 50× 0.75 NA objective. The probe depth at the laser wavelength of 488 nm is 55 nm. The sample geometry was $z(x,y)\bar{z}$, which is the allowed geometry for GaAs and InP LO phonons.

The relative concentration of C_{As} was determined with local vibrational mode (LVM) Raman spectroscopy. LVM's occur when a substitutional impurity atom has a much smaller mass than the mass of the host atoms. The vibrational mode is centered on the substitutional defect; it does not propagate through the crystal. The LVM of C_{As} has been observed previously by Raman spectroscopy at 583 cm^{-1} at 77 K.(Wagner, et al., 1992) The laser power was 250 mW and typical integration times were 1 hour. The intensity of the C_{As} LVM peak observed at 580 cm^{-1} below the Ar ion laser line was internally calibrated by ratioing the peak height to that of the 2nd-order phonon observed at 525 cm^{-1}.

3.4.4 Fourier transform infrared spectroscopy (FTIR)

FTIR spectroscopy is also used to measure the absorption by the C_{As} LVM. FTIR spectroscopy is a type of transmission spectroscopy in which a Michelson interferometer is used. Light from a broad band infrared source is collimated and incident on a beam splitter. The beam splitter creates two separate optical paths by reflecting half of the incident light and transmitting the remaining half. (See Fig. 3.10). In one path the beam is reflected by a fixed-position mirror back to the beam splitter. In the second path, the beam is reflected by a moving mirror which changes the path length of the second beam. The split beam is coherent and when the two beams recombine at the beam splitter interference phenomena are produced. The plot of intensity versus position of the combined beams is the interferogram. The Fourier transform of an interferogram is a spectrum of intensity versus frequency. The calculation of the Fourier transform requires a computer.

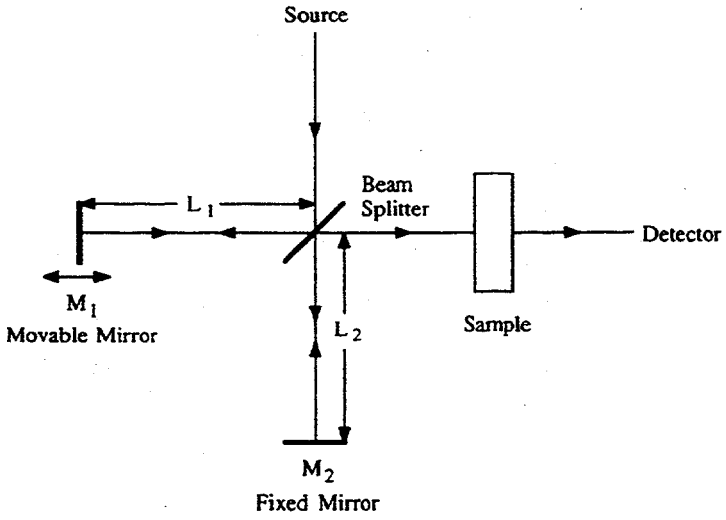

Figure 3.10. Schematic of a beam splitter in an FTIR spectrometer.

In the LVM measurements presented here, absorption spectrocopy is used. The absorption spectrum is calculated by dividing the sample spectrum by a reference spectrum and taking the negative logarithm. The reference spectrum is either a spectrum with no sample present in the sample holder or a spectrum of a reference sample. In this study, the reference spectrum is obtained with an undoped substrate of GaAs or InP which has not been implanted. I_0 represents the intensity of light after it passes through the reference material. Light passing through the sample material results in an intensity of $I_0e^{-\alpha x}$ where x is the thickness of the sample and α is the absorption coefficient. Therefore,

$$-\ln\frac{I_0e^{-\alpha x}}{I_0} = \alpha x \qquad [3.24]$$

where αx is referred to as absorbance. The result of the experiment is a plot of absorbance versus k. When the LVM of C_{As} absorbs light at its characteristic frequency this corresponds to a peak in the absorbance spectrum. The concentration of C_{As} can be determined by the area under the peak since

$$\alpha = n\sigma \qquad [3.25]$$

where n is the concentration of the absorbing defect and σ is the absorption cross section of the defect.

The C_{As} LVM occurs at 583 cm^{-1} at 4K.(Newman, et al., 1972) The absorption cross section for the C_{As} LVM was discussed in Chapter 2. Since reported values of the cross section vary widely, absolute concentration will be reported. Instead the area under the LVM peak is used as a relative measure of the concentration.

For FTIR experiments, samples approximately 1×1 cm^2 were cut and wedged, to eliminate Fabray-Perot interference. Samples are wedged by waxing a metal shim under one end of the sample before lapping and polishing. Following lapping and polishing the two faces of the sample are approximately 3° away from parallel. LVM measurements are performed in a Digilab FTS-80 Fourier transform spectrometer using a Ge:Cu IR

detector. Sample temperatures are held at 9K under flowing He in a Janis Super VP cyrostat.

3.4.5 Other Techniques

Photoluminescence measurements were performed at 4K in an immersion cryostat. The 488 nm line of an Ar laser was used for excitation. The penetration depth of this laser line in GaAs is approximately 50 nm. A PbS detector was for detection of PL from deep levels.

SIMS analyses were performed at Charles Evans and Associates using a CAMECA IMS-4f double focussing, magnetic sector ion microanalyzer. Cesium bombardment was used with SIMS monitoring of negative secondary ions. The background determines the detection limit in the SIMS experiments. For C, the background is approximately 1×10^{16} cm^{-3}. The raw data from the experiment is a profile of secondary ion counts vs. time. This data is converted to concentration vs depth. The conversion from ion counts to concentration is performed by using relative sensitivity factors determined from ion implanted standards. The conversion of sputtered time to depth is determined from stylus profilometer measurements of the analytical crater depths and the total sputter time. The depth scale is accurate to within 10%.

Chapter 4: Results and Discussion

4.1 GaAs:C implantation

As described in Chapter 2, C doping of GaAs by implantation is not as successful as doping during epitaxial growth. C implanted alone at energies and doses such that the peak C (bulk) concentration is greater than 5×10^{18} cm^{-3} results in activation of less than 10% of the implanted C. Co-implantation with Ga has been shown to significantly increase the activation.(Pearton & Abernathy, 1989) The sheet hole concentrations have been increased by an order of magnitude for doping levels above 10^{19} cm^{-3}. As originally proposed by Heckingbottom and Ambridge,(Heckingbottom & Ambridge, 1973) co-implantation of a complementary species increases the activation of the implanted dopant by maintaining the stoichiometry of the implanted layer. However, in the case of Ga co-implantation with C, the Ga is a much heavier ion and will cause significantly more radiation damage to the substrate. The increase in damage density is due to both the greater atomic mass of the Ga ion and the fact that the Ga ion must be implanted at higher energies to match the concentration profile with that of the C implant.

In the case of C implantation, the mechanism by which a Ga co-implant increases the activation is unclear. Clearly the Ga co-implant will maintain the stoichiometry of the layer. Therefore, the probability of C occupying an As site will increase. In addition, maintaining the stoichiometry of the layer will reduce the number of point defects remaining in the layer following annealing. It is well known that native defects can compensate intentional dopants in compound semiconductors.(Walukiewicz, 1988a) The increase in damage density caused by the Ga co-implant also provides additional vacancies for the C atoms to occupy. By identifying the mechanism by which the Ga co-implant increases the activation, the co-implant parameters can be optimized to provide the

maximum activation. For example, if the increase in damage density is the primary mechanism for increased activation then the implant parameters should be chosen such that the peak of the damage density created by co-implantation matches the peak of the C concentration. On the other hand, if maintaining the stoichiometry of the layer is the most important, then the peak of the Ga concentration (implanted Ga) should be matched to that of the C concentration.

The experiments described in this section are designed to elucidate the mechanism by which Ga increases the activation of implanted C. The co-implant process can then be optimized to attain the highest possible activation. The results from these studies can also provide information on increasing the activation of C implanted into other compound semiconductors and can provide insight into the general process of implantation in compound semiconductors.

4.1.1 Series of elements as co-implants

In this section, results are presented from a series of experiments which clarify the mechanisms by which co-implantation affects the electrical activity of implanted C in GaAs. The effects of stoichiometry and damage are separated by using a series of co-implant ions. The co-implant ions used were, in order of increasing atomic mass: B, N, Al, P, Ar, Ga, As, and Kr. The group III elements (B, Al, and Ga) help in maintaining the stoichiometry of the implanted region. The noble gases (Ar and Kr) should not affect the stoichiometry while the group V elements (N, P, and As) create even larger deviations in stoichiometry than implantation of C alone. As the atomic mass of the co-implant species increases, the radiation damage density in the substrate due to the implantation process increases. This increase is due to the larger mass of the implanted ion and the higher implantation energy required to match the C ion implantation profile.

GaAs substrates were solvent cleaned, etched, and implanted with singly ionized C ions at an energy of 40 keV and a dose of 5×10^{14} cm^{-2}. Following implantation of C, the co-implant was performed for individual samples. The dose and energy of the co-implant was chosen to match the profile of the C ions as calculated by the LSS theory.(Lindhard, et al., 1963) Table 4.1 indicates the dose and energy of each element implanted in this study. Figure 4.1 shows the C and Ar profiles as calculated using the Profile Code. The wafers were tilted 7° off the [100] axis during both implantations to prevent channeling. The substrates were held at room temperature during implantation. Following implantation, the samples were rapidly thermally annealed.

Secondary ion mass spectroscopy (SIMS) measurements of the samples both before and after annealing indicate that the actual concentration profiles are similar to the calculated profiles. Figure 4.2 shows the concentration as a function of depth for C and B after annealing. The experimental profiles are very similar to the predicted profiles.

Table 4.1 Implantation Parameters

Implant Ion	Atomic Mass (amu)	Energy (keV)	Dose (10^{14} cm^{-2})
C	12	40	5
B	11	30	6
N	14	40	5
Al	27	80	6
P	31	90	6
Ar	40	115	5
Ga	69	180	5
As	75	220	4
Kr	84	250	4

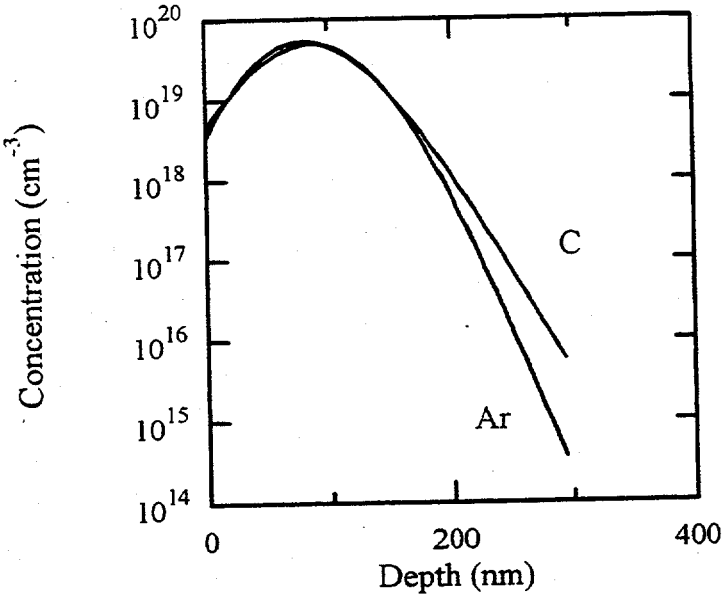

Figure 4.1 Theoretical ion implantation profiles for C and Ar as calculated by the Profile Code. Implantation conditions are listed in Table 4.1.

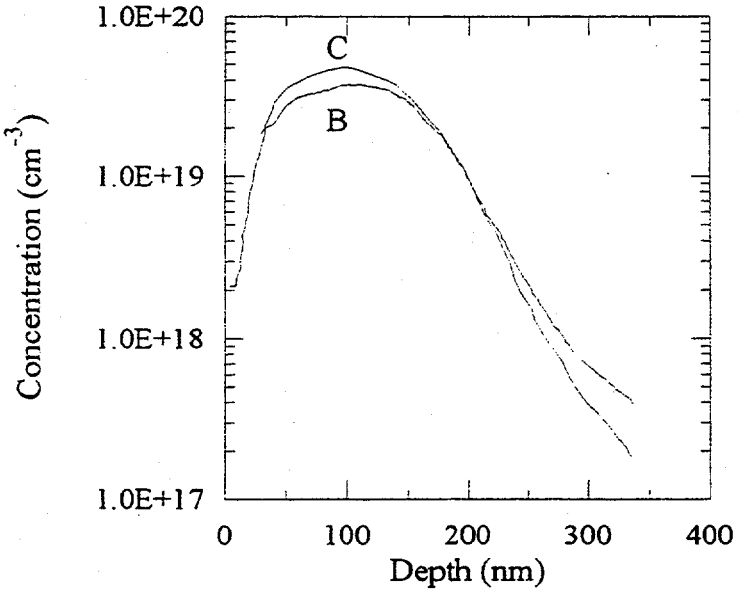

Figure 4.2. SIMS profile of implanted C and B. Implantation conditions are listed in Table 4.1.

Carrier concentration, mobility, and resistivity as a function of temperature were determined by van der Pauw geometry Hall effect measurements. The activation (or electrical activity) is then determined by dividing the sheet free carrier concentration (holes) by the implanted dose. The amount of structural damage caused by the implantation was characterized by channeling Rutherford backscattering spectrometry (RBS). Photoluminescence (PL) measurements of optically active deep levels were made at 4 K using the 488 nm line of an Ar laser. The relative concentration of C_{As} ($[C_{As}]$) was determined with local vibrational mode (LVM) Raman spectroscopy. The intensity of the C_{As} LVM peak observed at 580 cm^{-1} below the Ar ion laser line was internally calibrated by ratioing the peak height to that of the 2nd-order phonon observed at 525 cm^{-1}.

The extent of structural damage as measured by channeling RBS due to the various co-implant ions is shown in Fig. 4.3 for samples implanted with C+B, C+Al, and C+Ga. In addition, the spectra from an unimplanted sample and in a random direction are shown. The C only and C+N samples exhibit spectra similar to that of C+B. The light ions, C+B, C only, and C+N, cause only slight damage to the substrate as indicated by the increased backscattering yield relative to the standard (unimplanted) sample. The co-implant ions which have atomic mass greater than that of Al cause an amorphous layer to form at the surface of the substrate. The amorphous layer is approximately 120 nm thick for the samples implanted with C+Al, C+P, and C+Ar (only C+Al spectra is shown). For the C+Ga, C+As and C+Kr samples (only the C+Ga results are shown) the amorphous layer is approximately 140 nm thick. Following annealing at 950 °C for 10 seconds a nearly perfect crystal is recovered for the C+Ga case, however in the case of C+Kr some extended defects remain as shown in Fig. 4.4.

The sheet carrier concentration as a function of the depth of the amorphous layer as measured by RBS is shown in Fig. 4.5. For the co-implant ions from column III of the periodic table (B, Al, and Ga), the sheet carrier concentration increases with increasing

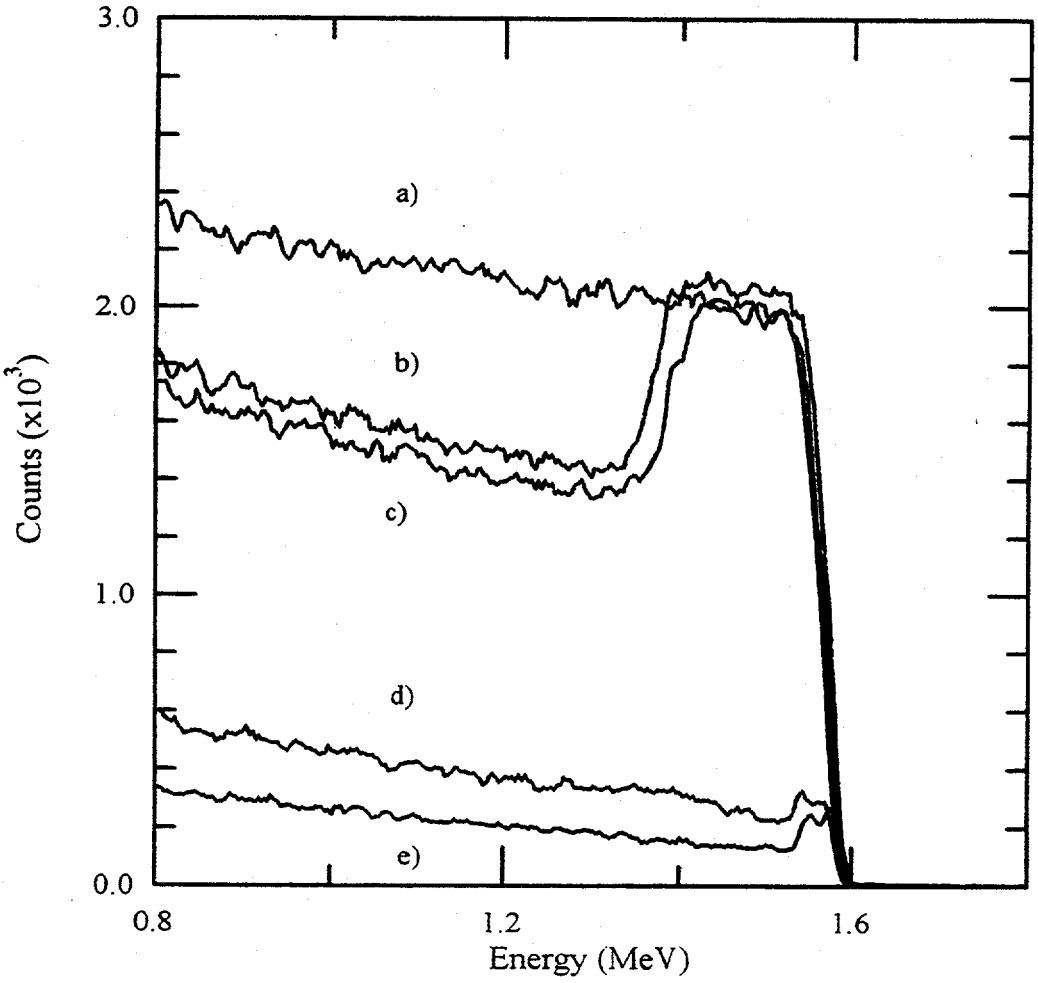

Figure 4.3. 1.95 MeV He^+ <111> aligned RBS spectra for a) random direction, b) C+Ga implant, c)C+Al implant, d) C+B implant and e) unimplanted sample. The amorphous layers at the surface of the C+Ga and C+Al samples are 140 and 120 nm respectively.

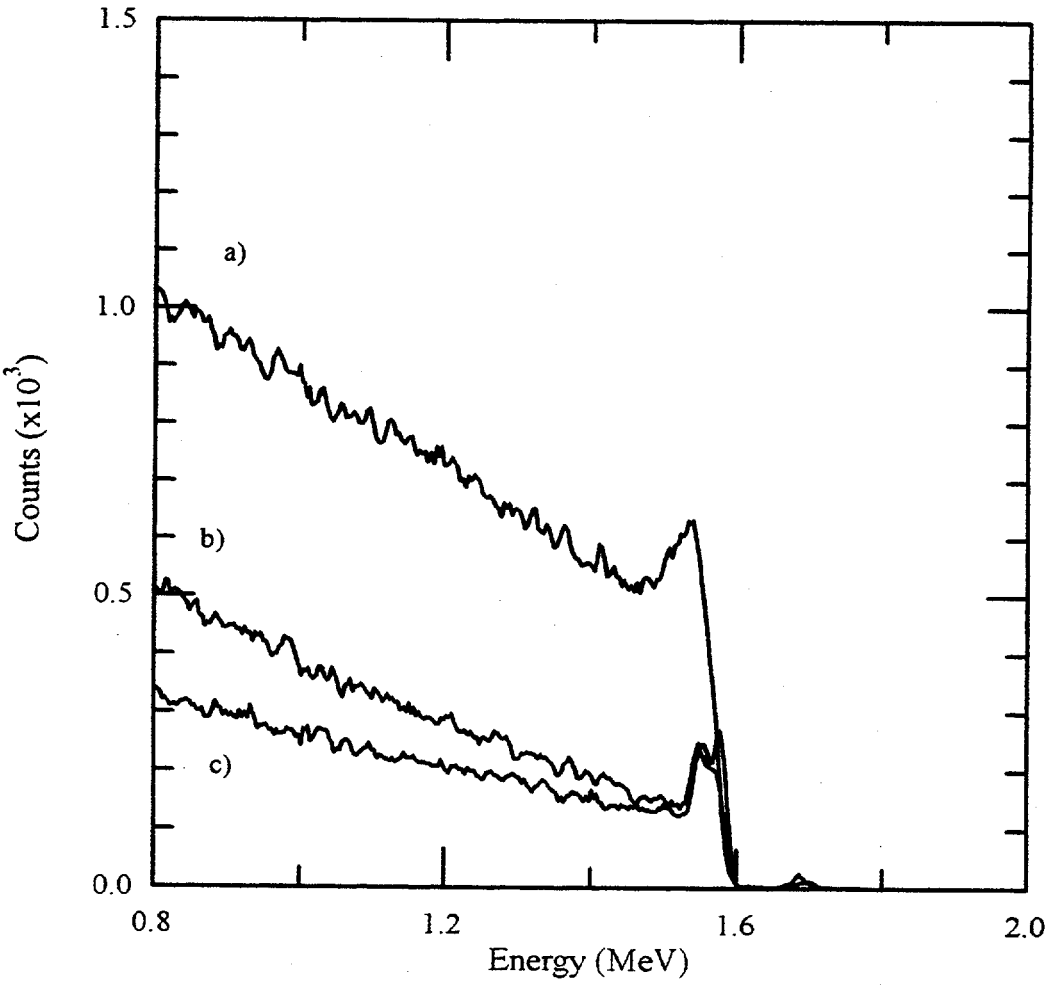

Figure 4.4. 1.95 MeV He^+ <111> aligned RBS spectra for implanted layers following annealing at 950°C for 10s; a) C+Kr implant, b)C+Ga implant, and c) unimplanted sample.

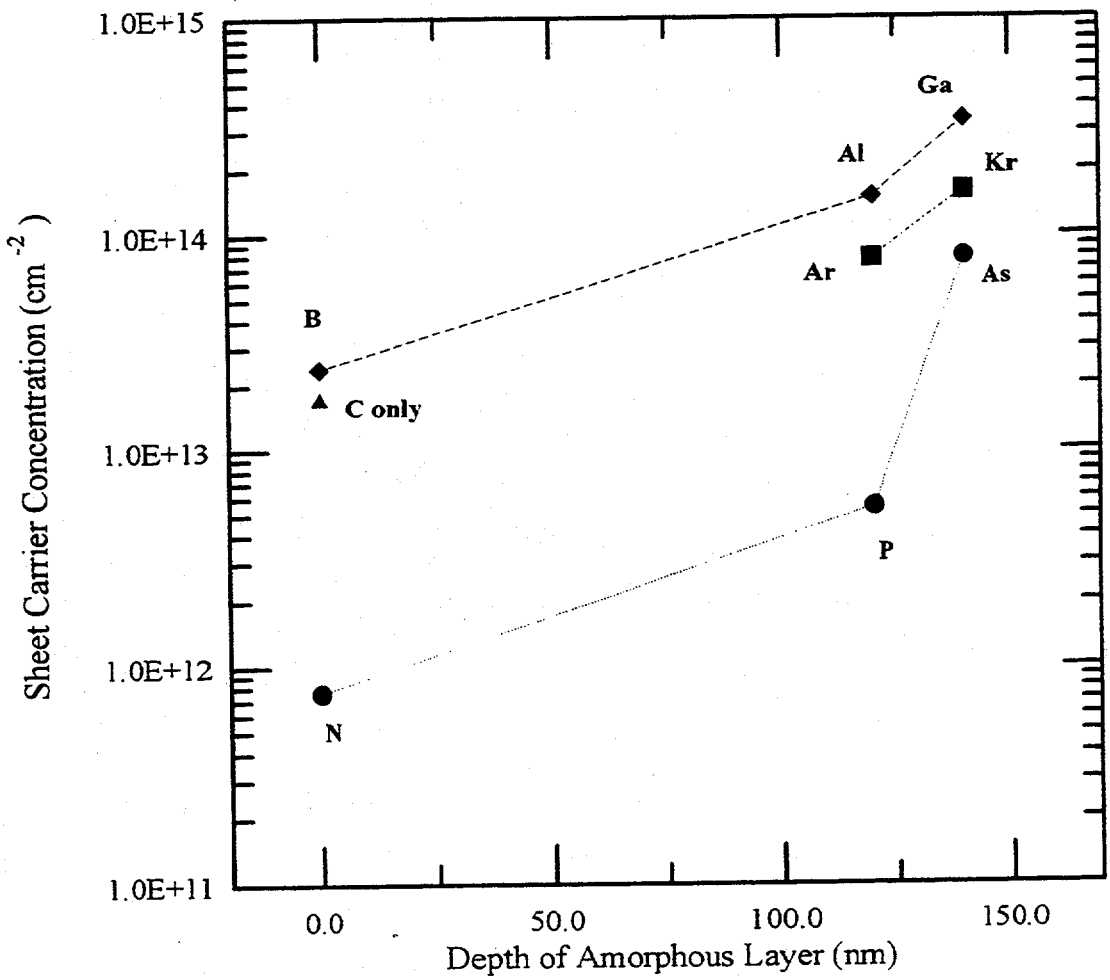

Figure 4.5. Free hole concentration as measured by Hall effect as a function of the depth of the amorphous layer as measured by RBS.

radiation damage. This trend is repeated for the co-implant ions from column V (N, P, and As) and for the inert gasses (Ar and Kr). In addition for co-implant ions which create similar amounts of radiation damage (e.g., Ga, As, and Kr), the highest sheet carrier concentration is attained for the group III co-implant followed by the co-implants which are inert gases. The group V co-implant has the least effect on the carrier concentration. In fact, both N and P co-implants decrease the sheet carrier concentration as compared with C implanted alone.

The LVM of C_{As} was measured using Raman spectroscopy. A typical Raman spectrum of the C+Ga sample is shown in Fig. 4.6. The relative height of the LVM peak as a function of the sheet carrier concentration is shown in Fig. 4.7. The peak height was normalized by the second order phonon peak. The peak height is plotted instead of the area under the peak since the line width of the LVM peak for each sample was limited by the resolution of the instrument. In general the height of the LVM peak increases with increasing carrier concentration with a few exceptions. Although the C+Ga sample has twice as many free carriers as the C+Kr sample the LVM peaks have nearly the same height. This trend is repeated for the C+Al and C+Ar samples. The concentration of C_{As} was below the detection limit of the instrument for the C+N and C only samples.

The Hall mobilities as a function of temperature for the C+Al, C+Kr, and C+Ga samples are plotted in Fig. 4.8. Although the C+Al and C+Kr have nearly the same free hole concentration ($p_S = 1.7\times10^{14}$ cm^{-2}) the mobility is significantly higher in the C+Al case. In fact, the mobility of the holes in the C+Kr case behaves very similarly to the C+Ga case however the free hole concentration in the C+Ga sample ($p_S = 3.3\times10^{14}$ cm^{-2}) is approximately twice as large as the hole concentration in the C+Kr sample. The mobilities attained for the C+Ga and C+Al samples are similar to mobilities reported for MOCVD and MOMBE GaAs epitaxial layers with similar C doping levels(Yamada, et al., 1989) which indicates good crystalline quality of the regrown layers.

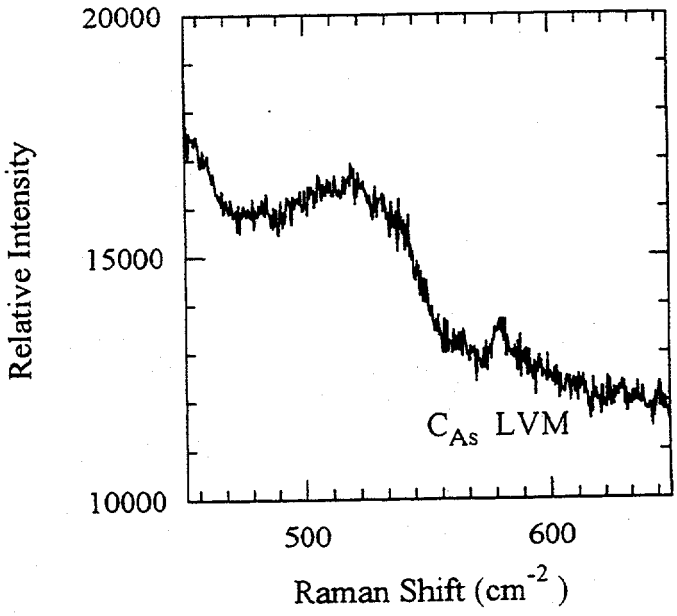

Figure 4.6. Typical Raman spectra with the C_{As} LVM peak at 580 cm^{-1} for sample implanted with C+Ga.

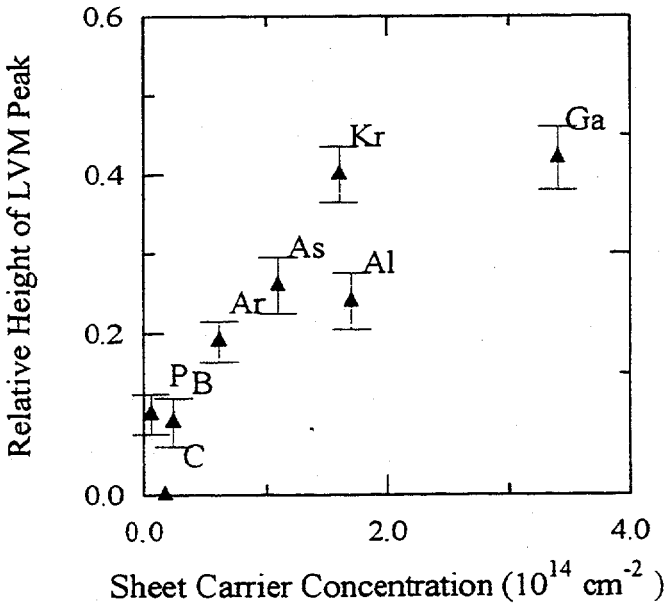

Figure 4.7. Relative peak height of the C_{As} local vibrational mode as a function of the sheet carrier concentration.

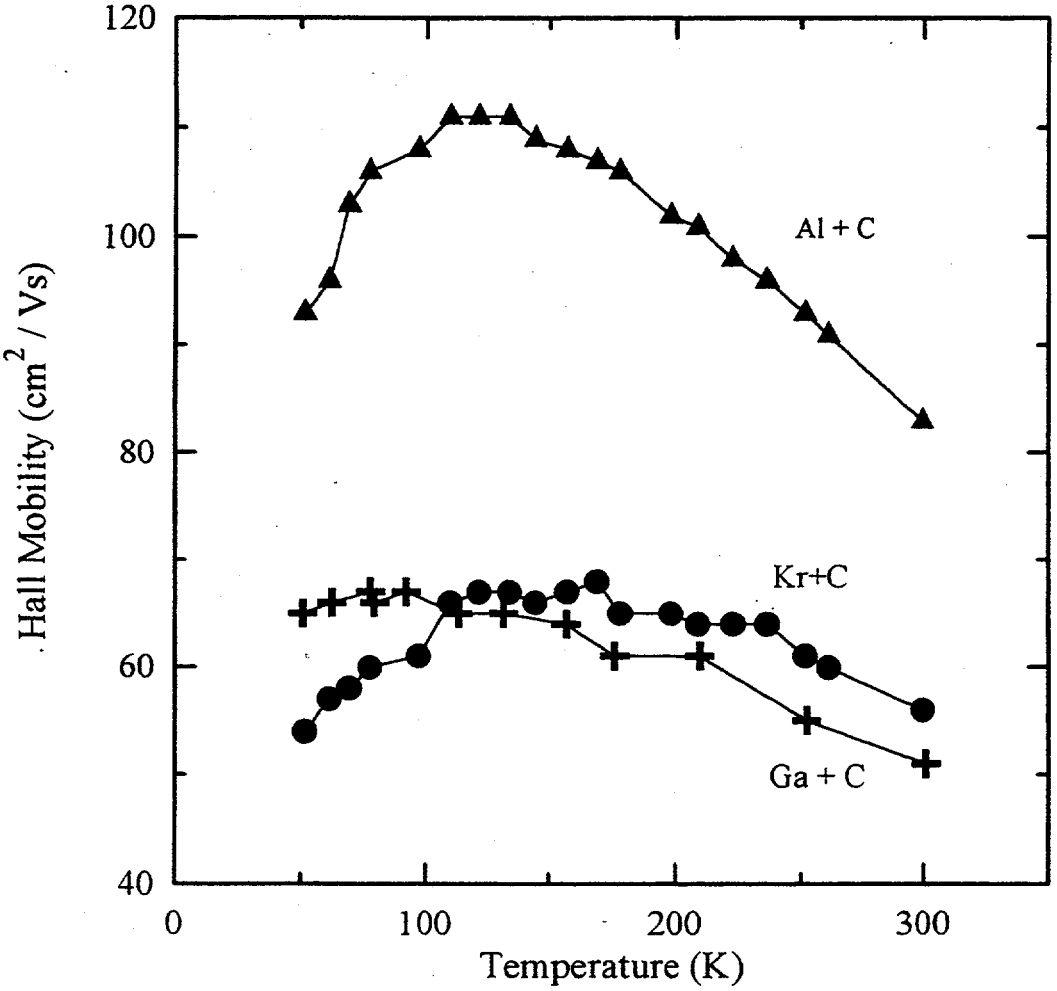

Figure 4.8. Hole mobility as a function of temperature as measured by van der Pauw geometry Hall effect.

The photoluminescence spectra for the C+Ga and C+Kr samples are shown in Fig. 4.9 and those of C+Al and C+Ar in 4.10. The C+Kr sample shows significantly more emission from deep levels peaking at the photon energy of approximately 1.1 eV above the valence band. Although a large peak is not seen in the C+Ar spectrum, the intensity of emission below 1.2 eV is significantly higher in the C+Ar sample compared to the C+Al sample.

By comparing the RBS spectra (Fig. 4.3) and the LVM spectra (Fig. 4.7) it is evident that as the radiation damage in the crystal increases the $[C_{As}]$ increases. For implantation of C alone or co-implantation with light ions, little radiation damage occurs. The concentration of defects is further reduced by self-annealing during the implantation process. In fact, the samples in which no amorphous layer forms (C+B, C only, and C+N) have $[C_{As}]$ which are at or below the detection limit of Raman spectroscopy. Co-implantation with heavier ions produces more extensive damage. Both the C+Al sample and the C+Ar sample have an amorphous layer of approximately 120 nm and the $[C_{As}]$ as determined by the height of the LVM peak is very similar in these two samples. Likewise, the C+Ga and C+Kr samples have a wider amorphous layer and a higher $[C_{As}]$ as indicated by the height of the LVM peak. Hence, one effect of the co-implanted ion is to increase the concentration of substitutional C_{As} by creating additional radiation damage in the substrate.

In addition to the damage created by co-implantation, the chemical identity of the co-implanted species has a significant effect. The free hole concentration in the samples is not linearly proportional to the $[C_{As}]$ as measured by LVM spectroscopy (Fig. 4.7). As an example consider the series of samples co-implanted with Ga, As, and Kr. In each of these samples an amorphous layer of 140 nm forms at the surface. The $[C_{As}]$ is nearly the same in the C+Ga and C+Kr samples, however, the carrier concentration in the C+Ga ($p_s=3.3\times10^{14}$ cm^{-2}) sample is nearly twice that of the C+Kr ($p_s=1.7\times10^{14}$ cm^{-2}) sample. Free carriers (holes) from the C_{As} acceptors in the C+Kr sample are lost either by

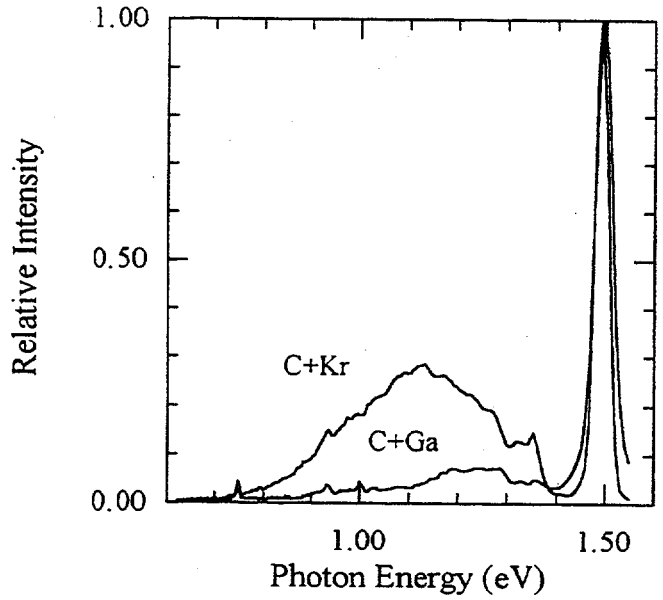

Figure 4.9. Photoluminescence spectra for C+Kr and C+Ga samples.

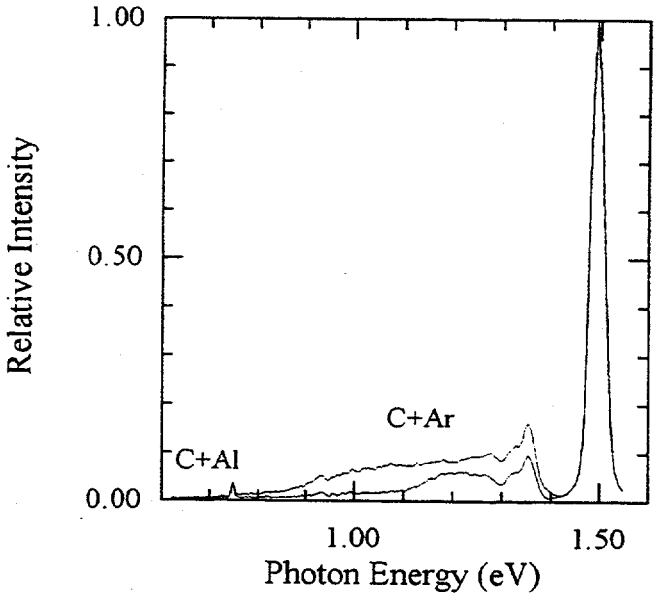

Figure. 4.10. Photoluminescence spectra for C+Ar and C+Al samples.

passivation or compensation by donors. In comparison, co-implantation with As reduces both the [C_{As}] and the concentration of free holes.

These differences can be understood in terms of combined lattice damage and stoichiometry effects. The radiation damage creates available sites for the C. Therefore in the C+Ga and C+Kr samples similar [C_{As}] result. In the case of As, the co-implant competes with the C for an As site. Hence the [C_{As}] is reduced. In the crystal co-implanted with Ga the implanted layer is closer to perfect stoichiometry than the sample co-implanted with Kr. The deviation from stoichiometry, i.e., the excess As atoms from the sites substituted by C, is accommodated by point or extended defects. As proposed by Walukiewicz(Walukiewicz, 1989) in p-type GaAs the defects related to the non-stoichiometry are predominantly donors. Such donor defects can act as compensating or passivating centers reducing the hole concentration even further. The As co-implant not only competes with the C for As vacancies, but it also introduces additional non-stoichiometry into the crystal further increasing the concentration of native defects and reducing the number of free carriers.

The C+Al, C+P, and C+Ar samples exhibit similar behavior to the crystals described above. An amorphous layer 120 nm thick forms at the surface in each case. Similar [C_{As}] are found in the C+Al and C+Ar samples which is lower than the [C_{As}] found in the C+Ga and C+Kr samples due to the reduced thickness of the amorphous layer. The C+P sample has a significantly lower [C_{As}] since P will compete with the C for the As site. Again, native defects result in a reduced free hole concentration when the co-implant is not a group III element.

The non-stoichiometric defects either compensate or passivate the C_{As} acceptors in the implanted layers. If the acceptors are compensated, then the mobility of the samples will be reduced, particularly at low temperatures (<77 K) where mobility is limited by ionized impurity scattering. However, if the acceptors are passivated, then samples with similar free carrier concentrations will have similar mobilities. Although the C+Al and

C+Kr samples have the same sheet hole concentration of 1.7×10^{14} cm^{-2} (Fig. 4.7), the low temperature mobility is higher in the C+Al sample (Fig. 4.8) whereas the $[C_{As}]$ is higher in the C+Kr sample. These results indicate that a considerable concentration of donor defects are present in the C+Kr sample. These defects both compensate the C_{As} acceptors and act as charged scattering centers reducing the hole mobility in the implanted layer. This inference is further corroborated by the data presented in Fig. 4.8 where the deep defect related photoluminescence is more intense in the C+Kr and C+Ar samples than in the C+Al and C+Ga samples.

A particularly interesting case is the C+B sample. The B co-implant creates little additional damage beyond what is caused by C alone within the sensitivity of channeling RBS. No amorphous layer is formed in the implanted substrate. Consequently, the B co-implant has only a stoichiometry effect on the electrical activity of the implanted C. However, the carrier concentrations in the C only and C+B samples are nearly identical within the experimental error of the technique. This result indicates that a heavily damaged or amorphous layer is required before the stoichiometry of the implanted layer will have an effect on the activation.

This series of samples shows that the ability of the implanted C to substitute for an As atom and contribute a free hole depends on the degree of disorder in the as-implanted lattice. Co-implantation with Ga dramatically improves the electrical activity of C acceptors. The highest sheet hole concentration of 3.2×10^{14} cm^{-2} corresponds to a volume concentration of about 3×10^{19} cm^{-3}. Is this the maximum attainable concentration or can it be increased further by a modification of the implantation and/or annealing processes? As discussed in Chapter 2, annealing studies of heavily C doped epitaxial films indicate that high temperature (800 to 900 °C) annealing reduces the concentration of electrically active C acceptors.(Höfler, et al., 1992)(Nozaki, et al., 1993) In very heavily doped samples with $p>5\times10^{19}$ cm^{-3} the high temperature annealing reduces the free hole concentration to between 2×10^{19} and 4×10^{19} cm^{-3}. The final hole concentration is

independent of the original hole or C concentration in the material before annealing. Since the activation of C implanted into GaAs requires annealing in the 800 to 950°C range, the hole concentration of about $3\times10^{19}cm^{-3}$ found in the Ga co-implanted sample is close to the maximum hole concentration that can be achieved by C implantation in GaAs

Both increasing the radiation damage and maintaining crystal stoichiometry in the implanted layer are necessary for high activation of C ions implanted into GaAs. The formation of heavily damaged layers improves substitutionality of C atoms on As sites. On the other hand, maintaining the stoichiometry of the implanted layer reduces the concentration of compensating native donors and increases the concentration of free holes.

4.1.2 Ga co-implant series

As described in the previous section, the role of co-implantation in increasing the activation of C is two-fold. Both increasing the radiation damage in the sample and maintaining the stoichiometry of the implanted layer increase the electrical efficiency of implanted C in GaAs. These results raise several additional questions. Can the activation of C in GaAs be increased even further by changing the implantation conditions? In the experiments described in the previous section the dose of the co-implant was closely matched to the dose of the C. In the experiment described in this section, the only co-implant species which is used is Ga but the dose is varied over an order of magnitude to determine if the activation can be increased even further.

The second question which will be addressed is the effect of regrowth of an amorphous layer on the electrical activation of implanted C. In the previous section, it was determined that additional radiation damage increases the amount of C substituting for As atoms. However, the extensive radiation damage due to implantation created an amorphous layer at the surface of the substrate. During annealing following implantation,

solid phase epitaxy (SPE) occurs. Does SPE emulate epitaxial growth and enhance the C activation, or is it merely the additional vacancies present as radiation damage increases that increases $[C_{As}]$?

In this experiment, each dose of Ga is implanted either at room temperature or with the sample cooled by liquid nitrogen. During implantation of GaAs at room temperature, dynamic annealing occurs.(Haynes & Holland, 1990) The lattice atoms (Ga and As) and the defects created during implantation have enough energy to diffuse and recombine. Implantation at lower temperatures (with the sample holder cooled by liquid nitrogen) limits the amount of dynamic annealing. Therefore, with all other implantation parameters held constant, implantation at low temperature will result in a larger defect density. For a given Ga dose and energy the amount of damage to the substrate can be changed without changing the effect of the co-implant on the stoichiometry of the layer.

GaAs substrates were solvent cleaned, etched, and implanted with singly ionized C ions at an energy of 40 keV and a dose of 3.5×10^{14} cm^{-2}. Following implantation of C, the co-implant was performed for individual samples. The dose and energy of the co-implant are given in Table 4.2. The co-implants were performed with the wafer held at

Table 4.2 Implantation Parameters

Implant Parameters	Co-implant Parameters	Temperature
C: 40 keV,	none	RT
3.5×10^{14} cm^{-2}	Ga: 180 keV, 7×10^{13} cm^{-2}	RT
for all samples	Ga: 180 keV, 7×10^{13} cm^{-2}	LN
	Ga: 180 keV, 3.5×10^{14} cm^{-2}	RT
	Ga: 180 keV, 3.5×10^{14} cm^{-2}	LN
	Ga: 180 keV, 7×10^{14} cm^{-2}	RT
	Ga: 180 keV, 7×10^{14} cm^{-2}	LN

room temperature or with the sample holder cooled with liquid nitrogen. The substrate temperature during low temperature implantations was held at 108 K. The dose rate for the Ga implantations was kept very low, < 0.1 $\mu A/cm^2$. The dose rate in these experiments is carefully controlled because this parameter also has an effect on the radiation damage which occurs during implantation. A higher dose rate heats the sample and increases the dynamic annealing. For implantations performed at low temperature, the dose rate must be kept low so the substrate remains at the same temperature throughout the implantation. Following implantation, the samples were rapid thermally annealed.

Carrier concentration, mobility, and resistivity as a function of temperature were determined by van der Pauw geometry Hall effect measurements. Using an electrochemical capacitance voltage profiler, the net space charge as a function of depth is measured. Throughout this thesis, the net space charge is assumed to be equal to the free carrier concentration within the implanted layer. The amount of structural damage caused by the implantation was characterized by channeling Rutherford backscattering spectrometry. FTIR spectroscopy was used to measure the C_{As} LVM.

The effect of the Ga co-implant dose on the depth of the amorphous layer in C implanted GaAs is shown in Fig. 4.11. As the co-implant dose increases, the thickness of the amorphous layer as measured by channeling RBS also increases. The amorphous layer is consistently reaches deeper for co-implants performed at low temperature relative to implants performed at room temperature due to the difference in dynamic annealing.

The sample which was implanted with Ga at a dose of 7×10^{13} cm^{-2} at room temperature is heavily damaged, but it does not become amorphous. This is indicated in Fig. 4.11 as an amorphous layer of zero thickness. This designation is not an accurate description of the amount of damage in the sample. TEM micrographs of the Ga implanted sample show that regions of the implanted layer are amorphous and other regions are crystalline. A more accurate description of the damage might be the concentration of vacancies in the implanted layer. However, measurement of this quantity

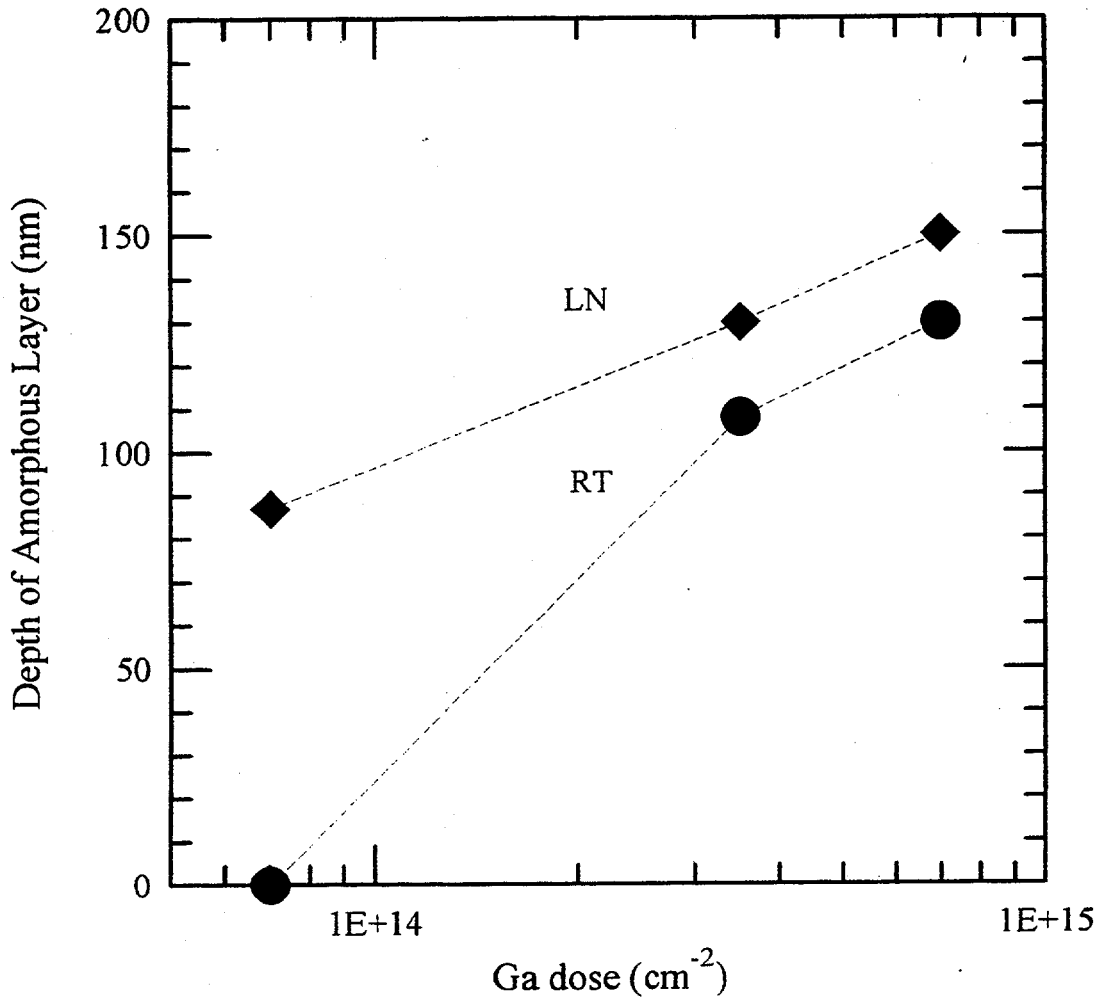

Figure 4.11. Depth of the amorphous layer as measured by RBS plotted as a function of the Ga dose.

is very difficult if not impossible. Therefore this sample will be described as having an amorphous layer 0 nm thick.

At a sufficiently high dose, the thickness of an amorphous layer created by implantation will saturate. However, the highest Ga dose used in this study, 7×10^{14} cm^{-2} at 180 keV, is not high enough for this to have occurred. From a study of Ge implanted into GaAs, the dose at which the damage saturates is approximately 2×10^{15} cm^{-2} when the implantation energy is 180 keV.(Yu, et al., 1994) The Ge isotope used has an atomic mass of 74 and the Ga isotope chosen has an atomic mass of 71. Since their masses are so similar the amount of damage created during implantation will be approximately the same at the same implantation energy. Therefore, a Ga dose of 2×10^{15} cm^{-2} would be required before the damage saturates.

The difference between heavily damaged and fully amorphous layers influences the extent of the regrowth following annealing. Consider the two samples implanted with Ga at a dose of 7×10^{13} cm^{-2}. The Ga co-implant performed at low temperature creates an amorphous layer 90 nm thick. The sample implanted at room temperature is heavily damaged but not fully amorphous. The as-implanted RBS spectra for these samples are shown in Fig. 4.12. During annealing, the amorphous layer created by implantation at low temperature regrows more perfectly than the implanted layer which is heavily damaged but not amorphous (Fig. 4.13). When the amorphous regions in the sample implanted at room temperature regrow they must eventually meet at their growth fronts. Sadana(Sadana, et al., 1984) found that implanted GaAs samples which were partially crystalline were not defect free following annealing. Dislocations and stacking faults were seen in high resolution TEM micrographs of the annealed samples. Similar behavior has been observed with detailed solid phase epitaxy studies in Si and Ge.(Csepregi, et al., 1977),(Csepregi, et al., 1978)

Figure 4.14 shows the effect of the co-implant dose and temperature on the sheet free hole concentration. As the dose increases, the hole concentration increases. Samples

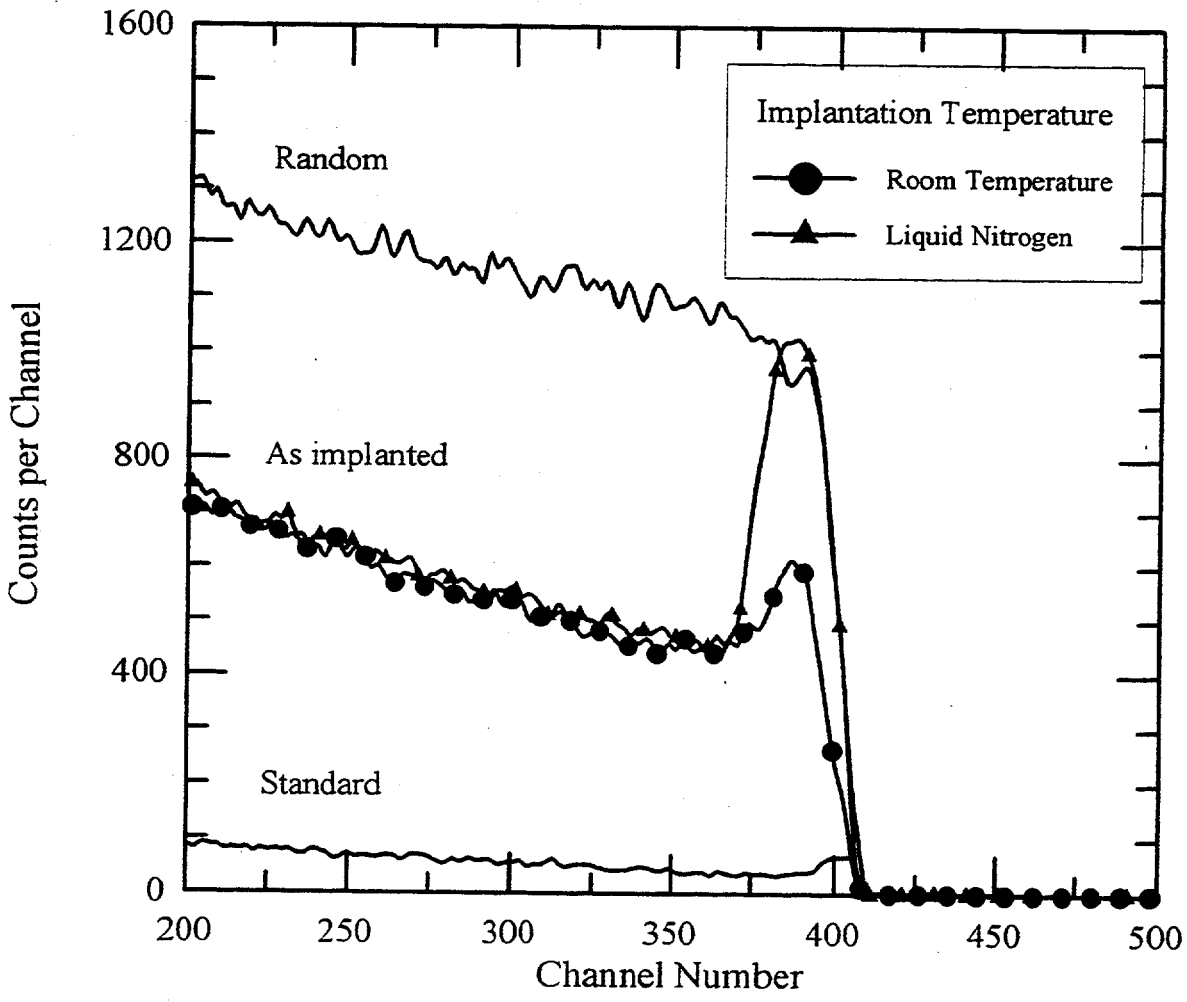

Figure 4.12. 1.95 MeV He^+ <111> aligned RBS spectra for layers implanted with C and Ga. The Ga dose is 7×10^{13} cm^{-2}.

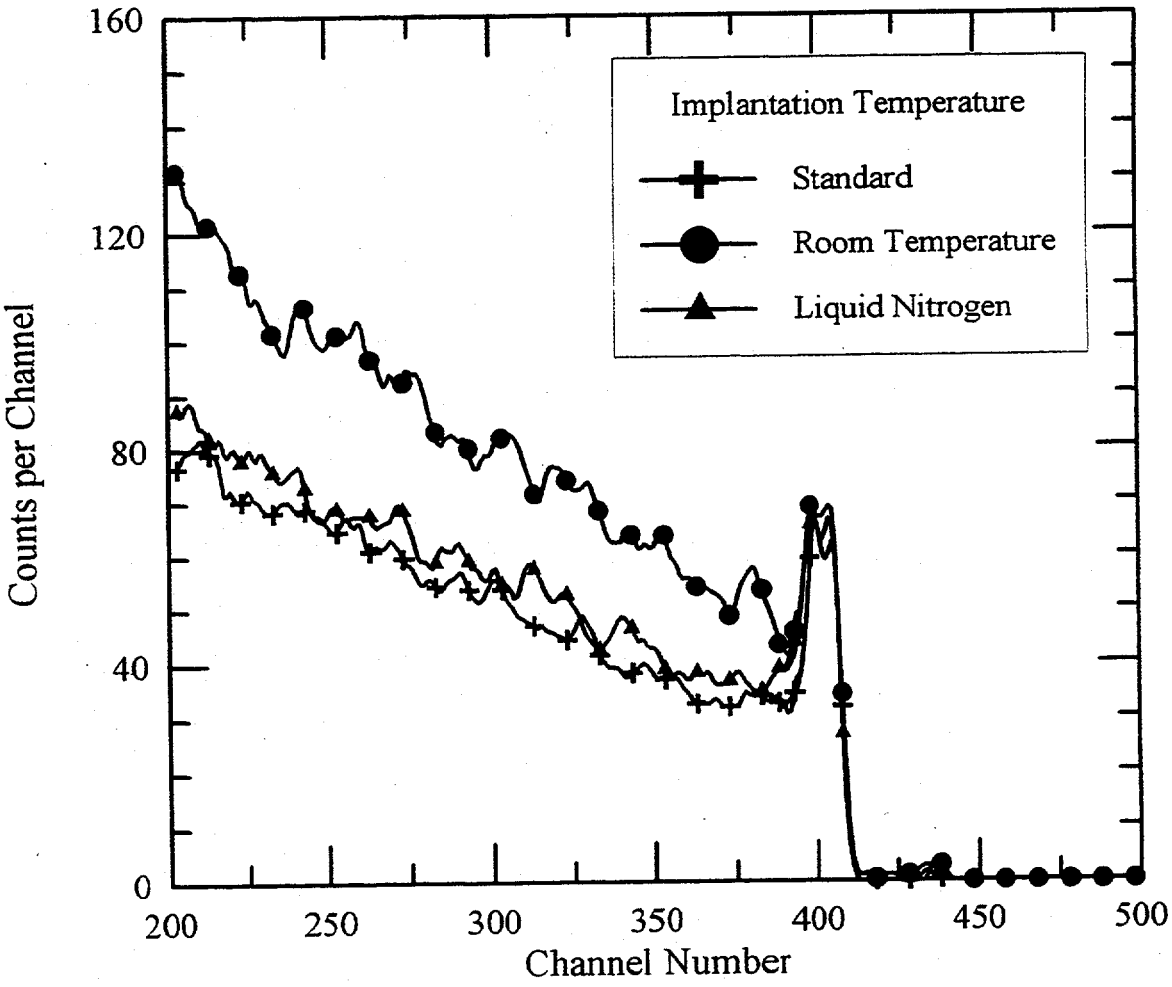

Figure 4.13. 1.95 MeV He^+ <111> aligned RBS spectra for layers implanted with C and Ga and annealed. The Ga dose is 7×10^{13} cm^{-2}.

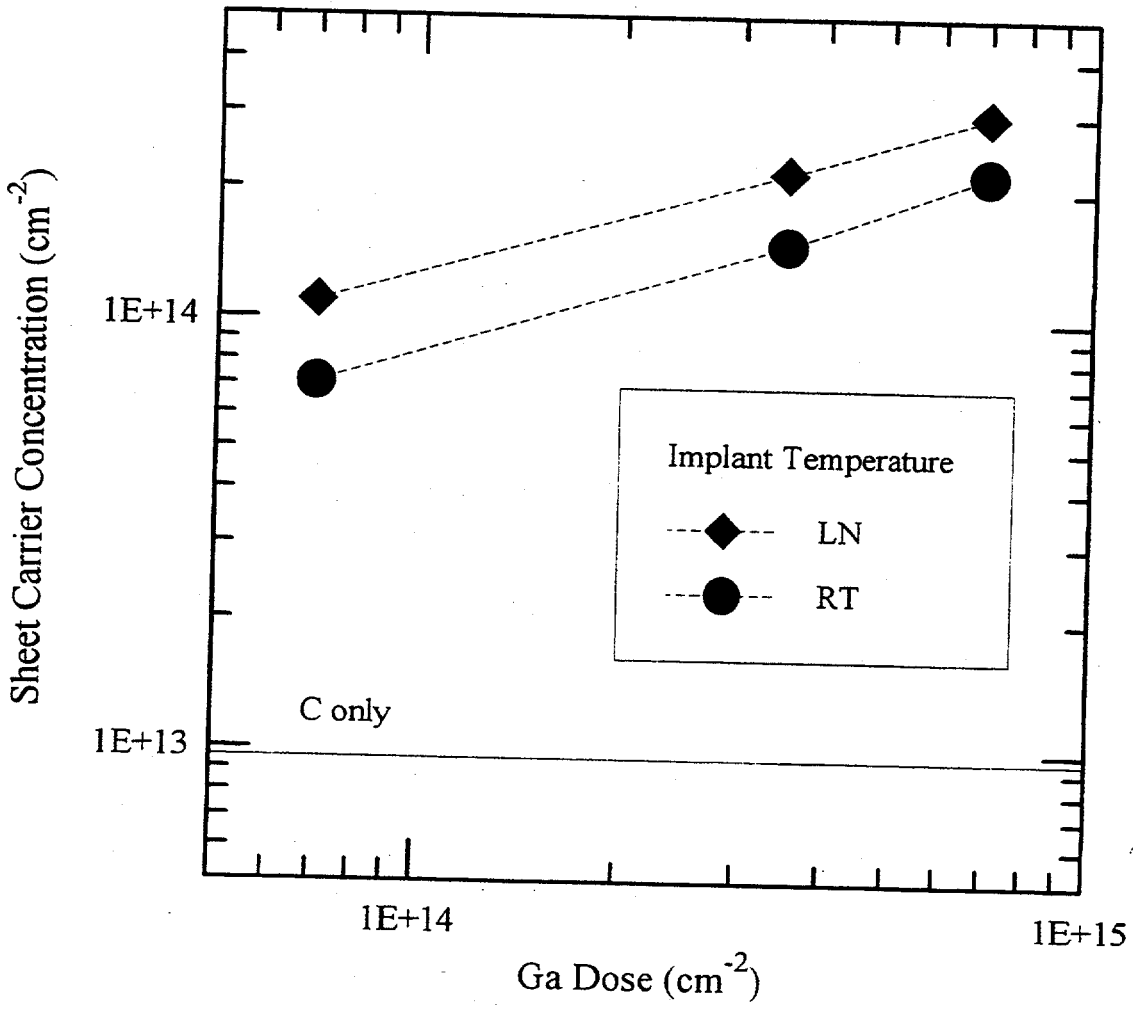

Figure 4.14. Free hole concentration as measures by Hall effect plotted as a function of the Ga co-implant dose for co-implantation at room temperature and low temperature.

which were co-implanted at low temperature have consistently higher sheet carrier concentrations. Considering the effect of the dose and temperature of the co-implant, it is evident that a correlation exists between the amount of radiation damage and the activation of implanted C.

How does the increase in radiation damage increase the activation of C? One model suggests that as the radiation damage increases, the concentration of vacancies increases. This increase in vacancies corresponds to an increase in the concentration of C_{As}. A second model would be that solid phase epitaxy of the amorphous layer during annealing emulates epitaxial growth of GaAs and this enhances the C activation. To address these issues, let us compare the samples implanted with Ga at a dose of 7×10^{14} cm^{-2}. The sample implanted at room temperature has an amorphous layer 130 nm deep. The sheet free hole concentration after annealing in this sample is 2.2×10^{14} cm^{-2}. In the sample implanted at low temperature the amorphous layer is 150 nm deep, and the sheet free hole concentration after annealing is 3×10^{14} cm^{-2}. The additional 8×10^{13} cm^{-2} free holes cannot be merely additional C atoms which occupy substitutional sites in the region between 130 and 150 nm below the surface. The average concentration of C in this region is 1×10^{19} cm^{-3} which then corresponds to 2×10^{13} cm^{-2} free holes if all C atoms in this region contribute a free hole in one sample but not in the other.

Consider the concentration of holes as a function of depth shown in Fig. 4.15 for the sample co-implanted with Ga at low temperatures at a dose of 7×10^{13} cm^{-2}. The depth of the amorphous layer in this sample is 90 nm before annealing. The amorphous to crystalline interface is near the peak of the C concentration profile. No significant change in the free hole concentration occurs at this depth. Therefore, the increase in free carriers as the amorphous layer increases in depth is due to an overall increase in damage density as the dose increases or when the implant is performed at low temperature.

Since the increase in free carriers is due to an overall increase in damage density, it could be expected that as the damage density increases the $[C_{As}]$ also increases. The area

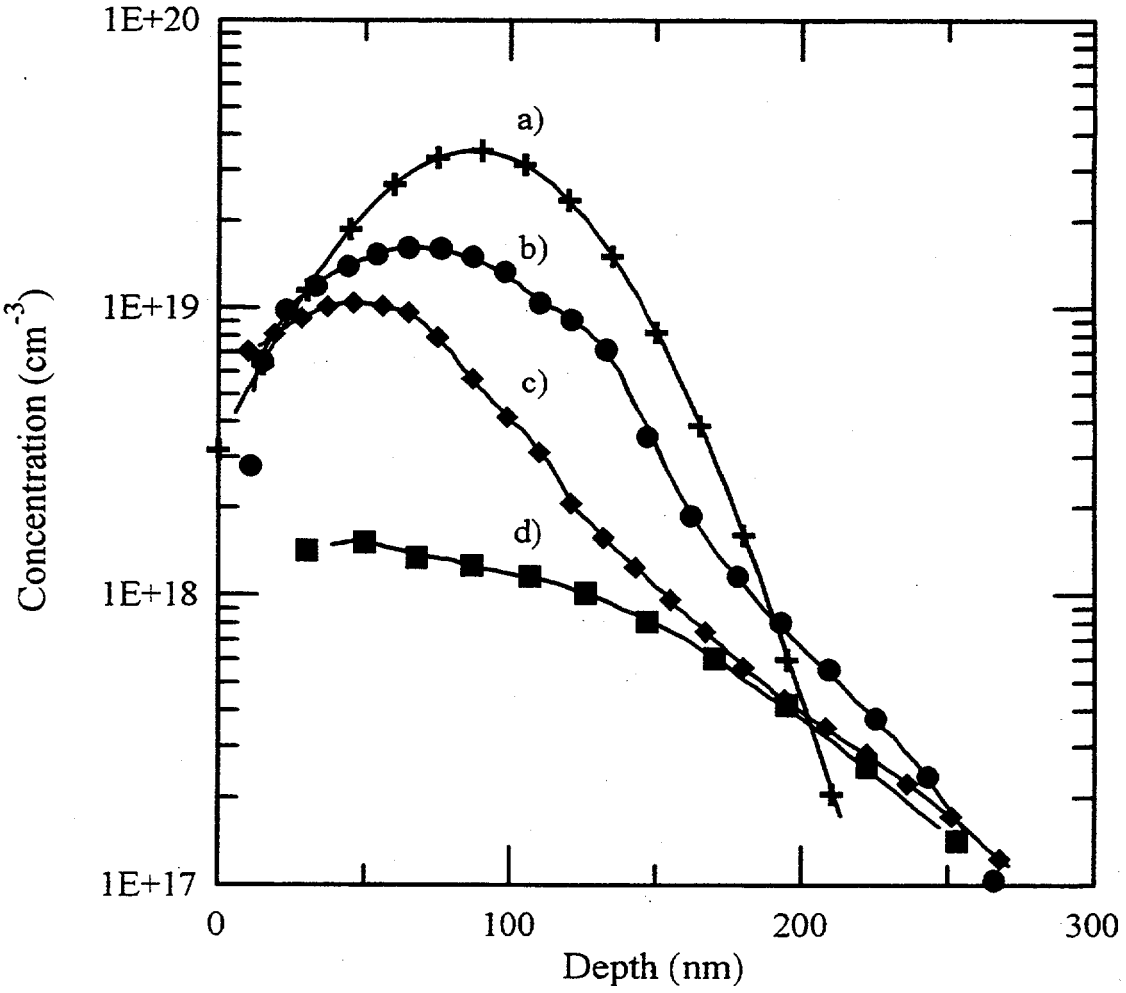

Figure 4.15. Carrier concentration as a function of depth measured by electrochemical capacitance voltage profiling for a) theoretical profile, b) Ga co-implant: 7×10^{14} cm^{-2}, LN, c) Ga co-implant: 7×10^{13} cm^{-2}, LN, and d) C only implant.

under the C_{As} LVM seen by FTIR spectroscopy is a measure of the $[C_{As}]$. In Fig. 4.16, the area under the C_{As} LVM peak is plotted as a function of sheet carrier concentration. In general, the area under the peak increases linearly with increasing sheet carrier concentration. This linear relation is expected if the increase in free holes is due to an increase in the $[C_{As}]$.

At high carrier concentrations (high doses of Ga co-implant) the area under the LVM peak appears to saturate indicating the $[C_{As}]$ becomes constant. In Fig. 4.17 the area under the LVM peak is plotted as a function of the amorphous layer thickness. As the amorphous layer thickness increases the $[C_{As}]$ also increases. Again, the data reinforces the model that the damage density increases the concentration of substitutional C_{As}. The saturation seen in Fig. 4.16 where the $[C_{As}]$ does not linearly increase with the carrier concentration at high levels of activation suggests that as determined in the previous section, damage is not the only mechanism controlling the activation. The stoichiometry of the implanted layer also plays a role in the activation. In this study, the highest dose of Ga creates a Ga rich implanted layer. The non-stoichiometry may further enhance the activation of C by limiting the native defects which compensate the C_{As} acceptors.

The activation in this study is one of the highest activation efficiencies attained for C implanted into GaAs. However the comparison of activation efficiencies from different studies must take into account the bulk concentration associated with the implantation parameters. The concentration profile depends on both the implant dose and energy. Once the co-implantation parameters are optimized, the limiting factor in activation of implanted C is the solid solubility of C in GaAs at the annealing temperatures required. At annealing temperatures above 650°C the hole concentration in epitaxial layers doped with C is also found to decrease. In very heavily doped samples with $p>5\times10^{19}$ cm^{-3} high temperature annealing reduces the free hole concentration to between 2 to 4×10^{19} cm^{-3}.

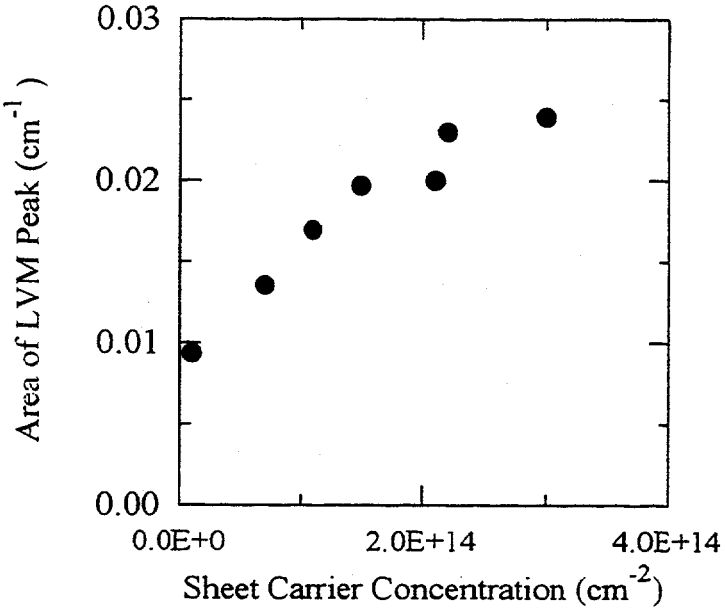

Figure 4.16. Area under the C_{As} LVM peak as a function of the free hole concentration.

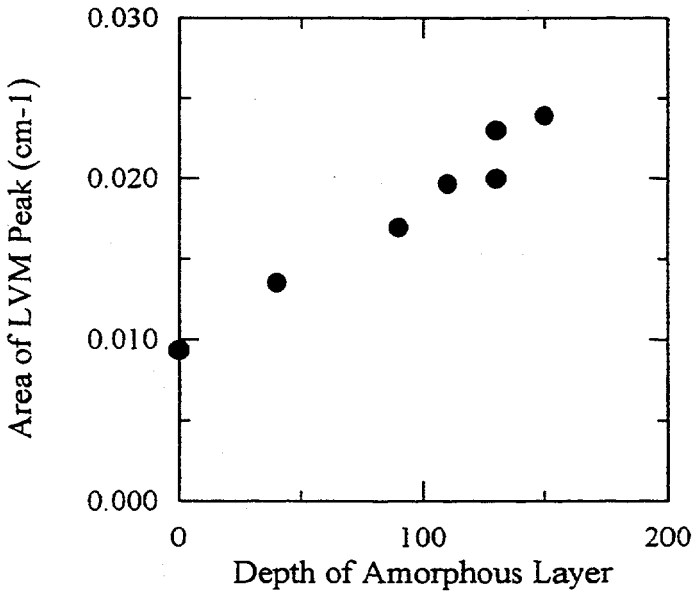

Figure 4.17. Area under the C_{As} LVM peak as a function of the depth of the amorphous layer.

The final hole concentration is independent of the original hole or C concentration in the material before annealing for such highly doped samples.

Several conclusions can be drawn from the set of experiments on C implantation in GaAs. First, Ga co-implantation is a reliable and reproducible method of attaining high activation efficiencies in C implanted GaAs. The activation efficiencies obtained allow C implantation to used as a viable doping technology in GaAs devices. Second, the Ga co-implant has two effects on the C activation. First, it creates additional damage in the lattice which allows the C to substitute for an As atom. Second, Ga has a stoichiometric effect on the C activation. By maintaining the stoichiometry of the implanted layer the number of compensating native defects is reduced which increases the concentration of free holes. Finally, there appears to be a solid solubility limit near 5×10^{19} cm^{-3} for C in GaAs at temperatures greater than 650°C which will affect the activation.

4.2 Inactive C in implanted and epitaxial layers

Although Ga co-implantation can increase the C activation to above 50%, the remaining C in the implanted layer remains inactive. In samples where C is implanted alone, a much larger fraction of the C is inactive. Various explanations for this behavior have been presented including self-compensation, interstitial C, precipitation, and compensation by radiation damage induced defects. No experimental evidence directly supporting any of these mechanisms has been published.

As discussed in Chapter 2, less than 100% efficiency of C doping is also a problem in annealed epitaxial layers heavily doped with C ($p > 5\times10^{19}$ cm^{-3}). Annealing above 650°C results in a reduction of the hole concentration without any outdiffusion of C. Independent of the original C concentration or the growth technique, the hole concentration tends toward an ultimate limit of approximately 5×10^{19} cm^{-3}. Further

annealing either for longer times or at higher temperatures does not result in any further decrease in the free hole concentration. Comparing these results with those of implanted C, these facts suggest that the solid solubility of C is approximately 5×10^{19} cm^{-3}.

In addition to the reduction in free carrier concentration, the mobility of the epitaxial layers also decreases. For a given temperature, the mobility is inversely proportional to the concentration of ionized impurities. The mobility of annealed epitaxial layers with a certain hole concentration is lower than as-grown epitaxial layers with the same hole concentration.(Höfler, et al., 1992) Therefore, the data suggests that compensating centers are being produced in these layers. Epitaxial layers doped with ultra high concentrations of C are strained in the as grown condition since the covalent radius of C is significantly smaller than that of Ga or As. Upon annealing, the strain in the layers is drastically reduced.

Researchers studying C doped epitaxial layers suggest the same mechanisms as those presented for implantation to explain the reduction in free hole concentration.(Höfler, et al., 1992)(Watanabe & Yamazaki, 1991)(Nozaki, et al., 1993) Again, no direct experimental evidence is shown to support any of the proposed mechanisms. It is important to understand the mechanism for the reduction of C activation. In addition, comparison of implanted and epitaxial layers would indicate whether the limitations are inherent to the GaAs:C system or are specific to the doping technique. Once the mechanism is known, processing steps can be designed to minimize this problem.

The discussion below will concentrate on two specific mechanisms which account for the majority of the inactive C in both heavily C doped epitaxial layers which have been annealed and in implanted layers. These two mechanisms are precipitation of C and compensation of C acceptors by native defects. Other mechanisms which have been suggested include C_{Ga} donors, lone C interstitials, C complexes, and misfit dislocations. No conclusive experimental evidence exists to support any of these mechanisms.

Although, they may occur in either epitaxial layers or implanted layers, the data presented here suggests that they do not play a major role in reducing the electrical activity of C.

4.2.1 Carbon precipitation

In this section, direct evidence of C precipitates in C-implanted GaAs and in epitaxially grown and annealed GaAs layers is presented. Peaks at 1585 cm^{-1} and 1355 cm^{-1} are observed in the Raman spectra of annealed C-doped samples and are unambiguously assigned to C-C sp^2 bonds. The identification of C precipitates with Raman spectroscopy provides an important new tool for understanding the behavior of C in III-V compound semiconductors. This method of characterization is very convenient because it is non-destructive and sensitive to the near surface region.

GaAs substrates were solvent cleaned, etched, and implanted with singly ionized C ions under various conditions as described in Table 4.3. Following implantation, the samples were rapid thermally annealed or furnace annealed at 850°C for 30 min. Carbon doped GaAs epitaxial layers were grown by MOMBE at 400°C by procedures reported elsewhere.(Konagai, et al., 1990) The hole concentration as measured by Hall effect is approximately 6×10^{20} cm^{-3}. A 1 cm^2 piece was furnace annealed at 850 °C for 3 hours.

In Raman spectroscopy of perfect crystals, the only phonons which are observed are Brillouin zone center phonons due to the requirement of k conservation. When impurities or disorder are introduced the conservation of k is relaxed and other phonons with a large density of states can be seen as well. In single crystal graphite one Raman active phonon exists as shown in Fig. 4.18. Once disorder is introduced into the crystal, other phonons can be seen in the Raman spectra of amorphous C and polycrystalline graphite. The term amorphous C refers to C which is predominantly sp^2-bonded but has no long range order. The Raman spectra of amorphous carbon (a-C) films consists of a

"G-band" centered between 1540 cm^{-1} and 1590 cm^{-1} (Fig. 4.19), and a "D-band" centered between 1340 cm^{-1} and 1390 cm^{-1}.(Robertson, 1991) The G-band corresponds to the zone center phonon (allowed phonon of graphite) which shifts slightly with the introduction of disorder. The D-band is created by disorder allowed phonons

Table 4.3. Implantation parameters and presence of Raman peaks for samples from this study.

Substrate	Doping Technique	Doping Parameters	Anneal Conditions	Raman Peaks
GaAs	None		None	NO
GaAs	None		950 °C, 10 s	NO
GaAs	Implant	C: $2x10^{15}$ cm^{-2}, 30 keV	None	NO
GaAs	Implant	C: $2x10^{15}$ cm^{-2}, 30 keV	950 °C, 10 s	YES
GaAs	Implant	Zn: $2x10^{15}$ cm^{-2}, 180 keV	950 °C, 10 s	NO
GaAs	MOMBE	C: $6x10^{20}$ cm^{-3}	None	NO
GaAs	MOMBE	C: $6x10^{20}$ cm^{-3}	850 °C, 3 hours	YES
InP	Implant	C: $2x10^{15}$ cm^{-2}, 30 keV	None	NO
InP	Implant	C: $2x10^{15}$ cm^{-2}, 30 keV	850 °C, 10 s	YES

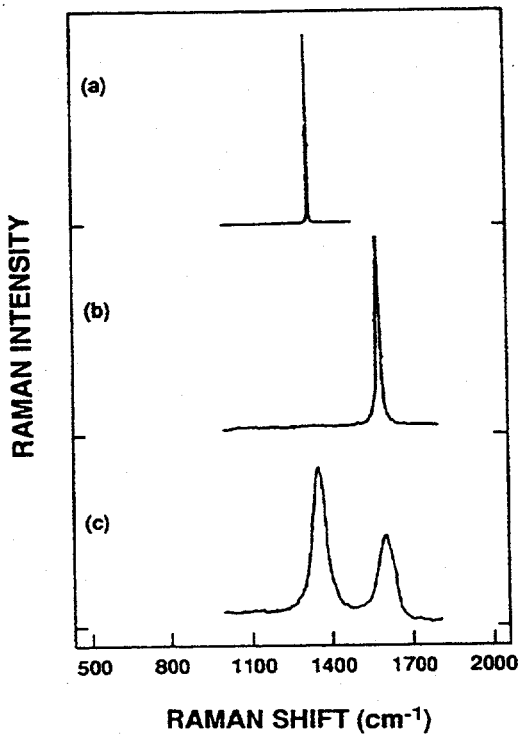

Figure 4.18. First order Raman spectra of (a) diamond, (b) graphite, and (c) microcrystalline graphite.(Schroder, et al., 1990)

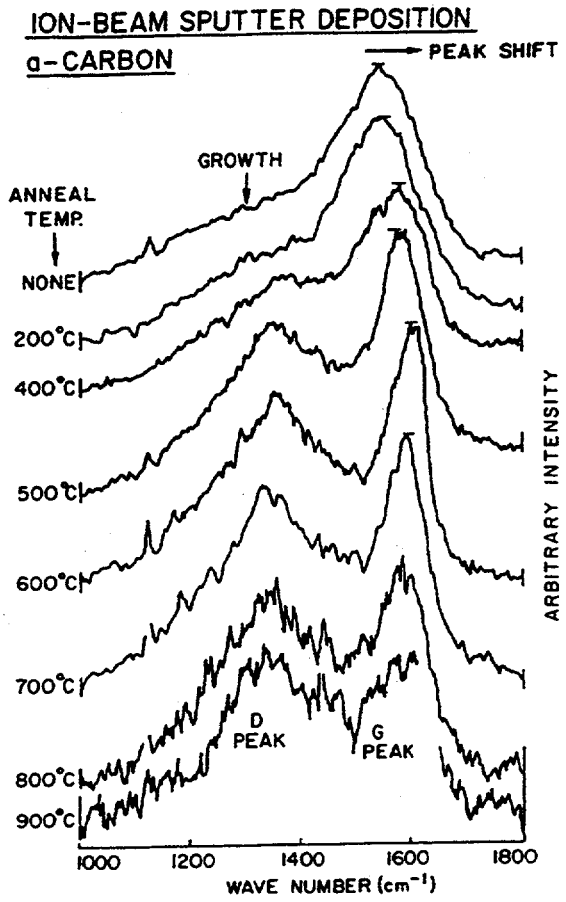

Figure 4.19. Raman spectra for a series of anneal temperatures up to 900°C in an ion-beam-sputter-deposited amorphous carbon sample.(Dillon, et al., 1984)

with a peak in their density of states of sp^2-bonded C as shown in Fig. 4.20. If C precipitates form in GaAs and they are of sufficient size and quantity, Raman spectroscopy can be used to identify them.

The Raman signature of sp^2-bonded C is unique. Presence of the G- and D- bands in a Raman spectrum indicate that "bulk-like" sp^2-bonded C is present. These two bands can be directly correlated with the phonon density of states of graphite. C modes in molecules have very different Raman frequencies. For example, in octene where there is a C=C double bond, the C=C stretch mode is found at 1650 cm^{-1}. In aromatic rings like benzene, the C-C stretch mode is seen at 1600 cm^{-1} and 1490 cm^{-1}.

Typical Raman spectra for various C-implanted GaAs and C-doped GaAs epitaxial layers are shown Fig. 4.21. The broad features centered near 1585 cm^{-1} and 1355 cm^{-1} are assigned to sp^2-bonded carbon. All of the samples in which these peaks appeared were annealed. These two peaks in the Raman spectra can be unambiguously identified as arising from C precipitates in the doped layer. Only bulk-like sp^2 bonded C can display such a Raman spectrum.

The detection limit for sp^2 bonded C in these experiments is estimated to be 0.25 monolayers of graphitic C which corresponds to an areal C density of 2.5×10^{14} cm^{-2}. This detection limit was determined from the Raman spectrum of single crystal graphite. A Raman spectrum from a sample of highly ordered pyrolytic graphite was collected for 60 seconds. Using the measured peak area, the collection time, the laser power and the laser probe depth, the optical cross-section of graphite is calculated. This cross-section is then used to determine the areal C density in the GaAs samples.

Raman spectroscopy is a surface sensitive technique with probe depth in GaAs of 55 nm. C contamination of the surface presents the principal difficulty in analyzing the Raman spectra in these experiments. A few GaAs substrates which were annealed had small C-C peaks in the Raman spectrum. Careful cleaning procedures for the samples and

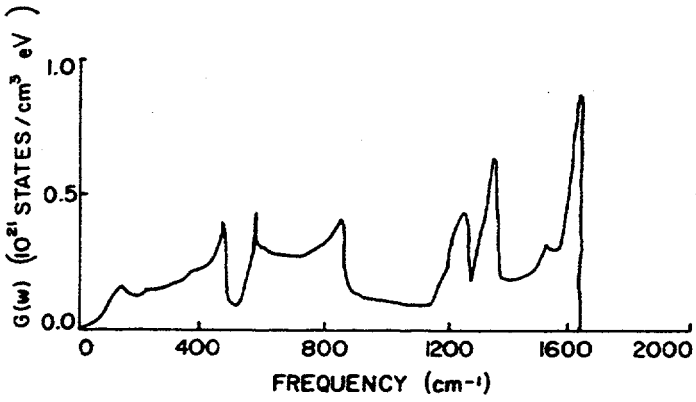

Figure 4.20. Graphite phonon density of states.(Dillon, et al., 1984)

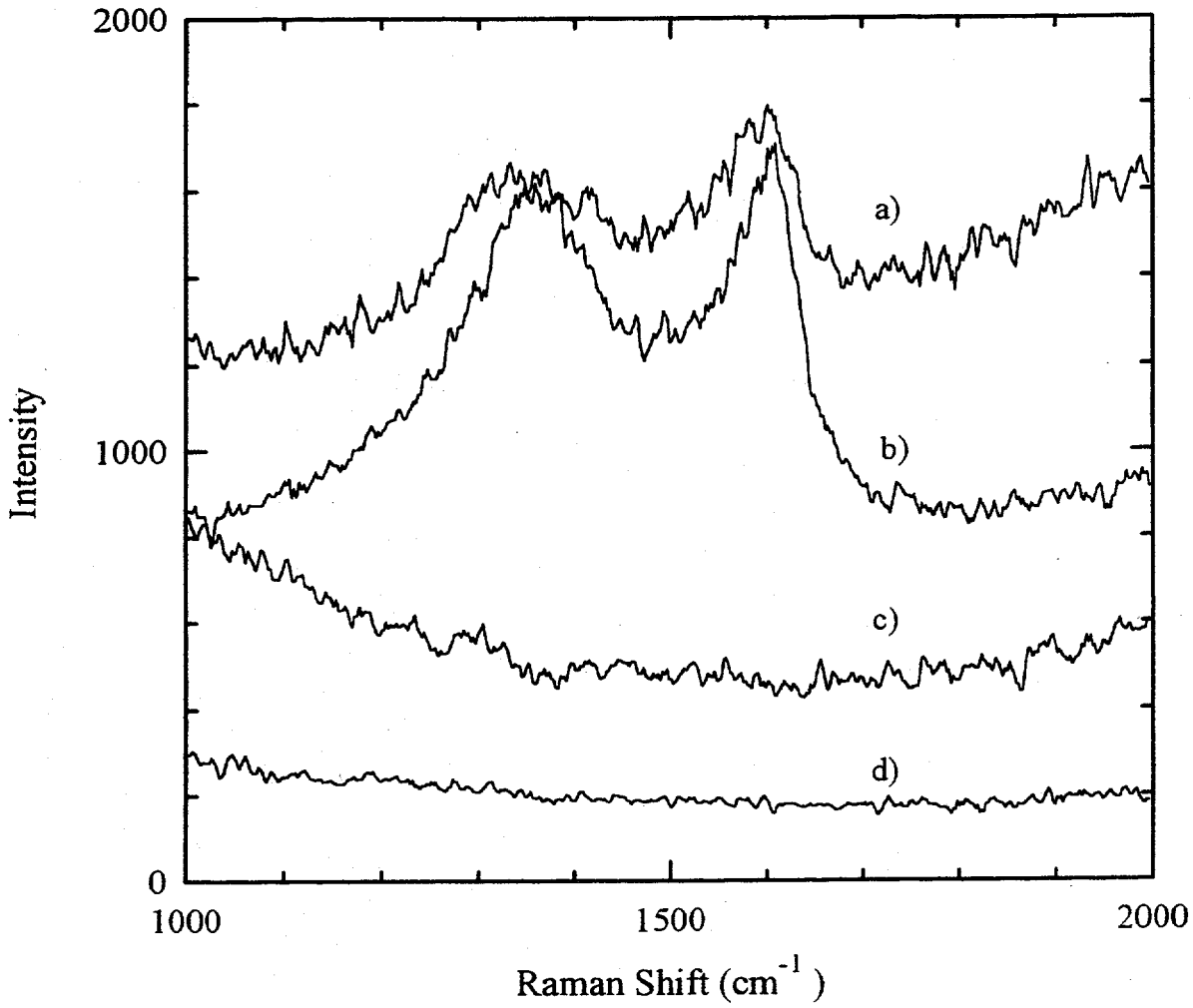

Figure 4.21. Raman spectra of carbon precipitates in GaAs for the following samples: a) C implanted and annealed, b) MOMBE-grown and annealed, c) implanted and not annealed, and d) annealed substrate.

cleaning and etching of the quartz chamber in the RTA and the ampoules used for furnace anneals eliminated this problem.

To study the affect of C contamination on the interpretation of the Raman results, several additional samples were characterized as described in Table 4.3. A piece of the GaAs substrate was processed and rapid thermally annealed in the same manner as the C implanted samples. The Raman spectrum for this sample is shown in Fig. 4.21(d). A second piece of the same substrate was implanted with Zn and annealed using the same annealing schedule. Neither of these samples exhibited any Raman peaks in the region from 1300 to 1600 cm^{-1}. Also, a sample which had been implanted with C but not annealed (Fig. 4.21c) did not exhibit any peaks in this region. However, all the samples which had been doped with carbon and annealed exhibited two Raman peaks centered near 1585 cm^{-1} and 1360 cm^{-1}.

As mentioned above, the most difficult part of this experiment is eliminating C contamination during the annealing. To completely eliminate the possibility that the Raman signal was caused by C contamination, GaAs samples were implanted with ^{13}C using the same implant conditions described above. The Raman spectra for samples implanted with ^{12}C and ^{13}C are shown in Fig. 4.22. In the samples implanted with ^{13}C the two peaks are shifted to lower frequency by 4% ($\sqrt{12/13}$) as expected. Therefore, the Raman peaks can only be a result of the C clustering of implanted C and not from environmental contamination.

The size of the C precipitates can be estimated from the Raman spectra by comparison to amorphous C films which have been studied extensively.(Robertson, 1991) The intensity ratio of the D- and G- bands, the I_d/I_g ratio is a function of sp^2 domain size in disordered graphite. An inverse relationship has been found between domain size, L_a, and I_d/I_g ratio in microcrystalline graphite by Tuinstra and Koenig:(Tuinstra & Koenig, 1970)

$$L_a(nm) = 4.4\ (I_d/I_g)^{-1}.$$

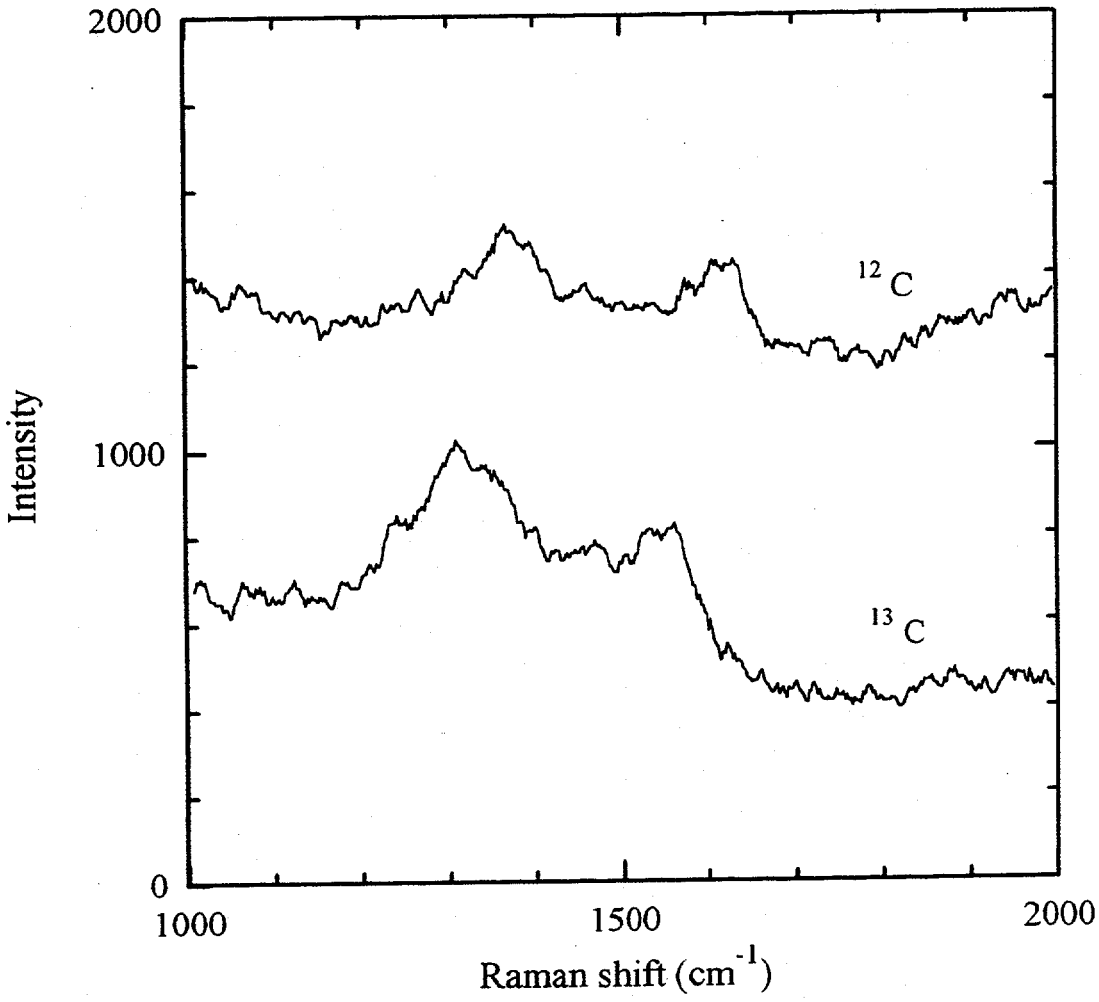

Figure 4.22. Raman spectra of C precipitates in GaAs implanted with either ^{12}C or ^{13}C.

(The Raman spectrum of single crystal graphite is a single "G-band" peak at 1580 cm^{-1}, i.e., $I_d/I_g = 0$.) This relationship breaks down with the very small domain sizes (<ca. 2 nm) found in a-C films grown at room temperature by sputtering or by chemical vapor deposition techniques. Dillon et al.(Dillon, et al., 1984) studied the Raman spectra of ion-beam-deposited films as a function of annealing temperature and concluded that they could use the Tuinstra and Koenig relationship to deduce the sp^2 domain size for films annealed above 800 °C. The spectra observed in this study are nearly identical to those observed by Dillon from ion-beam films annealed at 900 °C. The I_d/I_g ratios in the C doped samples (computed using the peak heights) are in the range of 0.8 to 1.0. Using the Tuinstra and Koenig relationship, the C precipitates have an average sp^2 domain size of 5 nm.

A simple, rough estimate of the minimum diffusion coefficient required for a C precipitate to form can be calculated. The interatomic spacing of graphite is 0.142 nm and therefore a particle 5 nm in diameter would contain approximately 750 carbon atoms, assuming the precipitate is a monolayer of graphite. In the GaAs sample implanted with C at 80 keV and at a dose of 1×10^{15} cm^{-2} the peak C concentration as calculated using the Profile code(Corporation,) is 6×10^{19} cm^{-3}. Given this concentration a volume of 1.2×10^{-17} cm^3 will contain 750 C atoms, and the C must diffuse 14 nm during the annealing to create the precipitate. Given the annealing conditions of 950°C for 10 s the diffusion coefficient required for precipitate formation can be estimated by:

$$x = (Dt)^{1/2}. \qquad [4.1]$$

D is then approximately 2×10^{-13} cm^2/s. You et. al.(You, et al., 1993) reported a diffusion coefficient of 7.8×10^{-15} cm^2/s for C diffusion in an As-rich atmosphere at 960 °C. The implanted layers can be considered to be As rich since implantation of C which occupies an As site disturbs the stoichiometry of the crystal towards the As rich condition. However the diffusion coefficient calculated here is more than 10 times higher than that of You. Two possible explanations exist for this effect.

First, diffusion is enhanced either by loss of group V elements at the surface or by radiation damage in the crystal due to the implantation process. To examine the role of the surface in the precipitation of C, two GaAs samples with the same concentration of implanted C were rapid thermally annealed. One sample was capped using the proximity method. The second was not capped. The surface of the second sample was noticeably degraded due to the loss of As. In this sample the C-C peaks were more intense. This result suggests that the loss of the group V element near the surface enhances precipitation.

Another possibility for the larger diffusion coefficient compared to those reported in the literature relates to the method of determining this quantity. In general, diffusion coefficients are determined with the use of SIMS. SIMS experiments do not give any information on the bonding configuration of the C. Therefore, these experiments do not take into account C diffusion to a precipitate within the C doped layer. C in a precipitate has not diffused beyond the original doped layer so this movement is not detected by SIMS.

You et al.(You, et al., 1993) studied C diffusion in MOCVD GaAs layers and $Al_{0.4}Ga_{0.6}As$/GaAs superlattices. In order to obtain satisfactory fits of the free hole concentration profiles after annealing both C_{As}^- diffusion and C_{As}^- reduction had to be considered. The fits presented were obtained with a diffusion equation which included a term describing hole reduction:

$$\frac{\delta C_s}{\delta t} = D_s \frac{\delta^2 C_s}{\delta x^2} - K C_s^2 \qquad [4.2]$$

where C_s is the concentration of C_{As}^-, D_s is the diffusivity of C_{As}^-, and K is the reduction coefficient of C_{As}^-. At 960°C, D_s was calculated to be 7.8×10^{-15} cm^2s^{-1} and K was found to be 5.3×10^{-23} cm^3s^{-1} for annealing in an As rich environment. The diffusion of C within the implanted or epitaxial layer in this work would not be considered in You's analysis as contributing to the diffusivity of C_{As}^- but rather to the reduction of C_{As}^-.

Furthermore, You et al. found that the diffusivity and reduction coefficient were dependent on the As_4 overpressure during annealing Annealing in As rich conditions resulted in a significant decrease in the free hole concentration. The hole concentration remained the same following annealing under Ga rich conditions. Analysis of the hole reduction resulted in extracted K values which were approximately proportional to $P_{As_4}^{1/4}$. Further analysis of the hole reduction data led them to conclude that the C_{As}^- reduction mechanism was due to a precipitation process. They further state that a C_{As}^- precipitation process is consistent with the fact that while p decreases in annealing, the net carbon concentration has practically not changes. You's results corroborate the mechanism of precipitation described in this thesis, and suggest that the diffusion to a precipitate is not included in typical measurements of the diffusion coefficient.

Although the above calculation was done with a monolayer of graphite, it is unlikely that the precipitates have this crystallographic form. A more accurate description of the precipitates is likely to be C clusters with sp^2-bonds. The clusters would be difficult to identify using diffraction since they have no long range order.

In conclusion, direct evidence of C precipitates in GaAs has been shown The Raman peaks are clearly not due to C contamination but come from the intentionally doped C. The precipitates are present in both implanted layers and epitaxially grown layers. Clearly this result raises further questions such as: the formation kinetics, the concentration of C in the precipitates, and the correlation of precipitate formation with activation. The Raman peaks are proportional to the amount of C which is in the precipitate so relative measurements can be made. However, unless the Raman cross-section is known, it is not possible to derive an absolute measurement. TEM measurements correlated with the Raman measurements would allow a quantitative determination of the amount of C in the precipitates

An experiment could be designed which would quantify the amount of C in precipitates and the effect of precipitation on the electrical characteristics of C doped

GaAs. Samples doped at similar levels by epitaxial growth and by implantation would be annealed using a series of annealing schedules. The samples would then by characterized with Raman spectroscopy, LVM spectroscopy, TEM, and electrical measurements. Correlating the $[C_{As}]$, hole concentration and precipitation as a function of the processing parameters would provide a clearer picture of the effects of precipitation. The formation kinetics of the precipitates could also be determined. Such information would be particularly useful to those using C doping for devices. This would make a great project for a future (present) graduate student. I had fully expected to perform this experiment however I underestimated the tenacity of C contamination and spent 6 months trying to eliminate it instead of performing this work.

4.2.2 Compensation by native defects

Precipitation clearly accounts for at least a portion of the inactive C in implanted and epitaxial GaAs:C. The existence of precipitates can account for the reduction in free hole concentration and the decrease in strain in annealed epitaxial layers. However, the decrease in mobility cannot be explained by precipitation. In degenerately doped semiconductors, mobility is inversely proportional to the number of ionized impurities. Precipitation reduces the number of ionized impurities hence the mobility should increase. Evidently, precipitation is not the sole contributor to the decrease in free hole concentration.

In this section the role of native defects in reducing the free hole concentration and mobility in GaAs:C will be examined. In implanted layers, radiation damage provides an abundant source of defects. In annealed epitaxial layers, the precipitation of C can also create defects. C which moves from an As site to a precipitate will create an As vacancy. The accommodation of the precipitate in the lattice can also create defects. A model

developed by Walukiewicz(Walukiewicz, 1988b) indicates that native defects will form complexes and change their electrical character to compensate intentional dopants. This reaction is controlled in part by the Fermi level stabilization energy which is an intrinsic property of the material.

The Fermi level stabilization energy, E_{FS} is determined by the Fermi-level position at metal semiconductor interfaces and the Fermi energy in heavily irradiated III-V compound and column IV semiconductors. The native defects created by electron irradiation damage cause the Fermi level to shift towards an ultimate position which is an intrinsic property of the material. That is, further irradiation does not cause the Fermi level to shift any further. A similar energy level at the metal-semiconductor interface is deduced from Schottky barrier heights. The deposition of more than a monolayer of metal causes the Fermi level to be pinned at the surface of the semiconductor. The observed Schottky barrier heights are determined by this pinning position and are only weakly dependent on the choice of metal. This level is found to be the same as the ultimate Fermi level (E_{FS}) measured following irradiation. Therefore it is determined that this level is an intrinsic property of the material. In Fig. 4.23 the band gaps and Fermi level stabilization energies are plotted for most of the III-V semiconductors.

The total energy required to form a native defect consists of the energy of structural change in the lattice and the electronic energy associated with changing the charge state of the defect. The electronic part of the energy depends on the location of defect levels relative to the Fermi level. Native defects within a III-V semiconductor can change their electrical character by forming complexes with other native defects, with intentional dopants, or with residual contaminants. In n-type GaAs, V_{Ga} has been found to be a stable defect but it transforms to a donor complex, $As_{Ga} + V_{As}$, in p-type material. Similarly V_{As} is a stable donor in p-type material, whereas $Ga_{As} + V_{Ga}$ is a stable acceptor in n-type crystals. The concentration of simple native defects is controlled by the following defect reactions

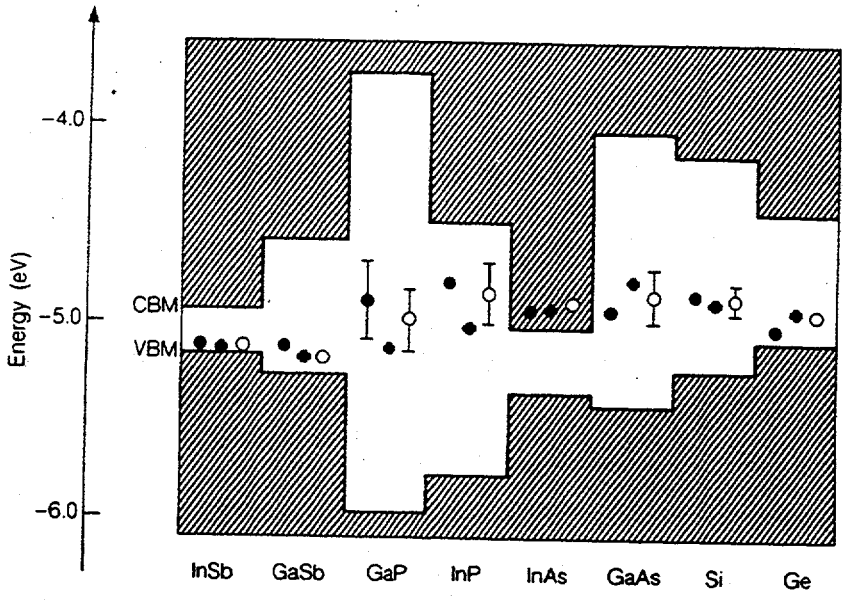

Figure 4.23. Position of the Fermi level stabilization energy deduced form the Fermi energy position in heavily irradiated semiconductors and from the Schottky barrier heights of metal-semiconductor interfaces.(Walukiewicz, 1988b)

$$As_{As} + V_{Ga} \longleftrightarrow As_{Ga} + V_{As} \qquad [4.3]$$

and

$$Ga_{As} + V_{Ga} \longleftrightarrow V_{As} + Ga_{Ga}. \qquad [4.4]$$

The transformation form acceptor-like defects on the left hand side of the above equations to donor-like defects on the right hand side requires only a single jump of an arsenic or gallium atom to one of the nearest neighbor sites.

The Fermi level stabilization energy is found to play a fundamental role in ion implantation experiments. In semiconductors where E_{FS} is located close to the conduction band, higher implant activation efficiencies are reported for donor-type impurities compared to acceptor type dopants. The opposite is true when E_{FS} is located near the valence band. An extreme case is that of InAs which is very difficult to dope it p-type. Implantation of virtually any element results in an n-type layer. This fact is a consequence of the position of E_{FS} which lies within the conduction band.

In heavily C doped GaAs, the Fermi level lies in or near the valence band. The Fermi level stabilization energy is found approximately 0.6 eV above the valence band. Therefore the energy of formation of donor-type defects is decreased by at least 0.6 eV. During annealing, As vacancies are created when C atoms move from substitutional sites to a precipitate. As vacancies are reported to be donors in p-type material. The C precipitate itself must displace part of the lattice creating native defects. In implanted semiconductors defects created during implantation will rearrange during annealing to form n-type complexes. Therefore, in both epitaxial growth and implantation, native defects are present in sufficient concentrations during annealing and the formation energy of donor defects is low enough that sufficient donor defects will form to affect the net carrier concentration.

Experimental evidence for the existence of native defects can be found in the measurement of the mobility and in PL experiments. GaAs epitaxial layers heavily doped with C and annealed exhibit a reduction in hole mobility as well as a reduction in free hole concentration. (Fig. 2.4 and 2.5). In the C implantation experiments described in Section 4.1.1 the 77K hole mobility for the C+Al, C+Ga, and C+Kr samples was compared. (Fig. 4.8) The Al+C and Kr+C had similar free hole concentrations however the C+Kr sample had a higher $[C_{As}]$ as measured by Raman LVM spectroscopy. The mobility of the C+Kr sample is significantly lower than the C+Al sample indicating the presence of compensating donor defects.

These defects may also be responsible for the increased PL intensity reported for annealed epitaxial layers and seen in the implantation studies described here. The PL spectrum for C+Kr samples is shown in Fig. 4.9. This spectrum is remarkably similar to those published by Watanabe(Watanabe & Yamazaki, 1991) (Fig 2.6) Watanabe's PL spectrum was recorded with heavily C-doped MOCVD layers ($p=1.3\times10^{20}$ cm^{-3}) annealed at 850°C. Both the MOCVD epitaxial layer and the C+Kr implanted layer exhibit a large broad peak centered around 1100 nm in their PL spectra.

The striking similarity between the results of precipitation experiments and PL experiments on both implanted and epitaxial GaAs:C layers suggest that the limitations in C doping of GaAs are inherent to this system and not particular to the doping technique. At low and moderate doping levels ([C]<1×10^{18} cm^{-3}) C readily incorporates as an acceptor in GaAs. Implants can be acceptably activated (>50%) and epitaxial layers are thermally stable. Slightly higher doping levels (1×10^{18} cm^{-3}<[C]<5×10^{19} cm^{-3}) require a Ga co-implant to activate more than 10% of the implanted C. Precipitation occurs in implanted layers at these doping levels which reduces the activation. The diffusion of C in implanted layers may be enhanced by radiation damage. Compensation by donor defects which are present due to radiation damage also limits the concentration of free holes. These intermediate doping levels are readily attained in epitaxial growth, and the layers are thermally stable.

Above doping levels of 5×10^{19} cm^{-3}, doping of GaAs with C becomes more difficult. Implantation is unsuccessful above this concentration. Doping levels higher than this can be achieved through non-equilibrium epitaxial growth, however these layers are not thermally stable. The solid solubility of C is exceeded, and the C will precipitate during annealing. The precipitation process decreases the $[C_{As}]$ and reduces the strain in the epitaxial layers. Precipitation also occurs in implanted layers. As well as precipitation, the free hole concentration is further reduced in both implanted and epitaxial layers through compensation by native defects.

4.3 InP:C

It is now appropriate to apply what has been learned about C doping of GaAs to other III-V compound semiconductors. As described in Chapter 2, the behavior of C in InP is very different than its behavior in GaAs. Implanted C substitutes for In and acts as

an donor however its activation is very low and co-implants seem to have little effect.(Pearton, et al., 1989) To compare the behavior of C in InP with that of the behavior in GaAs several C implants were performed.

InP substrates were solvent cleaned, and implanted with singly ionized C ions using the implantation conditions shown in Table 4.4. Following implantation of C, the co-implant was performed for individual samples. The co-implants were performed with the wafer held at room temperature or with the sample holder cooled with liquid nitrogen. The substrate temperature during low temperature implantations was held at 108 K. Following implantation, the samples were rapid thermally annealed.

Carrier concentration, mobility, and resistivity were determined by van der Pauw geometry Hall effect measurements. The activation is then determined by dividing the sheet free carrier concentration (holes) by the implanted dose. The amount of structural damage caused by the implantation was characterized by channeling RBS. Raman spectroscopy and FTIR spectroscopy were performed on selected samples

All of the implanted layers are n-type following annealing however the activation efficiencies are very low. Electrical data for all of the samples are presented in Table 4.4 In the series of three samples implanted with C at 40 keV at a dose of 5×10^{14} cm^{-2}, the activation was not higher than 5%. The results are not consistent, and P co-implantation seems to have little effect on the activation. When the P is implanted at room temperature the activation is worse than in the C only case. Low temperature implantation of P causes the activation to increases slightly.

Another series of samples was implanted with a slightly higher dose of C (7×10^{14} cm^{-2}) at twice the energy (80 keV). These implantation parameters result in a concentration profile (Fig. 4.25) with a peak concentration 3.6×10^{19} cm^{-3} of at 189 nm. P co-implants were performed at both room temperature and with the sample cooled by liquid nitrogen. In all cases activation is less than 1% regardless of the temperature of implantation or the use of a co-implant.

Table 4.4. Implantation parameters for InP. All samples are rapidly thermally annealed at 850°C.

Implant Parameters				Anneal-ing Time	Free Electron Conc.	Activ-ation	Resis-tivity	Mobil-ity
Ion	Energy (keV)	Dose $\times 10^{14}$ (cm-2)	Temp.	(s)	(cm-2)	(%)	(Ω cm)	($cm^2 \times V^{-1}s^{-1}$)
C	40	5	RT	10	1.7×10^{13}	3.4	3.5×10^{2}	1055
C+	40	5	RT	10	7.6×10^{10}	0.0	6.9×10^{4}	1202
P	90	5	RT					
C+	40	5	RT	10	2.7×10^{13}	5.2	4.5×10^{3}	51
P	90	5	LN					
C	80	7	RT	5	2.8×10^{12}	0.4	1.7×10^{3}	1361
C	80	7	RT	10	5.8×10^{12}	0.7	7.2×10^{3}	150
C+	80	7	RT	5	8.2×10^{9}	0.0	1.3×10^{6}	608
P	170	7	RT					
C+	80	7	RT	10	4.9×10^{8}	0.0	2.3×10^{7}	550
P	170	7	RT					
C+	80	7	RT	5	9.1×10^{8}	0.0	8.4×10^{6}	818
P	170	7	LN					
C	30	20	RT	10	3.9×1012	0.2	2.2×10^{3}	738
C	30	20	RT	60	1.7×1012	0.1	6.9×10^{3}	530
C	40 +	3.5 +	RT	10	5.5×10^{12}	0.2	1.8×10^{3}	620
	80 +	4.5 +		10	2.1×10^{12}	0.1	7.9×10^{2}	3670
	120 +	5 +		60	1.9×10^{12}	0.1	9.3×10^{2}	3510
	160 +	6 +		300	2.0×10^{12}	0.1	8.6×10^{2}	3540
	200	7						
C	40 +	3.5 +	LN	10	8.6×10^{11}	0.03	2.8×10^{3}	2600
	80 +	4.5 +		10	7.8×10^{11}	0.03	3.1×10^{3}	2640
	120 +	5 +		60	3.6×10^{11}	0.02	6.6×10^{3}	2570
	160 +	6 +		300	4.0×10^{11}	0.02	7.8×10^{3}	1995
	200	7						

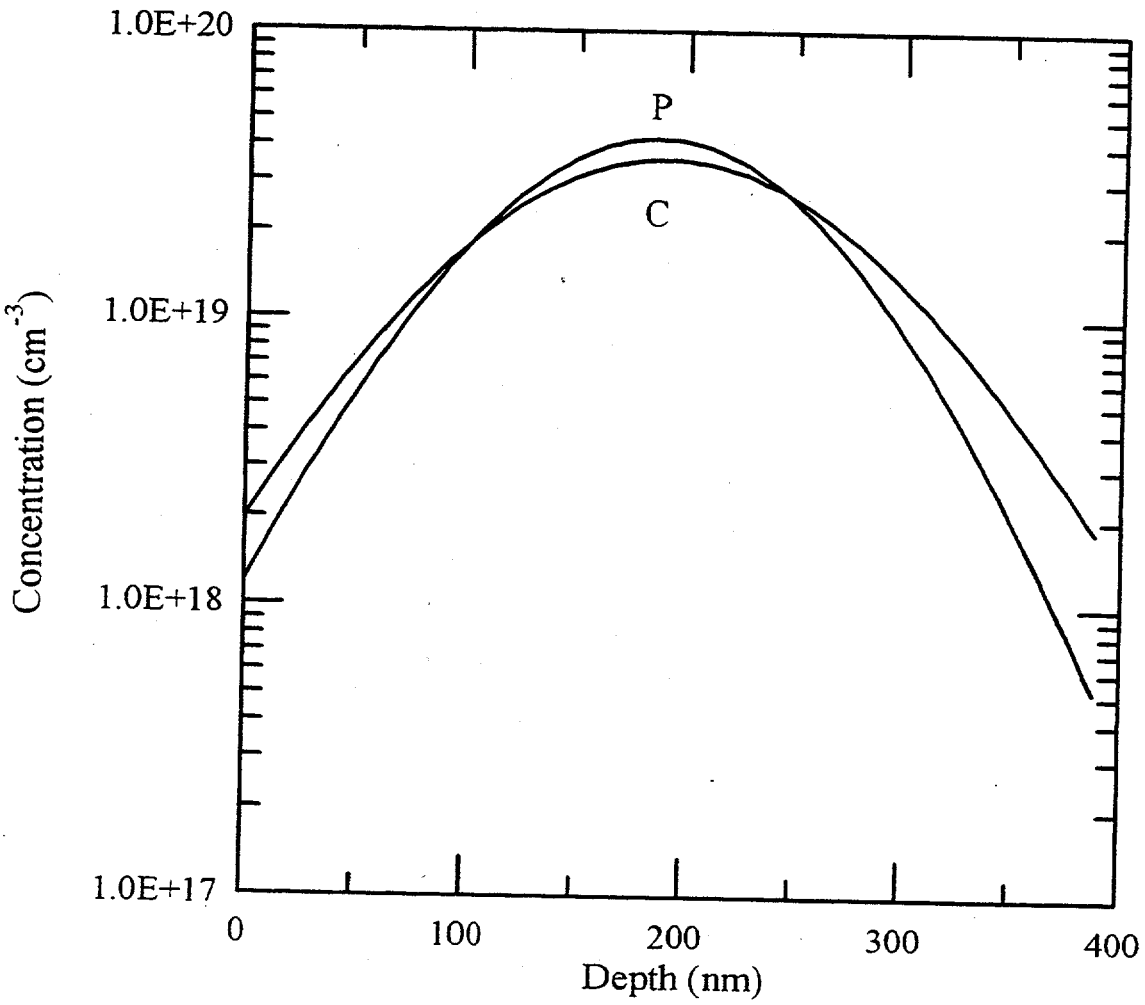

Figure 4.25. Theoretical ion profiles for C and P implantation into InP.

It is difficult to draw conclusions from this data since the results are inconsistent. The lattice location of the implanted C remains unknown. Is the C occupying substitutional sites? Is the C self-compensating, i.e., substituting for both In and P atoms? The electron mobility is one measure of the compensation in the implanted layer. Again the results are inconsistent. In the samples which were implanted with a C dose of 7×10^{14} cm^{-2}, the carrier concentration doubles from 2.8×10^{12} cm^{-2} to 5.8×10^{12} when the sample is annealed for 10 s instead of 5 s. While the carrier concentration doubles, the mobility drops by almost a factor of 10 from 1361 to 150 cm^2/Vs. If the mobility is inversely proportional to the number of ionized impurities then the mobility should be approximately 700 cm^2/Vs in the more active sample.

LVM spectroscopy is a direct measure of the concentration of substitutional dopants. The detection limit for FTIR experiments on the C_{As} LVM in GaAs is approximately 1×10^{14} cm^{-2}. To increase the probability of detecting a C LVM in InP, a heavily C doped layer was formed by implantation. A series of ^{12}C implants at various energies was performed to achieve a uniformly C doped layer, $[C] = 6\times10^{19}$ cm^{-3}, approximately 600 nm thick. (Fig. 4.26) The total dose of C was 2.6×10^{15} cm^{-2}. To detect the LVM in this sample at least 5% of the C must occupy an In site.

The samples were examined using FTIR spectroscopy to look for the C_{In} local vibrational mode. The $^{10}B_{In}$ LVM has been reported at 544 cm^{-1} and the $^{11}B_{In}$ has been found at 523 cm^{-1}. A simple ball and spring model would suggest that $^{12}C_{In}$ would be seen in the between 480 and 520 cm^{-1} if it existed. No peaks which could be attributed to C_{In} LVM were seen in either sample in the range from 460 to 520 cm^{-1} as shown in Fig. 4.27. This result suggests that C does not incorporate onto substitutional sites in InP.

It is possible that the $^{12}C_{In}$ LVM exists at a frequency similar to that of a 2nd order phonon in InP. If this is the case, the C_{In} LVM would not be detectable since the phonon absorption would mask any additional absorption by the LVM. As seen in Fig. 4.27, a large peak is present at 503 cm^{-1} in the absorbance spectrum of InP which

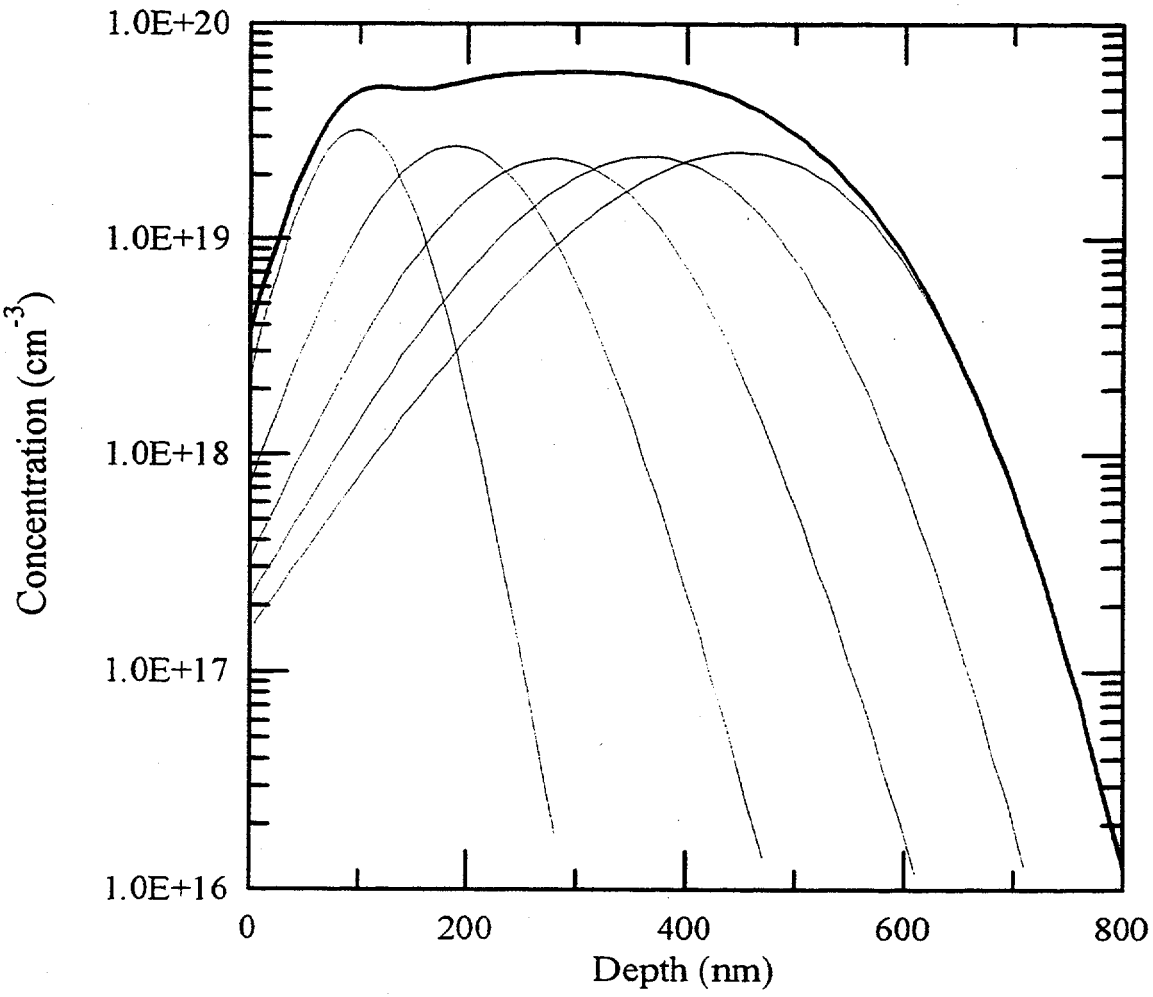

Figure 4.26. Theoretical concentration profile of C in InP with the following implantation schedule: 200 keV, 7×10^{14} cm^{-2}; 160 keV, 7×10^{14} cm^{-2}; 120 keV, 7×10^{14} cm^{-2}; 80 keV, 7×10^{14} cm^{-2}; 40 keV, 7×10^{14} cm^{-2}.

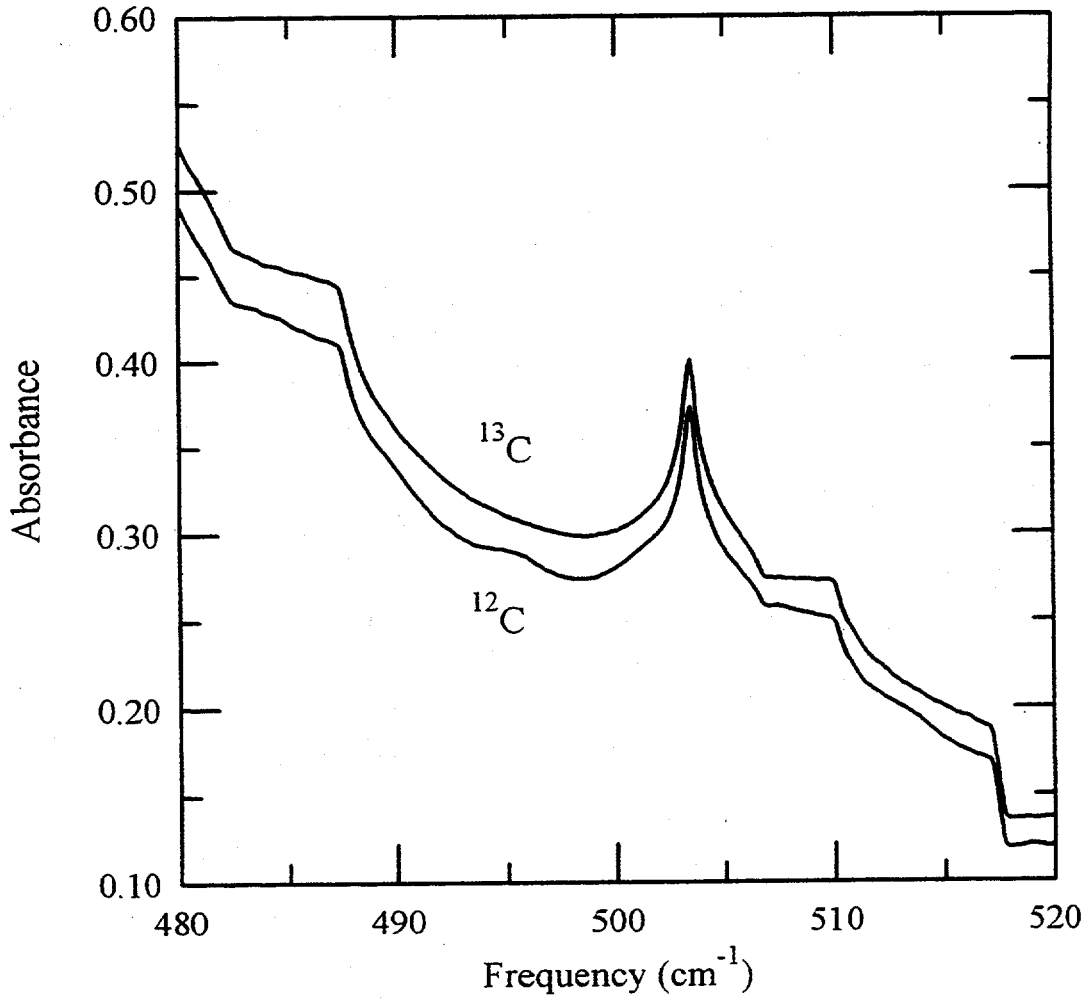

Figure 4.27. FTIR spectra of InP implanted with ^{13}C and ^{12}C.

corresponds to a second order phonon. This frequency is close to what would be expected for the $^{12}C_{In}$ LVM. Therefore the same experiment was performed with ^{13}C The same implantation schedule was used to implant samples with ^{13}C. No additional peaks were found in these experiments.

LVM experiments indicate that less than 5% of the implanted C are substitutional in InP. The C must then occupy other lattice sites within the crystal. One possibility is C precipitation as seen in GaAs. The Raman spectra for all of the C implanted InP exhibited the two characteristic peaks indicating that C precipitates form in the implanted layers.(Fig. 4.28) Comparison of GaAs and InP samples implanted with the same doses and energies of C suggests that precipitates form more readily in InP. At lower doses of C ([C] = 5×10^{14} cm^{-2}) precipitates were not seen in GaAs samples but still were seen in InP samples. Therefore a likely explanation for the behavior of C in InP is that it does not incorporate into substitutional sites easily. That is, C has a low solid solubility in InP and easily forms precipitates. The low solubility hypothesis is reinforced by the difficulty in doping InP with C during epitaxial growth. C doping is only successful at very low growth temperatures where the growth process is far from equilibrium.

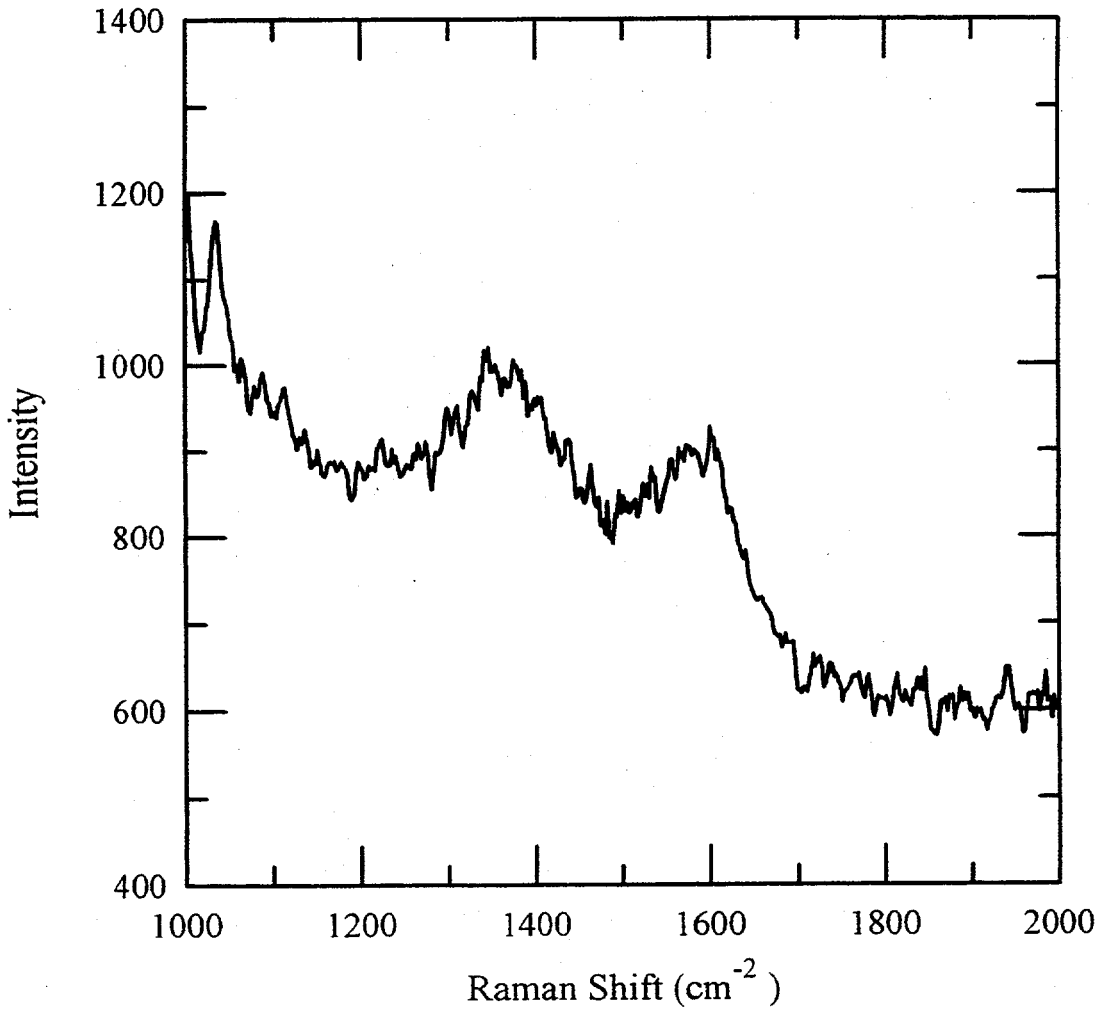

Figure 4.28. Raman spectrum of C precipitates in implanted InP.

4.4 A model to describe the behavior of carbon in III-V semiconductors

A phenomenological description of the behavior of C in III-V semiconductors will be presented in this section. This description is based on the data presented in this thesis and the data reported in the literature. The contribution of two factors to the lattice site of C will be detailed. These two factors are the chemical nature of the C atom and the Fermi level stabilization energy of the particular III-V semiconductor. In general, additional factors affect the substitutional site of impurities in compound semiconductors. These factors include the size of the dopant atom relative to the size of the host atoms and the natural valence of the dopant atom (i.e., a group II atom readily substitutes for a group III host atom but is not expected to substitute for a group V host atom)

C is a highly electronegative element. Its electronic configuration is $1s^2 2s^2 2p^2$. The lack of a full p shell contributes to its electronegativity. One definition of electronegativity is the ability of the atom to bind another electron in a covalent bond. The larger the electronegativity of an element the more strongly an atom of that element attracts electrons. On a scale in which the electronegativity of the elements range from 0.9 (K, Rb, and Cs) to 4.1 (F), C has an electronegativity of 2.5.

Pearson(Pearson, 1988) has proposed a scale of absolute electronegativity which is defined as the average of the first ionization energy and the electron affinity of the neutral atom. In this scale electronegativity refers to the potential of an atom to attract electrons to itself. On a scale in which electronegativity ranges from 0 to 10.41 eV, the electronegativity of C is 6.27 eV.

On either scale, the high electronegativity of C indicates it would prefer to act as an acceptor and bind an additional electron rather than act as a donor and contribute an electron to the conduction band. Si which has an electronegativity of 1.7, readily acts as a donor in most III-V compounds. Considering only the chemical nature of the dopant, C is expected to act as an acceptor, occupying the group V site.

Next consider the intrinsic properties of the particular semiconductor. In Section 4.2.3 the influence of the Fermi level stabilization energy on the formation of native defects was described. If E_{FS} is closer to the conduction band, all other things being equal, the material would prefer to be n-type. If E_{FS} is closer to the valence band then the material prefers to be p-type. Therefore, E_{FS} will influence the substitutional site of any dopant which is in principle amphoteric.

These two factors either cooperate or compete to determine the behavior of C. If E_{FS} is near the valence band, the material prefers to be p-type, then C is expected to be a very efficient acceptor. Clearly, experimental evidence reinforces this view. In Fig. 4.20, E_{FS} is plotted in the majority of the III-V compound semiconductors. In GaAs, GaP, and AlAs, E_{FS} is below midgap, and very high free hole concentrations can be achieved with C doping. In contrast, if E_{FS} is near the conduction band, these two factors oppose each other, and efficient doping with C cannot be expected. Again, experimental evidence supports the model. In InP and InAs where E_{FS} is near the conduction band, C acts as a very inefficient donor.

To more clearly illustrate this point consider the introduction of C into GaAs and InP as an acceptor. Assume that both crystals are p-type with a free hole concentration of 1×10^{19} cm^{-3}. At this free hole concentration, the Fermi level will be approximately at the top of the valence band. Next add one more C acceptor to these two crystals. The following reactions occur:

$$C^0 + V_{As}^{2+} \longrightarrow C_{As}^{-} + 3h^{+}, \qquad [4.5]$$

and

$$C^0 + V_{P}^{2+} \longrightarrow C_{P}^{-} + 3h^{+}. \qquad [4.6]$$

In GaAs the Fermi level stabilization energy (E_{FS}) is approximately 0.6 eV above the valence band. In InP E_{FS} is approximately 1.0 eV above the valence band. Therefore

$$E_{FS}(InP) = E_{FS}(GaAs) + 0.4eV. \qquad [4.7]$$

The energy of substitution for one C atom on a group V site is then 1.2 eV (3×(0.4eV)) more costly in InP than in GaAs. Hence, C is more likely to act as an acceptor in GaAs than in InP.

This model becomes even more interesting when applied to ternary compound semiconductors such as GaInP and GaInAs where the two pure binary compounds have very different E_{FS} levels. As reported in Chapter 2, the addition of more than 5% InP to GaP causes the free hole concentration to drop significantly. In GaInAs the material converts from p-type to n-type at a mole fraction of about 50% InAs.

The qualitative behavior of C can be described as follows. Due to the chemical nature of C, it prefers to occupy the group V site. If E_{FS} is below midgap, C will be a very efficient p-type dopant. In semiconductors where E_{FS} is above midgap, C cannot be easily incorporated and will be an inefficient donor. In these cases, either C will not incorporate or if already present due to a nonequilibrium process, it will readily precipitate during annealing.

5. Conclusions

Reproducible high activation of C implanted in GaAs has been achieved with a Ga co-implantation. Activation levels above 60% can be reproducibly attained with bulk concentrations approaching 5×10^{19} cm^{-3}. A likely application for this process may be found in the fabrication of nonalloyed contacts. A simple masking procedure would allow the implantation to be performed in a well-defined area. It is unlikely that implantation would replace C doping during epitaxial growth of more complicated structures such as HBTs or lasers. These devices can only be grown by epitaxial techniques and C doping is readily achieved in these techniques.

The mechanism by which the Ga co-implant increases C activation has been determined. The damage density due to implantation determines the concentration of implanted C atoms which substitute for As host atoms. The Ga co-implant also has a stoichiometric effect. Maintaining the stoichiometry within the implanted layers limits the concentration of compensating native defects. When the stoichiometry of the layer is not maintained, native defects will compensate a fraction of the C_{As} acceptors.

Direct evidence of C precipitation in GaAs and InP has been shown with Raman spectroscopy. Two peaks which are characteristic of sp^2 bonded C appear in both implanted C layers and epitaxial layers which have been annealed. Raman spectrocopy is a non-destructive characterization tool hence this technique provides an important new tool for determining the stability of C doping in all semiconductors.

The behavior of C in GaAs can be understood to be limited by the solid solubility of C which is approximately 5×10^{19} cm^{-3}. Above this concentration, the C precipitates. Furthermore, the presence of native defects compensates the C acceptors further reducing the electrical activation and the mobility. It is unlikely that C donors, lone C interstitials, 2

or 3 atom C complexes, or dislocations play a significant role in the electrical or structural behavior of C doped GaAs.

In InP, the behavior of C is found to be extremely different. C is an n-type dopant, occupying the In site, however its incorporation is difficult to control. Consistent results are hard to obtain with implantation. C precipitation as evidenced by Raman spectroscopy readily occurs in C implanted InP suggesting that C does not like to incorporate in the InP lattice.

The behavior of C in III-V semiconductors is controlled by the chemical nature of C and the intrinsic E_{FS} in the particular semiconductor. Due to its high electronegativity, C will readily occupy the group V site. If E_{FS} lies near the valence band, C acts as an efficient acceptor. When E_{FS} is near the conduction band, C does not readily incorporate in the material.

6. References

Abernathy, C. R., Pearton, S. J., Caruso, R., Ren, F., & Kovalchik, J. (1989). *Applied Physics Letters*, **55**(17), 1750 - 1752.

Abernathy, C. R., Pearton, S. J., & F.Ren (1990a). *Journal of Crystal Growth*, **105**, 375-382.

Abernathy, C. R., Pearton, S. J., Manasreh, M. O., Fischer, D. W., & Talwar, D. N. (1990b). *Applied Physics Letters*, **57**(3), 294.

Akatsuka, T., Miyake, R., Nozaki, S., Yamada, T., Konagai, M., & Takahashi, K. (1990). *Japanese Journal of Applied Physics*, **29**(4), L537-L539.

Ashen, D. J., Dean, P. J., Hurle, D. T. J., Mullin, J. B., White, A. M., & Greene, P. D. (1975). *Journal of the Physical Chemistry of Solids*, **36**, 1041.

Barthruff, D., Benz, K. W., & Antypas, G. A. (1979). *Journal of Electronic Materials*, **8**(4), 485-491.

Benchimol, J. L., Alaoui, F., Gao, Y., Le Roux, G., Rao, E. V. K., & Alexandre, F. (1990). *Journal of Crystal Growth*, **105**, 135-142.

Brozel, M. R., Foulkes, E. J., Series, R. W., & Hurle, D. T. J. (1986). *Applied Physics Letters*, **49**(6), 337.

Chan, Y. J., & Chen, C. H. (1993). *Applied Physics Letters*, **63**(8), 1092-1094.

Chen, H. D., Chang, C. Y., Lin, K. C., Chan, S. H., Feng, M. S., Chen, P. A., Wu, C. C., & Juang, F. Y. (1993). *Journal of Applied Physics*, **73**(11), 7851-7856.

Chin, T. P., Kirchner, P. D., Woodall, J. M., & Tu, C. W. (1991). *Applied Physics Letters*, **59**(22), 2865-2867.

Chiu, T. H., & Ditzenberger, J. A. (1990). *Applied Physics Letters*, **56**(22), 2219-2221.

Chiu, T. H., Tsang, W. T., Schubert, E. F., & Agyekum, E. (1987). *Applied Physics Letters*, **51**(14), 1109-1111.

Cockayne, B., Brown, G. T., & MacEwan, W. R. (1981). *Journal of Crystal Growth*, **54**, 9-15.

Csepregi, L., Kennedy, E. F., Mayer, J. W., & Signon, T. W. (1978). *Journal of Applied Physics*, **49**(7), 3906-3911.

Csepregi, L., Kullen, R. P., & Mayer, J. W. (1977). *Solid State Communications*, **21**, 1019-1021.

Cunningham, B. T., Baker, J. E., & Stillman, G. E. (1990a). *Applied Physics Letters*, **56**(9), 836-838.

Cunningham, B. T., Baker, J. E., Stockman, S. A., & Stillman, G. E. (1990b). *Applied Physics Letters*, **56**(18), 1760-1762.

Cunningham, B. T., Hasse, M. A., McCollum, M. J., Baker, J. E., & Stillman, G. E. (1989). *Applied Physics Letters*, **54**(19), 1905.

Davidson, B. R., Newman, R. C., Pritchard, R. E., Bullough, T. J., Joyce, T. B., Jones, R., & Oberg, S. (1993). *MRS Proceedings, Preprint.*

de Lyon, T. J., Buchan, N. I., Kirchner, P. D., Woodall, J. M., McInturff, D. T., Scilla, G. J., & Cardone, F. (1991a). *Journal of Crystal Growth*, **111**, 564-569.

de Lyon, T. J., Woodall, J. M., Kirchner, P. D., McInturff, D. T., Scilla, G. J., & Cardone, F. (1991b). *Journal of Vacuum Science Technology B*, **9**(1), 136.

Dillon, R. O., Woollam, J. A., & Katkanant, V. (1984). *Physical Review B*, **29**(6), 3482-3489.

Donnelly, J. P., & Ferrante, G. A. (1980). *Solid State Electronics*, **23**, 1151-1154.

Enquist, P., Hutchby, J. A., & de Lyon, T. J., (1988). *Journal of Applied Physics*, **60**(9), 4485-4493.

Enquist, P. (1990). *Applied Physics Letters*, **57**(22), 2348-2350.

Enquist, P. (1992). *Journal of Applied Physics*, **71**(2), 704-708.

Giannini, C., Fischer, A., Lange, C., Ploog, K., & Tapfer, L. (1992). *Applied Physics Letters*, **61**(2), 183-185.

Giannini, C., Gerardi, C., Tapfer, L., Fischer, A., & Ploog, K. H. (1993). *Journal of Applied Physics*, **74**(1), 77-81.

Guido, L. J., cunningham, B. T., Nam, D. W., Hsieh, K. C., Plano, W. E., Jr., J. S. M., Vesely, E. J., Sugg, A. R., N. Holonyak, J., & Stillman, G. E. (1990). *Journal of Applied Physics*, **67**(4), 2179-2182.

Guido, L. J., Jackson, G. S., Hall, D. C., Plano, W. E., & Holonyak, J., N. (1988). *Applied Physics Letters*, **52**(7), 522-524.

Han, W. Y., Lu, Y., Lee, H. S., Cole, M. W., Schauer, S. N., Moerkirk, R. P., Jones, K. A., & Yang, L. W. (1992). *Applied Physics Letters*, **61**(1), 87-89.

Hanna, M. C., Lu, Z. H., & Majerfeld, A. (1991). *Applied Physics Letter*, **58**(2), 164-166.

Hanna, M. C., & Majerfeld, A. (1991). *Applied Physics Letters*, **59**(16), 2001-2003.

Harris, J. S. (1971). The effects of dose rate and implantation temperature on lattice damage and electrical activity in ion implanted GaAs. In I. Ruge & J. Graul (Eds.), International Conference on Ion Implantation in Semiconductors (pp. 157). Berlin: Springer.

Haynes, T. E., & Holland, O. W. (1990). *Applied Physics Letters*, **59**(4), 452.

Haynes, T. E., & Holland, O. W. (1991a). *Applied Physics Letters*, **58**(1), 62-64.

Haynes, T. E., & Holland, O. W. (1991b). *Nuclear Instruments and Methods B*, **59/60**, 1028-1031.

Heckingbottom, R., & Ambridge, T. (1973). *Radiation Effects*, **17**, 31.

Hess, K., Stath, N., & Benz, K. W. (1974). *Journal of the Electrochemical Society*, **121**(9), 1208-1212.

Höfler, G. E., Höfler, H. J., Holonyak, N., & Hsieh, K. C. (1992). *Journal of Applied Physics*, **72**(11), 5318-5324.

Höfler, G. E., & Hsieh, K. C. (1992). *Applied Physics Letter*, **61**(3), 327.

Hoke, W. E., Lemonias, P. J., Weir, D. G., Hendriks, H. T., & Jackson, G. S. (1991). *Journal of Applied Physics*, **69**(1), 511-513.

Hunter, A. T., Kimura, H., Baukus, J. P., Winston, H. V., & Marsh, O. J. (1984). *Applied Physics Letters*, **44**(1), 74-76.

I. S. Corporation in Danvers, MA:

Iida, T., Makita, Y., Kimura, S., Winter, S., Yamada, A., Shibata, H., Obara, A., Niki, S., Fons, P., Tsai, Y., & Uekusa, S. (1993). *Applied Physics Letter*, **63**(14), 1951-1953.

Ilegems, M. (1977). *Journal of Applied Physics*, **48**(3), 1278-1287.

Ito, H., & Ishibashi, T. (1989). *1989 MRS Fall Meeting*.

Jewell, J. L., Harbison, J. P., Scherer, A., Lee, Y. H., & Florez, L. T. (1991). *IEEE Journal of Quantum Electronics*, **27**, 1332.

Jiang, H., Elliman, R. G., & Williams, J. S. (1994). *Journal of Electronic Materials*, **23**(4), 391-396.

Jones, R., Oberg, S., & Umerski, A. (1992). *Materials Science Forum*, **83-87**, 551.

Kamp, M., Contini, R., Werner, K., Heinecke, H., Weyers, M., Luth, H., & Balk, P. (1989). *Journal of Crystal Growth*, **95**, 154-57.

Kamp, M., Weyers, M., Heinecke, H., Luth, H., & Balk, P. (1990). *Journal of Crystal Growth*, **105**, 178-184.

Kibbler, A. E., Kurtz, S. R., & Olsen, J. M. (1991). *Journal of Crystal Growth*, **109**, 258-263.

Kobayashi, N., Makimoto, T., & Horikoshi, Y. (1987). *Applied Physics Letters*, **50**(20), 1435-1437.

Konagai, M., Yamada, T., Akatsuka, T., Nozaki, S., Miyake, R., Saito, K., Fukamachi, T., Tokumitsu, E., & Takahashi, K. (1990). *Journal of Crystal Growth*, **105**, 359-365.

Konagai, M., Yamada, T., Akatsuka, T., Saito, K., Tokumitsu, E., & Takahashi, K. (1989). *Journal of Crystal Growth*, **98**, 167-173.

Kopf, R. F., Schubert, E. F., Downey, S. W., & Emerson, A. B. (1992). *Applied Physics Letters*, **61**(15), 1820-1822.

Kuech, T. F., Wolford, D. J., Veuhoff, E., Deline, V., Mooney, P. M., Potemski, R., & Bradley, J. (1987). *Journal of Applied Physics*, **62**(2), 632-643.

Kushibe, M., Eguchi, K., Funamizu, M., & Ohba, Y. (1990). *Applied Physics Letters*, **56**(13), 1248-1250.

Lee, B. J., Houng, Y. M., & Miller, J. N. (1990). *Journal of Crystal Growth*, **105**, 168-177.

Leier, H., Marten, A., & Wolk, C. (1992). Highly carbon-doped AlGaAs/GaAs HBTs using otimized carbon implantation for the base contact. In International Symposium on GaAs and Related Compounds (pp. 699-704). Karuizawa: International Physics Conference Service.

Lindhard, J., Scharff, M., & Schiott, H. E. (1963). *Kfl. Danske. Videnskab. Selskab. Mat.-Fys. Medd.*, **33**(14).

Low, T. S., Skromme, B. J., & Stillman, G. E. (1983). *Inst. Phys. Conf. Ser.*, **65**, 515-522.

Makimoto, T., & Kobayashi, N. (1993). *Japanese Journal of Applied Physics*, **32**(9B), L1300-L1303.

Malik, R. J., Nottenberg, R. N., Schubert, E. F., Walker, J. F., & Ryan, R. W. (1988). *Applied Physics Letters*, **53**(26), 2661-2663.

McLevige, W. V., Vaidyanathan, K. V., Streetman, B. G., Ilegems, M., Comas, J., & Plew, L. (1978). *Applied Physics Letters*, **33**(2), 127-129.

Micovic, M., Evaldsson, P., Geva, M., Taylor, G. W., Vang, T., & Malik, R. J. (1994). *Applied Physics Letters*, **64**(4), 411-413.

Newman, R. C., Thompson, F., Hyliands, M., & Peart, R. F. (1972). *Solid State Communications*, **10**, 505.

Nozaki, S., Takahashi, K., Shirahama, M., Nagao, K., Shirakashi, J., & Tokumitsu, E. (1993). *Applied Physics Letters*, **62**(16), 1913-1915.

Paulson, W. M., & Tam, G. (1984). The characteristics of carbon implantes into semi-insulating GaAs. In D. C. Look & J. S. Blakemore (Eds.), Semi-Insulating III-V Materials 1984 (pp. 53-59). Shiva, Cheshire England:

Pearson, R. G. (1988). *Inorganic Chemistry*, **27**, 734.

Pearton, S. J., & Abernathy, C. R. (1989). *Applied Physics Letters*, **55**(7), 678.

Pearton, S. J., Chakrabarti, U. K., Abernathy, C. R., & Hobson, W. S. (1989). *Applied Physics Letters*, **55**(19), 2014.

Pearton, S. J., Hobson, W. S., Kinsella, A. P., Kovalchick, J., Chakrabarti, U. K., & Abernathy, C. R. (1990). *Applied Physics Letters*, **56**(13), 1263-1265.

Putz, N., Veuhoff, E., Heinecke, H., Heyen, M., Luth, H., & Balk, P. (1985). *Journal of Vacuum Science and Technology*, **B3**, 671.

Robertson, J. (1991). *Progress in Solid State Chemistry*, **21**, 199-333.

Sadana, D. K., Sands, T., & Washburn, J. (1984). *Applied Physics Letters*, **44**(6), 623.

Saito, K., Tokumitsu, E., Akatsuka, T., Miyauchi, M., Yamada, T., Konagai, M., & Takahashi, K. (1988). *Journal of Applied Physics*, **64**(8), 3975-3979.

Sansbury, J. D., & Gibbons, J. F. (1970). *Radiation Effects*, **6**, 269-276.

Schroder, R. E., Nemanich, R. J., & Glass, J. T. (1990). *Physical Review B*, **41**(6), 3738.

Shin, B. K. (1976). *Applied Physics Letters*, **29**(7), 438.

Shin, B. K., Ehret, J. E., Park, Y. S., & Stefinew, M. (1978). *Journal of Applied Physics*, **49**(5), 2988.

Skromme, B. J., Stillman, G. E., Oberstar, J. D., & Chan, S. S. (1984). *Applied Physics Letters*, **44**(3), 319-321.

Sohn, H., Weber, E. R., Nozaki, S., Konagai, M., & Takahashi, K. (1992). *Materials Research Society Symposium Proceedings*, **262**, 129-133.

Stockman, S. A., Fresina, M. T., Hartmann, Q. J., Hanson, A. W., Gardner, N. F., Baker, J. E., & Stillman, G. E. (1994). *Journal of Applied Physics*, **75**(8), 4233-4235.

Stockman, S. A., Hanson, A. W., & Stillman, G. E. (1992a). *Applied Physics Letters*, **60**(23), 2903-2905.

Stockman, S. A., Höfler, G. E., Baillargeon, J. N., Hsieh, K. C., Cheng, K. Y., & Stillman, G. E. (1992b). *Journal of Applied Physics*, **72**(3), 981-987.

Stringfellow, G. B., Koschel, W., Briones, F., Gladstone, J., & Patterson, G. (1981). *Applied Physics Letters*, **39**(8), 581.

Tamamura, K., Ogawa, J., Akimoto, K., Mori, Y., & Kojima, C. (1987). *Applied Physics Letters*, **50**(17), 1149-1151.

Temkin, H., & Bonner, W. A. (1981). *Journal of Applied Physics*, **52**(1), 397-401.

Theis, W. M., Bajak, K. K., Litton, C. W., & Spitzer, W. G. (1982). *Applied Physics Letters*, **41**(1), 70-72.

Tokumitsu, E., Kudou, Y., Konagai, M., & Takahashi, K. (1984). *Journal of Applied Physics*, **55**(8), 3163-3165.

Tu, K. N., Mayer, J. W., & Feldman, L. C. (1992). Electronic Thin Film Science for Electrical Engineers and Materials Scientists. New York: Macmillan Publishing Company.

Tuinstra, F., & Koenig, J. L. (1970). *Journal of Chemical Physics*, **53**, 1126.

van Berlo, W. H. (1993). *Journal of Applied Physics*, **73**(6), 2765-2769.

Wagner, J., Fischer, A., & Ploog, K. (1993). *Applied Physics Letters*, **62**(26), 3482-3484.

Wagner, J., Maier, M., Lauterbach, T., Bachem, K. H., Fischer, A., Ploog, K., Mirsh, G., & Kamp, M. (1992). *Physical Review B*, **45**(16), 9120-9125.

Walukiewicz, W. (1988a). *Journal of Vacuum Science and Technology B*, **6**(4), 1257-1262.

Walukiewicz, W. (1988b). *Materials Research Society Proceedings*, **104**, 483.

Walukiewicz, W. (1989). *Applied Physics Letters*, **54**(21), 2094.

Watanabe, K., & Yamazaki, H. (1991). *Applied Physics Letters*, **59**(4), 434-436.

Watanabe, K., & Yamazaki, H. (1993). *Journal of Applied Physics*, **74**(9), 5587-5595.

Yamada, T., Tokumitsu, E., Saito, K., Akatsuka, T., Miyauchi, M., Konagai, M., & Takahashi, K. (1989). *Journal of Crystal Growth*, **95**, 145-149.

You, H. M., Tan, T. Y., Gösele, U. M., Lee, S. T., Höfler, G. E., Hsieh, K. C., & Holonyak Jr., N. (1993). *Journal of Applied Physics*, **74**(4), 2450-2460.

Yu, K. M., Moll, A. J., Walukiewicz, W., Derhacobian, N., & Rossington, C. (1994). *Applied Physics Letters*, **64**(12), 1543-1545.

Zhang, K., Hwang, W., Miller, D. L., & Kapitan, L. W. (1993). *Applied Physics Letters*, **63**(17), 2399-2401.

Zhu, L. D., Chan, K. T., Wagner, D. K., & Ballantyne, J. M. (1985). *Journal of Applied Physics*, **57**(12), 5486-5492.